THESIS FOR THE DEGREE OF DOCTOR OF PHILOSOPHY (PHD)

The role of proteasomal complexes in the neurodegenerative Huntington's disease

by Azzam Aladdin

UNIVERSITY OF DEBRECEN
DOCTORAL SCHOOL OF MOLECULAR MEDICINE

DEBRECEN, 2021

THESIS FOR THE DEGREE OF DOCTOR OF PHILOSOPHY (PHD)

The role of proteasomal complexes in the neurodegenerative Huntington's disease

by Azzam Aladdin

Supervisor: Krisztina Tar, PhD

UNIVERSITY OF DEBRECEN
DOCTORAL SCHOOL OF MOLECULAR MEDICINE

DEBRECEN, 2021

Table of Contents

Abbreviations

A	Antimycin-A
ATGs	Autophagy-related proteins
BDNF	Brain-derived neurotrophic factor
Blm10	Bleomycin resistance 10
blm10Δ	BLM10 deleted strain.
BMA1	Bafilomycin A1
BSA	Bovine serum albumin
CAG	Cytosine, adenine, and guanine
Carboxy-H_2DCFDA	6-carboxy-2',7'-dichlorodihydrofluorescein diacetate.
cDNA	Complementary DNA
CFP	Cyan Fluorescent Protein
CHX	Cycloheximide
CNS	Central nervous system
DIC	Differential interference contrast
DMEM	Dulbecco's Modified Eagle's Medium-high glucose
DNM1L	Dynamin 1 like protein
Drp1	Dynamin-related protein 1
DUB	Deubiquitinating Enzyme
E1	Ubiquitin-activating enzyme
E2	Ubiquitin-conjugating enzyme
E3	Ubiquitin-ligating enzyme
ECAR	Extracellular acidification rate
EDTA	Ethylenediaminetetraacetic acid
ER	Endoplasmic reticulum
ETC	Electron transport chain
FACS	Fluorescence-activated cell sorting
FBS	Fetal bovine serum
FCCP	Carbonyl cyanide 4-(trifluoromethoxy)phenylhydrazone
FDR	False discovery rate.
Fis1	Mitochondrial fission 1
GFP	Green fluorescent protein
GST	Glutathione S-transferase
GTP	Guanosine triphosphate
HA	Hemagglutinin
HCD	Higher-energy collisional dissociation.
HCS	High content screening

HD	Huntington’s disease
HEAT	HTT, Elongation factor 3, protein phosphatase 2A, and TOR1.
HEPES	4-(2-hydroxyethyl) piperazine-1-ethanesulfonic acid, N-(2-hydroxyethyl) piperazine-N′-(2-ethanesulfonic acid)
HSF-1	Heat shock factor-1
HTT	Huntingtin gene
Htt	Huntingtin protein
IPTG	Isopropyl-β-D-1-thiogalactopyranoside
LC	Liquid chromatography
LC3	Light chain 3
LiAc	Lithium acetate
MAPK	Mitogen-activated protein kinase.
Mff	Mitochondrial fission factor
Mfn	Mitofusin
MG132	Carbobenzoxy-Leu-Leu-leucinal
MiD49	Mitochondrial dynamics proteins of 49 kDa
MiD51	Mitochondrial dynamics proteins of 51 kDa
MIEF	Mitochondrial elongation factor
MMP10	Matrix metalloproteinase-10
mODC	Mouse ornithine decarboxylase-C-terminal targeted for proteasomal degradation.
MS	Mass spectrometer
mtDNA	Mitochondrial DNA
MTR	Mitotracker Red CMXRos
N17	First 17 amino acids, N- region of Htt
NES	Nuclear export signal
N-Htt	N terminal huntingtin
OCR	Oxygen consumption rate
OD	Optical density
Opa1	Optic atrophy 1
OXPHOS	Oxidative phosphorylation
PA200	Proteasome activator 200 kDa
PAGE	Polyacrylamide gel electrophoresis
PBS	Phosphate buffered saline
PDC	Pyruvate dehydrogenase
PEG	Polyethylene glycol
Pen	Penicillin
PFA	Paraformaldehyde

PI	Propidium iodide
PI-3-P	Phosphatidylinositol 3-phosphate
PolyQ	Poly-glutamine
PolyUb	Polyubiquitin
PRD	Proline-rich domain
PRKN	Parkin RBR E3 ubiquitin-protein ligase
PTMs	Post-translation modifications
RIPA	Radioimmunoprecipitation assay
ROS	Reactive oxygen species
Rpn	Regulatory Particle Non-ATPase
Rpt	Regulatory Particle Triphosphatase
RT	Room temperature
RT-qPCR	Real-time quantitative polymerase chain reaction
scFvs	Single-chain Fv antibodies
SDS-PAGE	Sodium dodecyl sulfate-polyacrylamide gel electrophoresis
shRNAs	Small hairpin RNAs
Sirt 1	Sirtuin 1
Strep	Streptomycin
SUMO	Sumoylation
TBST	Tris-buffered saline with tween 20
TEV	Tobacco etch viral
TMRE	Tetramethylrhodamine ethyl ester
Ub	Ubiquitin
UPS	Ubiquitin-proteasome system
WT	Wild type strain
YPD	Yeast extract, peptone, dextrose
$\Delta\Psi m$	Mitochondrial membrane potential
19S-RP	19S-Regulatory Particle
20S-CP	20S-Core particle
2DG	2-deoxy-D-glucose

1. Introduction

Several neurodegenerative disorders are characterized by impairment protein degradation in neuronal cells. Ineffective clearance of misfolded proteins by the proteolytic pathways leads to the accumulation of toxic protein oligomers and aggregates in neuron cells. The dysregulation of ubiquitin-dependent and ubiquitin-independent proteasome activities plays an integral role in neurodegenerative diseases including Huntington's disease (HD) [1]. However, the precise role of proteasomal complexes in HD pathogenesis in extraneuronal tissues is not fully understood. Here we show that the ubiquitin-proteasome system responds to mutant huntingtin (Htt) in juvenile HD fibroblasts to protects cells. Moreover, the Blm10/PA200 activator family promotes the proteasomal degradation of N terminal Htt (N-Htt) fragments by a ubiquitin-independent pathway.

In the first study, we determined the crosstalk between mitochondria and the ubiquitin-proteasome system in juvenile HD fibroblasts. We found increased mitochondrial reactive oxygen species (ROS), and this increase is accompanied by a significant increase in the mitochondrial membrane potential ($\Delta\Psi m$). Moreover, mitochondrial oxidative phosphorylation (OXPHOS) does not reveal significant differences compared to control. Mitochondria function is controlled by the fission-fusion machinery. Thus, we measured the fission-fusion proteins. We found that fusion proteins are lower, this decrease leads to reduced mitochondria branching in diseased cells. We found also that juvenile HD fibroblasts are viable and both apoptosis and necrosis are relatively low similar to healthy control. On other hand, we demonstrated higher 26S proteasomal activity, which is associated with elevated Parkin in gene expression and protein level. Furthermore, we determined accelerated proteasomal degradation of mitofusin (Mfn)1 the mitochondrial fusion protein, which leads to reduced mitochondrial fusion. We suggest that juvenile HD fibroblasts respond to mutant Htt to balance mitochondrial structural loss by promoting proteasomal activity to protect cells.

In the second project, we determined the role of the Blm10/PA200 activator family in the proteasomal degradation of N-Htt fragments in a ubiquitin-independent manner. We conducted this part of our study using a combination of yeast and human HD models. We found that the deletion/depletion of the Blm10/PA200 family in the HD model drive to elevated mutant N-Htt aggregates formation and cellular toxicity. Moreover, the proteasomal activator Blm10/PA200 family interacts with soluble N-Htt fragments. The Blm10/PA200 family also promotes the activity of proteasome and accelerates the degradation of soluble N-Htt *in vitro*.

Overall, our results demonstrate how the ubiquitin-proteasome system (UPS) responds to mutant Htt, by enhancing the proteasomal degradation of specific Parkin substrates to protect the cells. Besides, the Blm10/PA200 activator family promotes the proteasomal degradation of toxic N-Htt fragments in a ubiquitin-independent manner. This activity leads to reduced aggregates formation and cellular toxicity. Here, we determined the value of enhancing the activity of the proteasomes by proteasomal activators. This activity may have the advantage to restore mitochondrial function and reduce the accumulation of toxic Htt species to attenuate cellular toxicity in HD.

2. Review of literature

2.1. Huntington's disease

Huntington's disease is an autosomal dominant neurodegenerative disorder [2]. HD patients are affected by a combination of symptoms ranging from movement disorders to psychiatric disturbances, and death usually occurs after 15-18 years of symptom onset [4]. The spread of this disease is estimated between 10.6 to 13.7 per 100,000 individuals in Europe [3-6]. The main hallmark of HD is the expansion of CAG repeats (≥ 40) in exon 1 of the huntingtin gene (*HTT*). The location of *HTT* is on chromosome 4. The mutation in the *HTT* gene leads to the generation of mutant Htt with abnormal polyglutamine repeats (polyQ) **(Figure 1)** [7]. Expanded polyQ makes the protein susceptible to be misfolded, and forming oligomers and aggregates with different levels of cellular toxicity [8, 9]. The length of polyQ correlates badly with disease progression. For example, greater than 60 glutamines (Qs) repeat in mutant Htt produces a more aggressive phenotype even in a juvenile age of HD patient **(Figure 1)**.

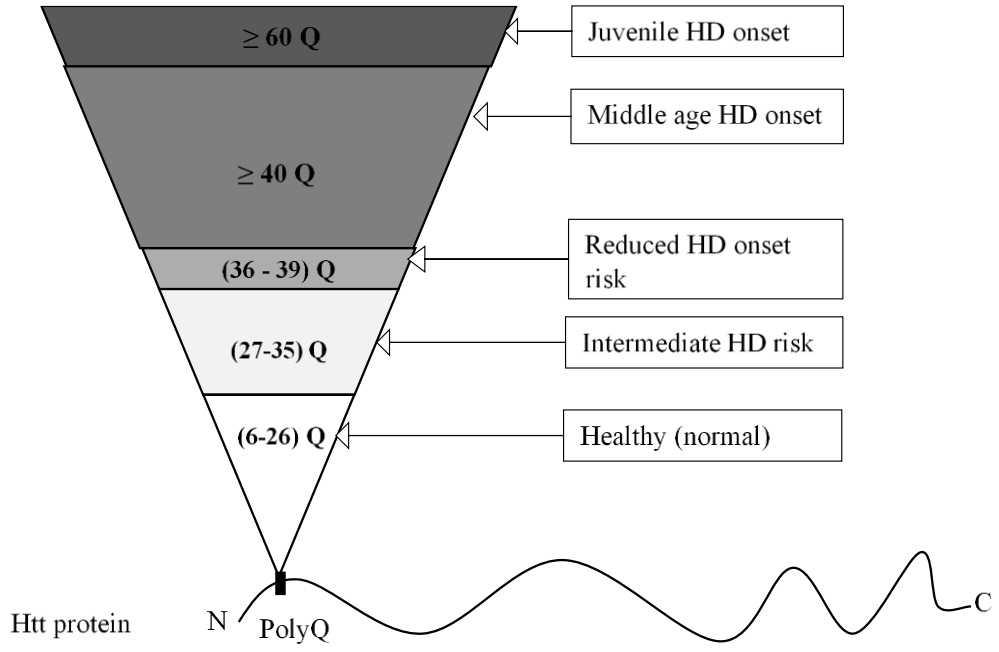

Figure 1. Schematic diagram of Htt sequence with different polyQ repeats, and the correlation between polyQ length and age-onset of HD *[10-14]. The severity and onset of HD are mainly correlated with the length of the polyQ track in mutant Htt. For example, if the mutant Htt of an HD patient contains more than 60Q, the HD manifestations will show even in the early age of an HD patient.*

In this chapter, we discuss the structure of Htt domains, which is important for our understanding of the cellular function of the Htt protein. Then, we consider the effects of mutant Htt in HD pathogenesis in different human tissues. We discuss the other hallmarks of HD, such as impairment of mitochondria and cellular proteostasis. Moreover, we spotlight the most promising therapeutic approaches that have been suggested by many studies.

2.2. The functions of huntingtin

Huntingtin is a large protein coded by the *HTT* gene. The Huntingtin gene consists of 67 exons, where exon 1 contains the CAG repeats, which is the vulnerable part in HD. Htt with a normal polyQ repeat such as 23 glutamines (23Q) includes 3144 amino acids. Wild-type Htt (MW 348 kDa) is a completely soluble protein. This protein is ubiquitously expressed throughout the human body with the highest level in neuronal cells [7, 15]. Most HD reports extensively study the toxic effects of the mutant N terminal fragment of Htt, because it contains expandable poly-glutamine **(Figure 1),** which is coded by exon 1 of mutant *HTT* [16, 17] **(Figure 2)**. This fragment consists of the first 17 amino acids of Htt called N-region (N17), follow by polyQ, then ~40 amino acids called a proline-rich domain (PRD) [18, 19]. The structure of N17 tends to fold as amphipathic α-helix [20, 21]. The function of N17 is to act as a nuclear export signal (NES) in the context of huntingtin and is subject to post-translation modifications (PTMs) of Htt [18, 22]. The polyQ stretch is a polymorphic region that adopts various structures like a random coil, extended loop, and α-helix. The structure of polyQ is also affected by the other protein regions [19, 20]. While the structure of PRD stretch is a polyproline helix, it plays a role in the interaction of Htt with the other proteins [23]. The C terminal of the Htt protein is coded by the remaining exons of *HTT* after exon 1. This part of Htt is not well studied. The most known structure in the C-terminal of Htt is HEAT (HTT, Elongation factor 3, protein phosphatase 2A, and TOR1) **(Figure 2)**. The structure of HEAT-repeats is antiparallel α-helices linked with loop [24, 25]. These domains have essential roles in protein-protein interaction [24]. However, the structure of Htt is variable. The structure depends on the structures of Htt domains, functions, and interactions with each other and other proteins [26]. In general, the structure and function of Htt are mainly controlled by PTMs.

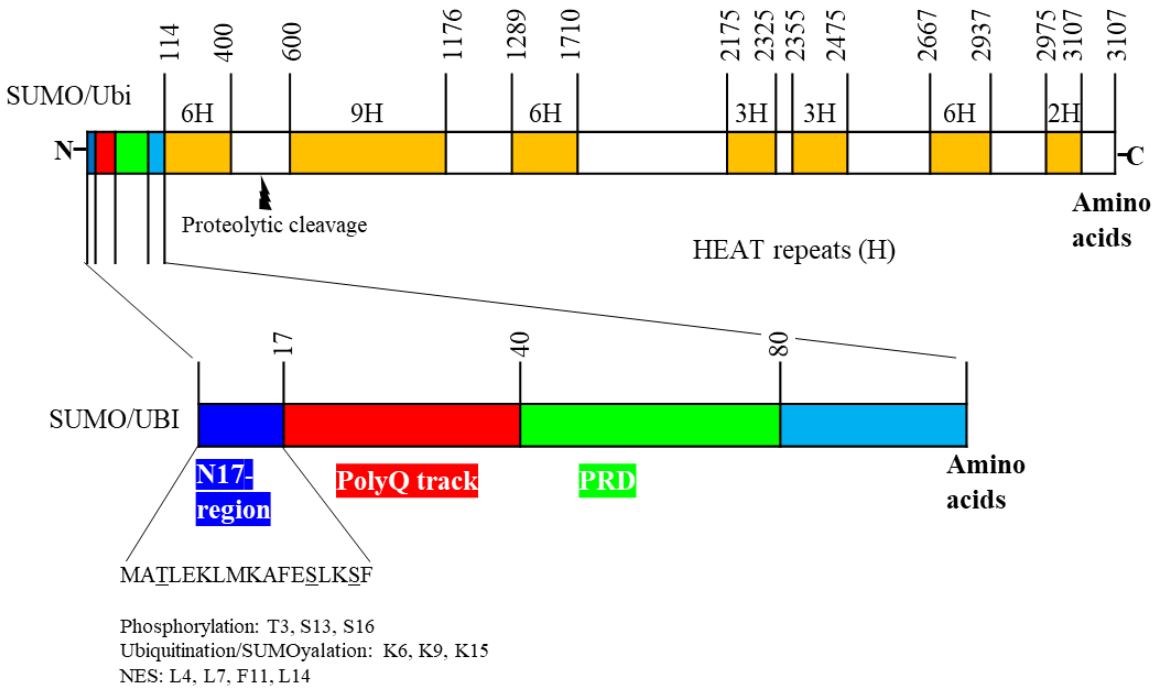

Figure 2. Diagram of huntingtin protein sequence and its regions*. The full length of the Htt sequence consists of ~3144 amino acids. The N-terminal region with 17 amino acids contains several PTMs sets, such as phosphorylation, ubiquitination, and nuclear export signal (NES) followed by a polyQ track with ~ 23Q and a proline-rich domain (PRD).*

Post-translational modifications have essential roles to regulate different functions of Htt [27]. PTMs such as SUMOylation, ubiquitination, phosphorylation, palmitoylation, and acetylation regulate the physiological function of Htt in healthy individuals. For example, SUMOylation helps to increase the capacity of Htt to suppress the transcription in the cell [17], where the ubiquitination affects many aspects of Htt such as subcellular localization and clearance [18, 22]. The full-length Htt has multiple sites to serve as a substrate for proteolysis [28]. These sites are between ~ 400-600 amino acids of the Htt sequence. Numerous reports identify several proteases that cleave within Htt such as caspases 2, 3, 6, calpain, and matrix metalloproteinase-10 (MMP10) [29-34]. The cleavage sites for these proteases are present within both wild-type and mutant Htt. These enzymes are expressing in various human tissues with different levels and activities. For example, caspase 6 is more active in the brain of HD patients, which promotes the generation of N-terminal Htt fragments [35]. The mutation in Htt probably prevents the normal function of Htt, which inhibits the function of caspase 6 in the case of expressing both proteins [36]. While caspase 3 can cleave within wild-type and mutant Htt in

neuron cells, which also could form N-huntingtin fragments [37]. The role of protease for wild-type Htt might inactivate some of the protein functions in healthy people [38]. Thus, the PTMs of Htt play as switches to activate and deactivate the particular or the whole protein function.

Huntingtin has multiple functions in development and physiology. The main function of Htt is essential for embryonic development [39-41]. For example, knockout of Htt in mice causes death for the mice embryos before 8.5 days of embryonic development, which means before the formation of the nervous system [41]. Moreover, cell death is elevated in Htt knockout mice, which indicates the role of Htt as anti-apoptosis in the cells [41]. This is supported by the overexpression of Htt in neuron cells, which protects the cells from apoptosis. Whereas the silencing of *HTT* in neuron cells leads to increased apoptosis [42-44]. The mechanism which explains how Htt has a role as anti-apoptosis is not fully studied. However, two possible mechanisms could explain this: First, that Htt can prevent the assembling of the pro-apoptosis complex Hip1-HIPPI, and the second is that Htt directly inhibits the activation of caspases 9 and 3 [42, 45], which regulate apoptosis signaling networks. The other important function that Htt is a player during the transcription process. Where Htt interacts with various transcription factors and regulatory proteins [46]. For instance, Htt indirectly regulates the production of the brain-derived neurotrophic factor (BDNF). Wild-type Htt inhibits the repressor element of the BDNF gene, which leads to an increase in the transcription of BDNF [47]. Huntingtin has an essential role in vesicles and organelles trafficking in the cell. The Htt also regulates BDNF on its transcriptional level and encourages BDNF vesicular trafficking in neuronal cells [48]. The knockdown of Htt leads to reduced transport of BDNF's vesicles [49]. Htt accumulates at synaptic terminals of neurons and interacts with synaptic vesicles and cytoskeletal proteins to regulate numerous synaptic activities between the cells [50]. Moreover, the impairment of mitochondria trafficking was reported in neurons of Htt knockout mice, and progressive degeneration was shown in the brain of the same mice [51]. Other studies suggested that Htt interplays in autophagy functions [52, 53], which regulate the trafficking of autophagosomes and their transport throughout the axon of neuron cells [54]. The understanding of the different sights of Htt functions leads to a comprehensive knowledge of mutant Htt and suggests potential approaches for HD therapy.

2.3. Mutant huntingtin

Mutant Htt contains an expanded polyQ tract in the N terminal of the Htt protein. As we discussed before, many proteases can cleave in mutant Htt within the range of approximately 400-600 amino acids, which then releases the toxic N-terminal Htt in neuronal cells. The

released fragments with mutant polyQ have more cytotoxicity than the mutant Htt protein itself [55]. It was also suggested that mutant N-terminal Htt fragments may initially be present in the cell as soluble fragments, and later can form oligomers, and then insoluble aggregates [56, 57]. Protein aggregation occurs when the concentration of mutant polyQ reaches a certain threshold in the cytosol [58]. The presence of mutant polyQ leads to a change in the structure of mutant Htt and influences the disease effects in the cell [59]. Emerging pieces of evidence have been proposed the importance of studying the effects of mutant Htt in extraneuronal and neuronal HD tissues [60, 61]. These studies could provide a better understanding of the disease, and could suggest more HD models for drug testing.

2.4. The manifestations of HD in the central nervous system

The central nervous system (CNS) is the most susceptible part in HD patients. The post-mortem brain of HD is 19% lower in total volume compared to the normal human brain [62]. The main vulnerable region in the brain is the striatum in the basal ganglia, where most of the GABAergic medium spiny neurons are lost [63]. The other parts are affected also, such as the cerebral cortex [62], and the hypothalamus [64]. They influence numerous impairments in their related tissue.

2.5. The manifestations of HD in peripheral tissues

The mutant Htt protein is widely expressed throughout the patient tissues [4]. Huntington's disease manifests in fibroblasts, skeletal muscles, the cardiovascular system, blood cells, the digestive tract, etc. [4, 61, 65-69] **(Figure 3)**. The abnormal manifestations in HD extraneuronal tissues are not all secondary responses to brain dysfunction, but most of these signs are directly caused by the expression of mutant Htt in the cell [70-73]. Studies that use HD peripheral tissues directly contribute to our comprehension of HD pathogenesis [4]. Therefore, the HD pathology in the peripheral tissues, such as severe atrophy of skeletal muscle [4], heart failure [74, 75], and weight loss [76], might have a substantial contribution to the disease progression. Several HD effects in the peripheral tissue are also summarized in **(Figure 3)**.

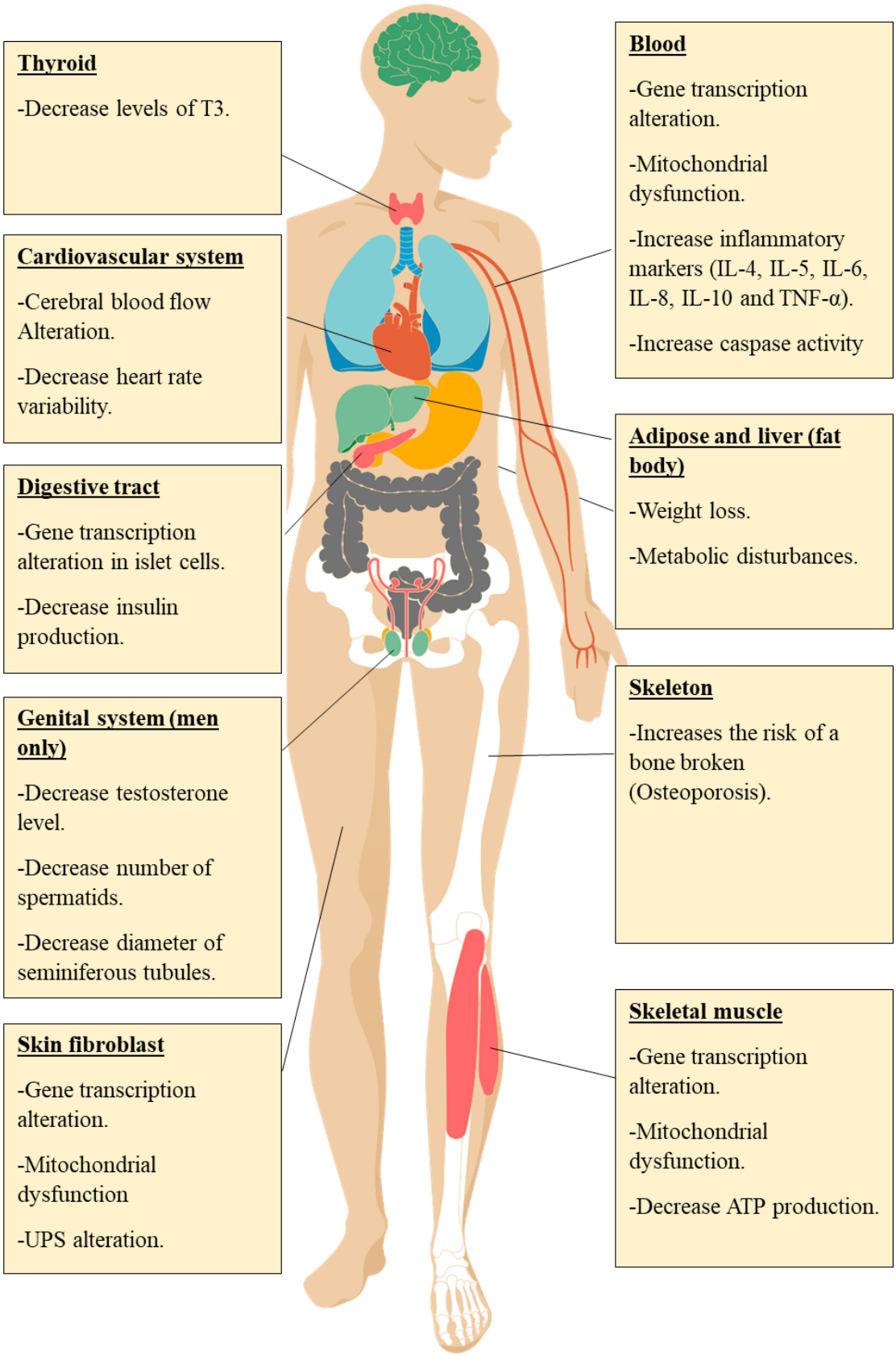

Figure 3. The effects of HD in peripheral tissues. *Mutant Htt protein is ubiquitously expressed throughout the HD patient's body, which is leading to widespread abnormalities in peripheral cells [4, 61, 65-69].*

2.6. HD models

HD cell models are valuable tools to investigate and interpret the hallmarks of Huntington's disease. Many inducible cell models have been developed and used to study HD pathogenesis in a highly controlled manner. For instance, the *Saccharomyces cerevisiae* (*S. cerevisiae*) HD model is based on the phenomenon that the genome of yeast does not contain an ortholog of the *HTT* gene. The changes in the phenotype of the yeast HD model are only caused by the effects of expressing mutant protein. Therefore, yeast is a powerful model to compare the behavior of human wild-type and mutant N terminal Htt fragments in the cells. It is a perfect model to understand the degradation of soluble fragments, and the effects of the mutant Htt on cellular toxicity and aggregates formation [77]. Other powerful models are human cell models, which have been used to study HD pathogenesis in different mammalian tissues. Multiple human cell lines have neuronal phenotypes including the SH-SY5Y neuroblastoma cell line. This cell line can reproduce many features of HD pathology after transient expression of the mutant N terminal Htt fragments [78]. Recently, different primary cell types were isolated from different tissues of HD patients. These cells express the full length of the mutant Htt protein. This feature makes primary cells a good model to study the effects of mutant Htt on intracellular pathways of various tissues [4, 61, 65-69]. For example, mutant huntingtin has a significant impact on mitochondrial function in skin fibroblasts of HD patients [61, 79]. Recently, the direct conversion of skin fibroblasts into functional neurons is become possible by silencing the polypyrimidine-tract-binding (PTB) gene [80, 81]. Trans-differentiation HD fibroblasts into neuron-like cells could be a promising model to study HD pathogenesis in neurons [80].

HD mice models were used to study many aspects of HD *in vivo*. These models were obtained by transgenic and knock-in techniques. Two classes of HD mice models were modified, some of them are expressing the mutant N terminal fragments, whereas the others are expressing the full-length of mutant Htt. The transgenic R6/1 and R6/2 mice have a predictable onset and fast disease progress [55, 82]. These features make this model great for drug discovery studies. As another example is the BACHD model, a transgenic mouse with a full-length mutant human *HTT* that contains 97 CAG repeats. This model is used mainly to study the effect of specific mutations in N17 [83]. This technique was used to replace the mouse *HTT* gene with a human mutant *HTT* containing the pathogenic CAG repeat. This model is powerful to study the metabolic changes in an early stage of HD.

2.7. What did we learn from HD models?

Diverse HD models have been used to understand HD pathogenesis. As well as the mutant Htt expresses in different human tissues, mutant Htt can influence many downstream effects in neuronal and peripheral cells [69, 84]. Mutant Htt influences several mechanisms in neuronal cells such as transcription process, intracellular signaling [84, 85], mitochondria dysfunction [86], endocytic recycling [87], synaptic impairment [88], etc. The dysfunction of mutant Htt drives dysregulation of multiple pathways in cells that are summarized in **(Figure 4)**.

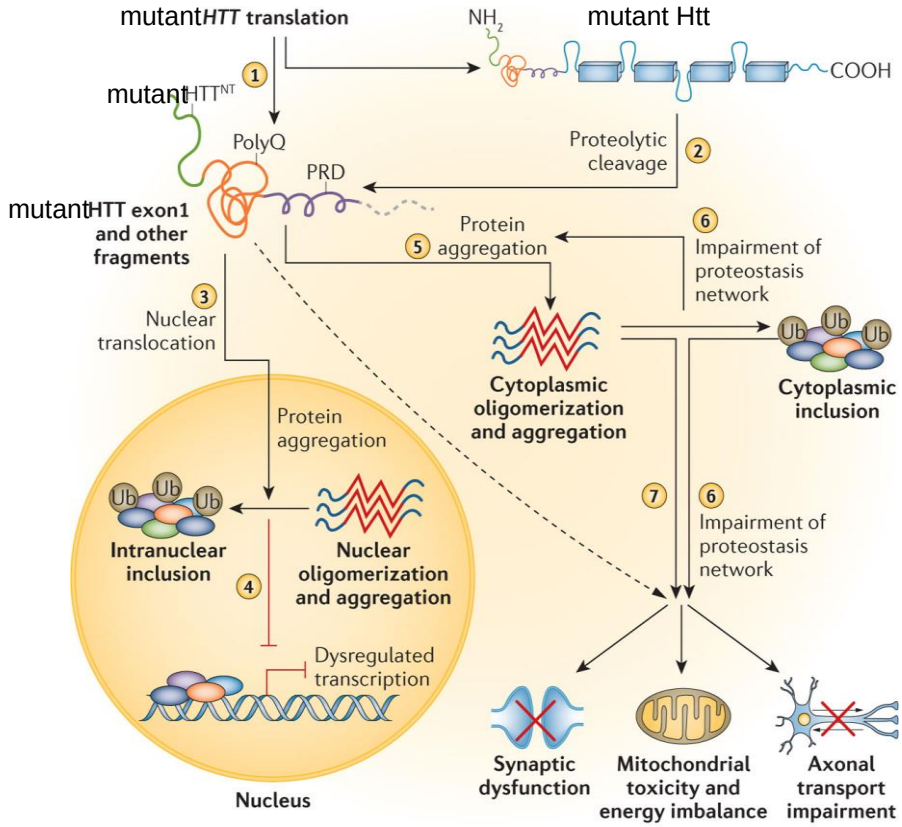

Figure 4. Summary of pathogenesis in HD neuronal cells. ***(1)*** *Mutant HTT is translated into mutant Htt with extended polyQ.* ***(2)*** *Native mutant Htt proteins are cleaved by proteolysis to generate additional toxic fragments.* ***(3)*** *Mutant Htt fragments are either transported into the nucleus or remain in cytosol.* ***(4)*** *Mutant Htt fragments are accumulated in the nucleus forming oligomers and insoluble aggregates. All forms can interact with transcription factors.* ***(5)*** *Mutant Htt fragments also form oligomers and aggregates in the cytoplasm.* ***(6)*** *The aggregation of mutant Htt fragments is elevated due to the failure in the proteostasis network in the cell, which also drives a global cellular dysfunction.* ***(7)*** *The HD manifestation in neuronal cells is translated as synaptic dysfunction, mitochondrial dysregulation, energy imbalance, and axonal transport impairment. Figure 4 adapted from Nature reviews Disease primers, Vol. 1, "Huntington disease", p: 1-21, Bates, G.P., et al., 2015.*

The alteration of numerous mechanisms is observed in various HD peripheral cell models, such as in transcription [89-91], the UPS [92, 93], and mitochondria functions [66, 67, 94]. These changes are often similar to the dysregulation mechanisms in neurons. Many studies in HD skin fibroblasts have reported the alteration of the transcription processes of different genes. The expression of the dynamin 1 like (*DNM1L*) gene encodes for Drp1 a mitochondrial fission protein is altered in HD fibroblasts [95, 96]. This could lead to changes in the Drp1 protein level. The increase of the Drp1 protein level further leads to mitochondria fragmentation in neuron cells [97]. However, the alteration in mitochondria structure of HD cells could cause changes in mitochondria integrity.

2.8. Mitochondrial integrity in HD

Mitochondria are tiny organelles in eukaryotes and the powerhouses of the cell. Mitochondria produce energy in the form of adenosine triphosphate (ATP) through the process of cellular respiration. The dysfunction of mitochondria is a key pathological process in HD in the CNS and numerous peripheral tissues. Therefore, we are going to discuss different aspects of mitochondrial defects in a number of HD models.

2.8.1. Mitochondrial respiration in HD

Mitochondrial respiration is a series of metabolic reactions and processes involving oxygen, this process converts the energy stored in carbon fuels to ATP. The major pathway that provides energy is OXPHOS. Oxidative phosphorylation is defined as an electron transport through the complexes I-IV driving electrons from the oxidation of NADH and $FADH_2$, this oxidation is coupled with phosphorylation of ADP to ATP at complex V.

Most functions in the cell are highly dependent on mitochondrial respiration and ATP synthesis. In an early study of the postmortem brain of HD patients, Stahl and Swanson have reported that mitochondria function is disturbed in HD neuron cells [98]. The following studies on HD postmortem brain of either juvenile or adult-onset have revealed that mutant Htt is correlated with abnormal mitochondria morphology [99, 100]. Other studies were also measured decreased activities of mitochondria complexes II, III, IV, and alterations in ATP/ADP ratio [101-104]. The cellular energy defects in HD are not only shown in the brain, but are also noticed in peripheral tissues, such as skin fibroblast [66], muscle [94, 105], and lymphoblasts [104]. Sarah et al. reported that ATP generation is decreased in skin fibroblasts of juvenile HD patients, but this decrease is independent of age and duration of disease [66]. The ATP deficiency in HD fibroblast is caused by defects in mitochondrial complex II activity [66].

Taken all together, mitochondria dysfunction is an important contributor to HD pathogenesis in different tissues of patients.

2.8.2. Mitochondrial membrane potential in HD

Mitochondrial membrane potential is generated by complexes I, III, and IV (proton pumps). These complexes are fundamental components during the OXPHOS process by pumping the protons into the intermembrane space. The accumulation of protons in the intermembrane space forms a proton gradient (ΔpH). ATP is generated by moving down the gradient concentration by crossing the protons through ATP synthase into the matrix [106]. In HD studies, isolated mitochondria from lymphoblasts cells from HD patients showed a decrease in ΔΨm. When HD lymphoblasts are stressed, the ΔΨm is lost. This indicates that the ΔΨm is affected by the toxic polyQ expressing in the cell [107].

2.8.3. Mitochondrial oxidative stress in HD

Oxidative stress is an overproduction of reactive oxygen species that trigger many toxic effects in the cell [108]. ROS includes non-radicals (H_2O_2, ROOH, HOCL, etc.) and free radicals ($O_2^{\bullet-}$, $ROO^{\bullet}$, $HOO^{\bullet}$, etc.) compounds. The main source of ROS is electron leakage at the level of complexes I and III from the mitochondrial electron transport chain (ETC) [109, 110], and the electron added to O_2 produces the superoxide anion ($O_2^{\bullet-}$) [108, 111-113].

The mitochondrial ROS, ΔΨm and the activity of ETC complexes are highly correlated to each other in two different pathways [114]. First, a decrease in ΔΨm could drive to increase ROS production when mitochondrial respiration is inhibited. Second, the ΔΨm is dropped by uncoupling, which leads to a decrease in the rate of ROS production [115]. On the other hand, the increase ROS production induces mitochondria fission. It was reported that mitochondria fragmentation occurs when the neuron cells were treated with H_2O_2 [116]. In general, mitochondrial dysfunction, ROS production, alteration in mitochondrial fission-fusion machinery, all are interdependent.

2.9. The importance of mitochondrial fission-fusion

Mitochondria can not be produced de novo. Therefore, the mitochondria proliferate as preexisting organelles grow and divide. Mitochondria contain their own mitochondrial DNA (mtDNA) and have their mechanisms for translating proteins necessary for respiration. However, most mitochondrial proteins are coded within the genome and synthesized in the cytoplasm [117-119]. Throughout the mitochondrial lifecycle, the mitochondria merge and separate again. Mitochondrial fission-fusion plays an essential role in the maintenance of functional mitochondria when the cells are subjected to metabolic alterations. The fusion is

used to mix and unify the mitochondrial compartment, while fission produces morphologically and functionally separate mitochondria [120]. Fusion helps to relieve mitochondrial stress by blending the contents of partially damaged mitochondria as a form of complementation. Fission is important to generate new mitochondria, which may be required for cell function. Moreover, the fission process contributes to quality control by allowing the elimination of damaged mitochondria, this process may facilitate apoptosis in high levels of cell stress [121]. Damaged and excess mitochondrial are removed by autophagy [122]. Fission and fusion are important for cell growth, mitochondrial distribution, and maintaining a healthy mitochondrial network. These processes have significant implications in mitochondrial functions and have a crucial role in the pathogenesis of many diseases, which the energy impairment as a manifestation of the disease.

2.10. Mitochondrial fission-fusion impairing in HD

Mitochondria are highly dynamic organelles in the cell. The mitochondrial fission-fusion machinery controls the constant changing of energy requirement in the cells [123]. The mitochondrial fission-fusion proteins regulate this machinery. The fission protein Drp1 is a cytosolic protein with GTPase activity [124]. Drp1 has a number of receptors on the outer mitochondria membrane. These receptors are Fis1, Mff, MiD49, and MiD51 [125]. To date, the precise mechanism of mitochondrial fission is still confusing. The best suggestion for mitochondrial fission is that a mitochondrial fission site is marked as pre-construction by an unknown mechanism, and this site is presented before the arrival of Drp1 [126]. Then, Drp1 forms an assembly surrounding the outer membrane as a ring using Fis1 as a receptor [127, 128]. The hydrolysis of GTP by the GTPase activity of oligomerizing Drp1 causes a site constriction on the mitochondria's outer membrane. [128]. On the other hand, the fusion proteins with GTPase activity are Mfn1 and Mfn2 and are located in the outer mitochondria membrane, where Optic atrophy 1 (Opa1) is located at the inner mitochondria membrane [129]. The fusion process requires both the outer and inner mitochondria membranes. The Mfn1 and Mfn2 promote the fusion of the mitochondria outer membrane [130-132], while Opa1 facilitates the inner mitochondrial fusion [133-135]. Mitochondrial fission-fusion is a brief process of ‘kiss and run’. When the $\Delta\Psi m$ is increased the mitochondria are more prone to fusion. Whilst the $\Delta\Psi m$ is decreased, once the mitochondria tend to undergo the fission process [136].

The fission-fusion balance is altered in HD neuron cells. This alteration is caused by dysregulation of mitochondrial fission-fusion gene expression and protein levels [86]. Studies using the post-mortem brain of HD patients showed that the mitochondria are fragmented, and

the gene expression of Mfn1 and Mfn2 are decreased. Gene expressions of Drp1 and Fis1 are increased affecting mitochondrial morphology [137, 138]. Mitochondrial fragmentation is observed in neuronal and peripheral cells of HD models [139-141]. Song et al, confirmed that an increase in mitochondrial fission in HD cells is the hallmark of the disease. In this study also, the authors proposed that the mutant Htt directly interacts with Drp1, this interaction leads to an increase in the GTPase activity of Drp1 and mitochondrial fragmentation [142]. This and many factors could stimulate mitochondria fission in HD cells. Oxidative stress is also enhanced mitochondrial fragmentation [116, 143, 144]. Thus, the accumulation of dysfunctional mitochondria may cause apoptosis in neuronal HD cells. Mitochondria are key players in HD neurodegeneration. Finding strategies to understand the different aspects of mitochondria could help to develop therapeutic strategies for HD disorder.

2.11. Mitochondria as a promising therapeutic target in HD

Mutant Htt directly or indirectly associates with multiple aspects of mitochondrial dysfunction, which lead to decreased ATP production, increased oxidative stress, and cell death. These defects are potential targets for HD therapy. For example, reducing ROS concentration is an objective for HD therapy [145]. Therefore, a number of components with antioxidant properties have been examined in HD models. The treatment with ascorbate improves R6/2 mice behavior [146]. Recently, it was demonstrated that a new antioxidant BN82451 protects the cells from ROS and increases the life span of the R6/2 mice HD model [147]. The most promising reagent for HD therapy is coenzyme Q10. It has antioxidant properties and roles in transferring electrons in ETC [148]. Treatment with Q10 showed improved motor performance, reduced striatal atrophy, attenuated weight loss, and increased survival of mice HD models [149, 150]. In clinical trials, however, low doses of Q10 did not show a major difference in HD patients. Therefore, an optimized increasing dose is required to obtain the fit concentration for potential therapy [151]. However, **Table 1** summarizes numerous therapeutic agents that target mitochondrial dysfunctions in HD models.

Table 1. Summary of the promising therapeutic strategies targeting mitochondrial functions. *These strategies were tested in different HD models.*

Therapeutic agents	**Experimental HD model**	**Pathway and outcome**	**Study references**
Butyrate or phenylbutyrate	▪Mouse YAC128 (express mutant Htt-128Q). ▪Striatal cells STHdh$^{111/111}$ (express mutant Htt-111Q).	-enhances pyruvate dehydrogenase (PDC) activity and this is associated with a rescue of mitochondrial function and motor phenotypes.	[152]
Resveratrol	▪Striatal and cortical cells from YAC128 mouse (express mutant Htt-128Q). ▪Mouse YAC128 (express mutant Htt-128Q).	-links with sirtuin 1 (Sirt 1) activation, the rescue of mitochondrial function, enhances expression of mitochondrial encoded ETC genes and, and improves motor phenotypes in YAC128 mice.	[153]
MitoQ and SS31 (Mitochondria-targeted antioxidant)	▪Striatal cells STHdh$^{111/111}$ (express mutant Htt-111Q).	-alter the expression of genes involved in mitochondrial fission-fusion dynamics and reduce mutant Htt protein	[154]
Mdivi-1 (Drp1 inhibitor)	▪Striatal cells STHdh$^{111/111}$ (express mutant Htt-111Q).	-promotes mitochondrial fusion, which is associated with the inhibition of excessive mitochondrial fission, and modulation of mitochondrial ROS production to improve mitochondria function.	[155, 156]
Mild perturbation of ETC	▪*Caenorhabditis elegans (C.elegans).* *C.elegans* (mutant Htt- different lengths of polyQ- eGFP).	-Mitochondrial stress regulates cytoplasmic proteostasis and health span during aging by coordinating the long-term activity of heat shock factor-1 (HSF-1) in *C.elegans*.	[157, 158]

2.12. Cellular proteostasis in HD

The dysregulation of proteostasis is another hallmark of Huntington's disease. Proteostasis is a balance between protein expression in the cell with the exact concentration, at the precise location with appropriate folding [159]. Protein concentration in cells is mainly controlled by protein clearance or turnover, which is organized by ubiquitination [160]. The process of ubiquitination is catalyzed by three enzymes cascade, consist of ubiquitin-activating (E1) enzyme, a conjugating (E2) enzyme, and ligase (E3) enzyme **(Figure 5).** It is believed that E3

ligases such as Parkin are the key for substrate recognition, and contribute to the specificity of the ubiquitin reaction [161]. The polyubiquitin (polyUb) chains are conjugated at different lysine residues (K6, K11, K27, K29, K33, K48, and K63) or N-terminal of methionine (M1) with different Ub chain topologies [162]. Each chain structure defines how the protein will behave or turnover in the cell. For example, the K48 linked ubiquitin chain will be the signal for protein proteolysis [163]. The attached polyUb can also be removed by the deubiquitinating (DUB) enzymes family.

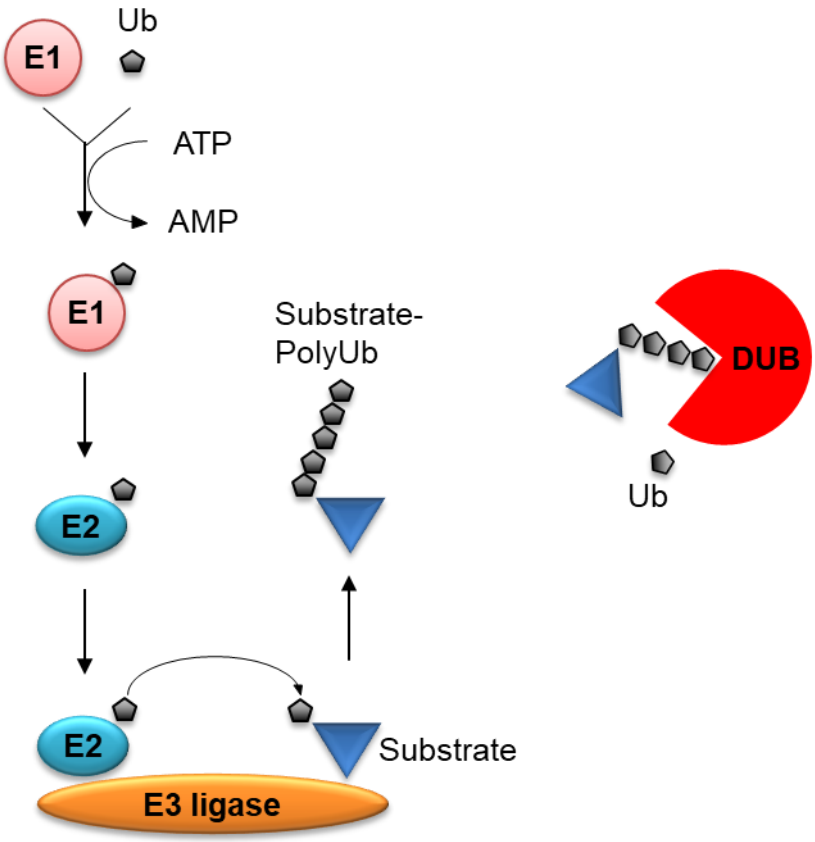

Figure 5. Overview of the ubiquitination system in the cell*. First, the E1 enzyme activates the ubiquitin and transfers it to the E2 enzyme. Second, the E2 enzyme cooperates with the E3 ligase to transfer the ubiquitin to the substrate. The linked polyUb chain can be removed by DUB enzymes.*

It is well known that the huntingtin protein can be ubiquitinated and degraded by the major proteolytic systems. These systems are the UPS, and the autophagy/lysosome machinery. Therefore, understanding these pathways in HD will give a great advantage to eliminate the toxicity of mutant Htt in HD cells.

2.13. Autophagy in HD

Autophagy is an intracellular process. It removes damaged organelles, long-lived proteins, and macromolecules. Autophagy is initiated by the generation of phosphatidylinositol 3-phosphate (PI-3-P) rich regions in the endoplasmic reticulum (ER). These regions form pre-autophagosomal structures such as phagophores. The level of PI-3-P is regulated by Beclin-1. The autophagosome assembles to envelop the substrate with the activities of LC3 proteins, and autophagy-related proteins (ATGs). Then, the autophagosome transfers the cargo to the lysosome for degradation [164-166].

The dysregulation of autophagy is increasingly considered to play essential roles in neurodegenerative diseases including HD. Mutant Htt influences various aspects of the autophagy pathway such as the initiation and trafficking of autophagosomes [167]. It was observed in HD fibroblast that Beclin-1, the key initiator of autophagy is reduced [168]. Because mutant Htt competes with the deubiquitinase Ataxin-3 for binding with Beclin-1. The results of this competition are increasing ubiquitination and degradation of Beclin-1 by the proteasome, which leads to impaired autophagy initiation [168]. Thus, disruption of the beginning of autophagy reflects the loss of huntingtin function in HD [169, 170]. Moreover, mutant Htt interacts with p62, the autophagosome adaptor. p62 is the receptor for the cargo, which can bind to ubiquitin and LC3. This interaction influences the affinity for substrate and LC3 and impairs the autophagic flux [169]. The function of Htt as a scaffold protein plays a key role in autophagosome trafficking. It was suggested that in HD neuronal cells, mutant Htt impairs autophagosome transport throughout the axon, reducing the fission of autophagosome with lysosome, and defects the degradation of cargo [168, 169]. The impairment of autophagy is affected mainly by the toxic effects of mutant Htt in the cells.

2.14. The ubiquitin-proteasome system in HD

The ubiquitin-proteasome system is the pathway for protein degradation by the proteasome in the cytosol and nucleus. The UPS regulates a large array of substrates and a number of cellular processes. The degradation of the substrate by UPS is tagged by polyUb that is linked with K48 residue [171]. The unfolded protein can enter the 26S proteasome for degradation **(Figure 6A)** The 26S proteasomal complex consists of a 20S core particle (20S-CP), which is capped at one or both ends by a 19S regulatory particle (RP) that named also proteasomal activator (PA)700 **(Figure 6A)**.

PA700 (MW~700 kDa) is a large protein complex, contains multiple subunits with diverse activities such as ATPase, reverse chaperon, and deubiquitinating enzyme, etc. For example,

PA700 from *S. cerevisiae* contains 17 subunits, such as AAA-ATPase (Rpt1–6) and non-ATPase (Rpn1–12) subunits. These subunits are arranged into two sub-complexes: a base and a lid **(Figure 6B)**. The base contains 9 subunits including polyubiquitin-interacting protein S5a, whereas the lid contains 8 subunits with a lack of ATPase activity. The lid is the upper sub-complex of PA700, which has the deubiquitinating function. The base acts as a reverse chaperone to unfold the substrate and to facilitate the gate opening of 20S-CP. Then the unfolded protein can be "sneaking" into the narrow pore of CP-20S for degradation. [172-174]. The UPS regulates numerous pathways in the cell, due to the diverse proteins that are degraded by the 26S.

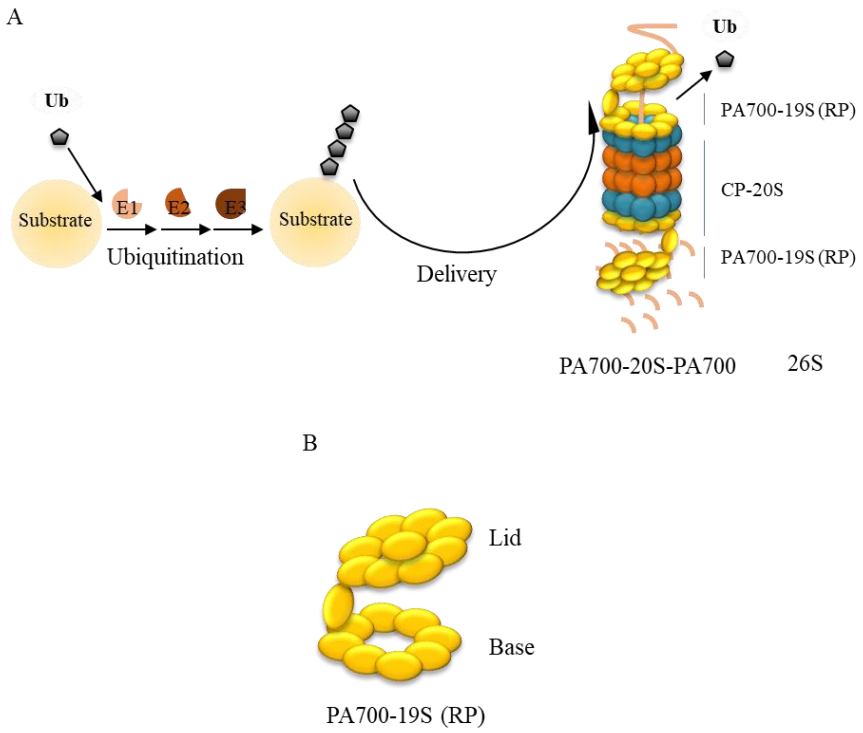

Figure 6. Schematic of the ubiquitin-proteasome system. (A) *Schematic diagram of protein degradation by the UPS.* ***(B)*** *Schematic representation of sub-complexes of the proteasome activator PA700-19S.*

The UPS provides highly effective regulation of mitochondria dynamics. The UPS is involved in the degradation of outer mitochondrial fission-fusion proteins [175]. In human cells, the mitochondria undergo the fission process, when Fis1 and Drp1 accumulate on the mitochondria outer membrane, whilst the Mfn1 and Mfn2 proteins are ubiquitinated and degraded by the 26S proteasome. On the other hand, the mitochondria are fused (fusion) in case of degradation of

Drp1 and Fis1 by UPS, where Mfn1 and Mfn2 accumulate on the outer mitochondria membrane, this accumulation plays a pivotal role in the mitochondria fusion process [176] **(Figure 7).**

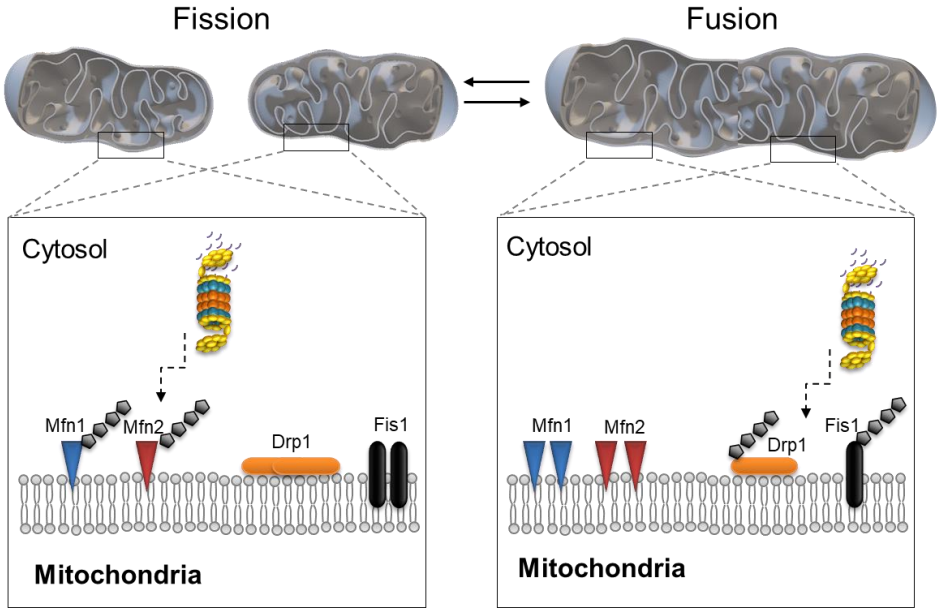

Figure 7. The crosstalk between the mitochondrial fission-fusion machinery and the UPS in normal condition. *In the fission process, Mfn1 and Mfn2 proteins are ubiquitinated and degraded by the 26S proteasomal complex, where Fis1 and Drp1 proceed with fission. During the fusion process, Drp1 and Fis1 are degraded by UPS, whilst Mfn1 and Mfn2 help the mitochondria for fusion.*

It was reported that mutant Htt can be ubiquitinated and be a potential substrate for the 26S proteasomes for degradation [177]. It was also found that the proteasome is present in the aggregates of mutant Htt, which indicates the direct implication of UPS in HD [177]. It was suggested also that the proteasomes can assembly with the insoluble aggregates [178]. The assembly of proteasomes to aggregates is probably reversible and dynamic [179]. Thus, the proteasomes are still functional and able to reach the substrates even in the presence of mutant Htt species [178]. In an i*n vitro* study, it was reported that mutant Htt aggregates do not inhibit the proteasomal activity [180], whereas the extracted mutant polyQ fibril from *in vivo* studies can inhibit the proteasomal activity [178], which suggest that the ubiquitination of aggregates could play an important role in the defect of 26S proteasome complex in HD cells [181]. Besides, it was proposed that mutant polyQ stretches could clog the proteasomes. The activity of the clogged proteasomes is inhibited, and these clogs prevent the peptides from passing the proteasomes [182, 183]. However, these data are conflicted with other data showing that N

terminal fragments are completely degraded by the proteasomes [184, 185]. Therefore, it is difficult to conclude the role of the UPS activity in the degradation of mutant Htt. Hence, more studies are needed to confirm the exact role and mechanism of proteasomal function in HD pathogenesis.

2.15. The core particle 20S-CP proteasome

The core particle consists of 28 subunits, assembles in 4 heptameric with dyad-symmetric rings, which form a cylinder shape proteasome [186, 187] **(Figure 8)**. The unfolded protein can enter each of the two gates. Each gate is formed from seven α-type subunits. The other two rings in the middle form the inner chamber. Each ring of the inner chamber is created from seven β-type subunits **(Figure 8)**. The inner chamber is the house for proteolytic active sites for the potential cleaving of peptides. In eukaryotic cells, only three of seven β-type subunits have active sites, therefore the proteasome has six active sites. These sites are caspase-like, trypsin-like, and chymotrypsin-like activities, which are presented by the β1, β2, and β5 subunits respectively [184, 185, 188] **(Figure 8).**

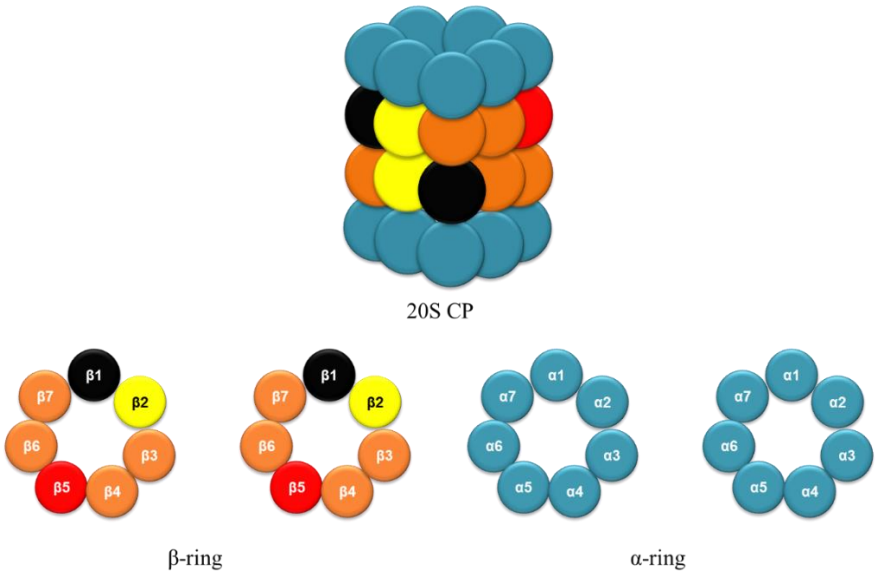

Figure 8. Schematic representation of the 20S-CP proteasome, and its subunits. *The a subunits control the gate opening of the 20S, where β subunits contain subunits, which have protease activities.*

The 20S-CP proteasome itself can degrade short peptides in a ubiquitin- and ATP-independent manner [189]. The mechanisms that control the gate opening at the α ring level are not well understood. It is thought that the binding of an unfolded protein to the α ring could induce the gate opening [190, 191]. It was reported that one-fifth of the total proteins in the cell are degraded by the proteasomes in a ubiquitin-independent manner [192]. This pathway may

provide an alternative mechanism for UPS to degrade unfolded and small proteins. For example, p53 a key regulator of the cell cycle is degraded by both ubiquitin independent and dependent pathways [193]. Moreover, the highly oxidized or misfolded proteins are degraded by 20S-CP proteasome under cellular stress [194, 195]. The degradation by the 20S-CP proteasomes is a passive pathway, which needs only an unstructured region in the protein to perform this process [196].

In general, the degradation by proteasomes is often dependent on ubiquitination and ATP [197]. However, a wide range of proteins is degraded by ubiquitin-independent or by both proteasomal degradation pathways [198, 199]. The specificity and function of the 20S-CP are well regulated by PA700, and proteasomal activator families Blm10/PA200 and PA28(αβγ). PA700 is a proteasomal activator in ubiquitin and ATP-dependent manner as we discussed before. On the other hand, PA28αβγ and Blm10/PA200 families regulate the proteasomal function in a ubiquitin and ATP-independent manner. Moreover, these activator families can form hybrid proteasome complexes with PA700. The exact cellular function of hybrid proteasomes is still not completely understood. These hybrid proteasomes may have more proteolytic specificities than proteasomes that capped with single or double of one type of proteasomal activator **(Table 2)**. Thus, the diversity of proteasomes can control vast different of substrates that put the proteasomal complexes as the main target to study a number of diseases.

Table 2. Types of proteasomal complexes have been identified with assemblies of different proteasomal activators. *These proteasomes were identified by different studies [190, 200-202].*

Proteasome	**Proteasome activator**	**Proteasome structure**
20S	-	CP
26S	19S (PA700)	PA700-CP
30S	19S (PA700)	PA700-CP-PA700
Hybrid proteasome	19S (PA700) 11S (PA28αβ)	PA28αβ-CP-PA700
Proteasome-PA200 singly capped	Blm10/PA200 family	PA200-CP
Proteasome-PA200 doubly capped	Blm10/PA200 family	PA200-CP-PA200
Hybrid proteasome	19S (PA700) PA200	PA200-CP-PA700
Proteasome-PA28αβ doubly capped	11S (PA28αβ)	PA28αβ-CP-PA28αβ
Proteasome-PA28γ doubly capped	11Sγ (PA28γ)	PA28γ-CP-PA28γ

2.16. The regulation of 20S-CP proteasome in a ubiquitin-independent manner

The capacity of the 20S-CP proteasomes in a ubiquitin-independent manner is significantly enhanced by PA28(αβγ) and Blm10/PA200 activators families [200, 203, 204]. PA28 is known as the 11S regulator. It has three different subunits PA28α, PA28β, and PA28γ, and these subunits are arranged in a heptameric structure [205, 206]. These subunits are assembled in three different structures in mouse as PA28α7, PA28β7, and PA28α4β3 [207]. While mammalian PA28 is mainly assembling in asymmetric PA28α4β3 complex [207]. In general, the PA28α and PA28β are found only in the cytosol, but all three PA28(αβγ) isoforms predominantly present in the nucleus [208, 209]. The diverse locations of PA28 and its function in the degradation of unfolded small proteins make it a target to study its role in HD. Seo et al. reported that the overexpression of PA28γ drives to recover the proteasomal function and increases cell viability in different HD cell models [93]. In their following study, they used YAC128 mice as an *in vivo* HD model. They also reported that overexpression of PA28γ by gene therapy leads to an increase the proteasomal activity in the striatum, as well as improved motor coordination, and behavioral abnormalities symptoms in this model [210]. The accumulating data indicate the importance of enhancing the 20S-CP proteasomal function in a ubiquitin-independent manner. This also attracted us to study the Blm10/PA200 family as a proteasomal activator, and its role in the degradation of peptides such as N terminal Htt fragments.

2.17. The Blm10/PA200 activator family

PA200 is a proteasomal activator with MW ~200 kDa, it is mostly located in the nucleus and also found in the cytosol of human cells [211]. The homolog of yeast *S.cerevisiae* is bleomycin resistance 10 (Blm10) with MW ~245 kDa. Blm10 shows about 20% amino acid sequence similarity compared to PA200 protein [212-216]. The structural studies by cryo-electron microscopy show that PA200 is a monomeric protein, it contains 32 HEAT-repeats-like modules from almost every α-helix. While Blm10 also contains HEAT-repeats, they are formed from all α-helix present in the protein [216]. The Blm10/PA200 family has a dome architecture that binds to the gate of CP-20S, and HEAT-repeat associates this binding [216-218]. PA200 utilizes its C-terminal (Tyr-Tyr-Ala) to trigger an α-ring of CP-20S gate to rearrange the α subunits for gate opening [218]. The structure of PA200 has two holes formed by a lot of positively charged residues, which allow unfolded proteins to go through PA200 into the 20S-CP for potential degradation [218]. Whereas, Blm10 has a small opened slot that also leads unfolded protein to move toward the axial channel of the proteasome [216]. The Blm10/PA200

family can assemble with 20S-CP forming a number of proteasomal complexes, which were determined in either *in vivo* or *in vitro* studies. The Blm10/PA200-CP proteasomes are found as different complexes. For example, Blm10/PA200-CP can form a hybrid proteasomal complex with PA700, which is found *in vivo* [219, 220] **(Table 2).** Moreover, the core particle can assemble with PA200 and form singly and doubly capped proteasomes. These proteasomes were recognized *in vitro* and isolated from testes of bovine and mammalian, while Blm10-20S-CP complexes were found *in vitro* and isolated from yeast strains [186, 202, 219, 221, 222] **(Table 2).** The current knowledge about specific substrates for the Blm10/PA200 family is very limited. The Blm10/PA200 proteasomal activators enhance caspase-like and trypsin-like protease activities of β1 and β2 –subunits, respectively [211, 216, 219, 223, 224]. The Blm10/PA200 family accelerates the turnover of Dnm1 in yeast and unstructured proteins such as Tau. PA200 facilitates the degradation of acetylated histone in a ubiquitin- and ATP-independent manner. Furthermore, PA200 is essential for cell survival in stressed cells [220]. Collectively, the Blm10/PA200 family plays multiple roles in the cell starting from its function as proteasomal activator to their role as regulator of a number of cellular functions.

2.18. Therapeutic strategies for HD by targeting the proteasomal systems

The most promising fields for HD therapy development are to decrease mutant Htt levels in a patient's neuronal cells [225, 226]. Gene silencing approaches to lowering mutant *HTT* monogenic expression in HD have been extensively studied. Even though these efforts are very promising, but it is still at the beginning of the way. Decreasing mutant *HTT* expression with siRNA improved the neuropathology and the phenotype in HD mouse models [181, 227-229]. But, these attempts to silence or delete mutant *HTT* only in HD human proteins are failed [230]. One of the main reasons caused this failure, that the gene therapy targeting mutant *HTT* not only suppresses the production of the mutant *HTT* but also wild-type *HTT*. The decreased level of the wild-type Htt protein caused problems in HD patients [230]. However, increasing the activity of proteasomal systems is an alternative manner to help the cell to remove mutant Htt [231]. Direct re-modulating of proteasomal complexes can be a therapeutic approach for HD. For example, overexpression of PA28γ can improve the cellular viability in HD neuronal cells and mouse models [93, 210]. The overexpression of different E3 ligases is another potential strategy to lower mutant Htt aggregation, by encouraging mutant Htt ubiquitination, and then degradation of the toxic Htt by the proteasomes [232-235]. Multiple therapeutic approaches that have been focused on decreasing mutant Htt are listed in **Table 3.**

Table 3. Summary of promising therapeutic approaches by modulating the UPS in different HD models*. Various HD therapeutic strategies are targeting UPS. Most of these strategies are still under development and have been tested using different HD models.*

Therapeutic approach	**Experimental model**	**Pathway and outcome**	**Study reference**
Sulforphane	▪HEK293 and Hela cells (express mutant Htt-74Q GFP). ▪Mouse model (transgenic UPS function [236], express mouse Htt). ▪Rat HD51 model (express mutant Htt-51Q). ▪Mouse HD (C57BL/6) induced by 3-nitroproprionic acid (express mouse Htt).	-activates pathways of Keap1-Nrf2-ARE, inhibits pathways of mitogen-activated protein kinase (MAPK), and NF-kB to activate UPS.	[237-239]
Rolipram	▪Mouse R6/2 (express mutant Htt-150Q).	-inhibits phosphodiesterase4 and activates protein kinase A to activate UPS.	[240]
Amiloride, Benzamil	▪Neuro2a cells (express mutant Htt-60Q-EGFP or mutant Htt-150Q-EGFP).	-rescue acid-sensing ion channel (ASIC), based on acidotoxicity that inhibits UPS.	[241]
PROTAC	▪Fibroblast cells from HD patients (express full-length mutant Htt 47Q or 68Q).	-A cellular inhibitor of apoptosis protein 1 (cIAP1) mediates UPS by linking a ligand for ubiquitin ligase with probs for mutant Htt aggregates degradation.	[242]
PEST-C4 Single-chain Fv antibodies (scFvs)	▪Striatal cells (express mutant Htt-72Q) from mouse HDR6/1	-Mouse ornithine decarboxylase-C-terminal targeted for proteasomal degradation (mODC)-(PEST) mediates UPS degradation of mutant Htt aggregates.	[243]

These findings show new insight into the possible modulation of UPS, which provides the most promising therapeutic avenues to overcome soluble mutant Htt. The way to find treatment for HD by removing the toxic role of mutant Htt is still a long way. Understanding more pathways that could eliminate the mutant polyQ will add more potential strategies for HD therapy.

3. Aims and objectives

3.1. Aims

Protein degradation by proteasomal complexes plays the main role in the regulation of a wide range of basic cellular processes and cleaning misfolded proteins. The implication of proteasomal complexes in different pathways of HD pathogenesis is still not entirely understood. Therefore, we investigated the roles of proteasomes in the pathogenesis of HD in two different manners. On one hand, we studied how the activity of the proteasomes in a ubiquitin-dependent manner affects mitochondria function in extraneuronal cells. On the other hand, we explored the potential role of the Blm10/PA200 activator family on the proteasomal degradation of N-Htt fragments in a ubiquitin-independent manner. Thus, our aims in this study are:

- To investigate the crosstalk between the ubiquitin-proteasome system and mitochondria in juvenile HD fibroblasts.
- To determine the role of the proteasomal activator Blm10/PA200 family in the degradation of the toxic N terminal Htt fragments.

3.2. Objectives

This study will address the following objectives:

1- Measure intracellular ROS production and mitochondria membrane potential, which reflect mitochondria function in juvenile HD fibroblasts.

2- Evaluate the glycolysis and mitochondria respiration in juvenile HD fibroblast.

3- Identify the cellular viability, which may be affected by mitochondrial alterations.

4- Determine the alteration in mitochondrial dynamics and function.

5- Evaluate the activity of UPS in juvenile HD fibroblast, and the effect of this activity in the turnover of specific UPS substrates.

6- Determine the effects of absence Blm10/PA200 proteasomal activator on aggregates formation from the toxic N-Htt, and cellular toxicity of the aggregates in an HD yeast model.

7- Investigate the interaction between the Blm10/PA200 family with soluble fragments and aggregates from toxic N-Htt.

8- Confirm the role of the Blm10/PA200 family regarding aggregate formation in the human neuroblastoma cell line.

9- Evaluate the activity of the proteasome in the presence of the Blm10/PA200 family in the degradation of soluble N-Htt fragments.

10- Determine and specify the contribution of Blm10/PA200 in the degradation of soluble fragments of wild-type and mutant N-Htt by mass spectrometry (MS).

4. Material and Methods

All chemicals and reagents were purchased from Sigma-Aldrich (St. Louis, MO, USA) except where stated otherwise.

4.1. Cell models, growth media, and culture conditions

We performed our study using different types of cells as experimental HD models to study various aspects of Huntington's disease.

4.1.1. Juvenile HD fibroblasts

Primary skin fibroblasts from juvenile healthy and patients with HD [80, 244]. These cells were obtained from Coriell Institute for Medical Research's NIGMS Human Genetic Cell Repository **(Table 4)**. The donors' approval and privacy documents were addressed and authorized by the Coriell Institute.

Table 4. Characterization of CAG repeats in exon 1 of the HTT gene in the fibroblasts from juvenile healthy control and two HD patients *[244]. Huntingtin gene presence as two copies in human cells. CAG1 refers to the CAG (cytosine, adenine, and guanine) repeat size of HTT in the first allele, CAG2 refers to CAG size in the second allele.*

Name	Type	Sex	Symbol	CAG1	CAG2	Age at sampling	Age of onset
AG07095	Healthy control	Male	16Q	NA	NA	2	NA
GM04281	Juvenile HD	Female	68Q	71	17	20	14
GM05539	Juvenile HD	Male	86Q	97	22	10	2

Fibroblasts were cultured in Minimum Essential Medium Eagle (MEM), supplemented with 10% non-heat inactivated fetal bovine serum (FBS) (Gibco™, Gaithersburg, MD, USA), 2 mM L-glutamine and 100 units/ml penicillin (Pen) and 100 µg/ml streptomycin (Strep) termed as complete MEM (CMEM). The cells grew in a cell culture incubator under standard conditions at 37 °C and 5% CO_2. To avoid any effects of cellular senescence on human fibroblasts, we performed our experiments using the cells within passage numbers 7 and 14.

4.1.2. SH-SY5Y cell line

SH-SY5Y neuroblastoma (European Tissue Culture) is a human cell line derived from the SK-N-SH cell line. The growth medium for SH-SY5Y consists of Dulbecco's Modified Eagle's Medium-high glucose (DMEM), heat-inactivated 10% FBS (Gibco™, Gaithersburg, MD, USA), 2 mM L-glutamine, 1 mM sodium pyruvate, and 100 units/ml Pen-100 µg/ml Strep

antibiotic solution, which termed as complete DMEM (CDMEM). The cells grew under standard conditions at 37 °C and 5% CO_2.

4.1.3. PA200 depleted cell line and its corresponding control

We used a previously generated stable PA200 depleted SH-SY5Y cell line (shPA200) and its control counterpart with an empty pGIPZ-GFP vector [245]. The stable shPA200 and control cells were grown in CDMEM media. Complete DMEM was supplemented with 1.25 µg/ml puromycin as the cells selection factor, which was removed before 24 hr of the day of the experiment.

4.1.4. Yeast strains

Yeast strains used in this study are isogenic to BY4741 and BY4742, which derive from *S. cerevisiae* S288C [246]. Complete gene deletion and yeast transformation were accomplished by the Lithium Acetate method as described by Gietz et al. [247]. Briefly, yeast and plasmid DNA were resuspended in polyethylene glycol (PEG) and lithium acetate (LiAc) solution (40% w/v PEG, 0.1 M LiAc in Tris-EDTA buffer), followed by 40 min incubation at 30 °C, and 7 min at 42 °C. Then, the yeast was plated on a selection medium. The cells grew in standard synthetic complete media (0.67% w/v yeast nitrogen base, 2% w/v glucose and necessary amino acids) or yeast extract, peptone, and dextrose (YPD) media (2% w/v of Difco peptone, 1% w/v of yeast extract, 2% w/v of glucose). Then, cells were seeded onto solid selective synthetic complete media with reduced amino acids at 30 °C for selecting the transformed yeast. The yeast strains **(Table 5)** grew in YPD media at 30 °C and were harvested at the log phase with approximate optical density $(OD)_{660}$ nm ~1 for potential study.

Moreover, we studied the phenotype of yeast strains expressed N terminal huntingtin fragments, which contain a specific length of polyglutamine such as N-Htt25Q as wild type or N-Htt103Q as mutant fragments. The original and transformed strains are listed in **Table 5**. The cells grew overnight in synthetic media with 2% v/v raffinose as a carbon source and reduced amino acids for plasmid selection. The transformed yeast strains were induced with 2% v/v galactose for N-Htt with polyglutamine expression or with 2% v/v raffinose as uninduced yeast. The cells were incubated for 18 hr to reach the OD_{660} nm ~ 0.4 mid-log phase. The induced and uninduced cells were spotted by drop-out the media onto solid synthetic media. Then the colonies were observed daily for yeast phenotype study.

Table 5. List of yeast strains used in this study. *The transformed strains are expressing N-Htt fragments under galactose induction.*

Strain	Genotypes	Ref.
S288C	*MATα SUC2 gal2 mal2 mel flo1 flo8-1 hap1 ho bio1 bio6*	[248]
BY4741	*MATa his3Δ1 leu2Δ0 met15Δ0 ura3Δ0*	[249]
BY4742	*MATΔ his3Δ1 leu2Δ0 lys2Δ0 ura3Δ0*	[249]
yMS122	*MATa his3D1 leu2D0 met15D0 ura3D0 PRE1tevProA (HIS3) GalpHA3Blm10(Kan)*	[219]
yMS94	*MATa his3D1 leu2D0 met15D0 ura3D0 PRE1 tevProA (HIS3) blm10:Nat*	[219]
yMS268	*MATα his3Δ1 leu2Δ0 met15Δ0 lys2Δ0 ura3Δ0*	[220]
yMS131	*MATα his3Δ1 leu2Δ0 met15Δ0 ura3Δ0 blm10Δ::NatMX*	[250]
yMS285	*MATα his3Δ1 leu2Δ0 ura3Δ0 rpn4Δ::KanMX*	[250]
yMS476	*MATα his3Δ1 leu2Δ0 met15Δ0 ura3Δ0 PRE1TEVProA(HIS3)*	[223]
yMS1371	*MATα his3Δ1 leu2Δ0 met15Δ0 ura3Δ0+ pYES2-Htt25Q-CFP*	[251]
yMS1377	*MATα his3Δ1 leu2Δ0 met15Δ0 ura3Δ0+ pYES2-Htt103Q-CFP*	[251]
yMS1372	*MATα his3Δ1 leu2Δ0 lys2Δ0 ura3Δ0 rpn4Δ::HphMX+ pYES2-Htt25Q-CFP*	This study
yMS1392	*MATα MATα his3Δ1 leu2Δ0 lys2Δ0 ura3Δ0 blm10Δ::NatMX+ pYES2-Htt25Q-CFP*	This study
yMS1378	MAT*α his3Δ1 leu2Δ0 lys2Δ0 ura3Δ0 rpn4Δ::HphMX+ pYES2-Htt103Q-CFP*	This study
yMS1393	*MATα MATα his3Δ1 leu2Δ0 lys2Δ0 ura3Δ0 blm10Δ::NatMX+ pYES2-Htt103Q-CFP*	This study

4.2. Plasmids constructs

The plasmid pHM6-Q23 (Addgene, Watertown, MA, USA) contains the wild-type length of CAG repeats of exon 1-*HTT*, while pHM6-Q74 (Addgene, Watertown, MA, USA) contains the mutant length of CAG repeats. Both plasmids express N-Htt with a specific number of glutamines with a hemagglutinin (HA) tag. These plasmids are a kind gift from David Rubinsztein [252]. These plasmids were transiently transfected in SH-SY5Y, and shPA200 and its corresponding control cell lines. The pGEX-5 plasmids express either wild-type N-Htt with 18Q tagged with Glutathione S-transferase (GST), or mutant N-Htt with 51Q. Both plasmids were obtained from Ron Kopito at Stanford University, CA, USA. The site between GST and N Htt was modified by adding a tobacco etch virus (TEV) protease cleavage site encoding regains. The GST tag preserves the expressed mutant N-Htt in a soluble form. Hence, upon GST cleavage the mutant N-Htt directly forms aggregates [180, 253]. The plasmid control pGEX-4T-2 was a kind gift from Anita Boratkó, University of Debrecen, Debrecen, Hungary. The plasmids pYES25Q-CFP, and pYES103Q-CFP express N-Htt25Q and N-Htt103Q fused

with CFP under the GAL1 promoter in the yeast HD model. These plasmids were a kind gift from Michael Sherman, Boston University School of Medicine, Boston, USA [254].

4.3. Reactive oxygen species measurement in juvenile HD fibroblasts

Cellular reactive oxygen species in juvenile HD fibroblasts were analyzed using 6-carboxy-2',7'-dichlorodihydrofluorescein diacetate (Carboxy-H_2DCFDA) (Thermo Fisher, Waltham, MA, USA). Carboxy-H_2DCFDA is a nonfluorescent molecule. This reagent is easily converted into a fluorescent green when the acetate groups are removed by the oxidation effects of intracellular ROS. In our experiment, fibroblasts were cultured in a six-well plate, each well contains 10^5 cells. On the next day, culture media was replaced with MEM contains 2% FBS and 1 µM Carboxy-H_2DCFDA, followed by 30 min incubation at 5% CO_2 and 37 °C. Then, the cells were rinsed with phosphate-buffered saline (1X PBS; 137 mM NaCl, 2.7 mM KCl, 10 mM Na_2HPO_4, 1.76 mM KH_2PO_4, pH 7.4), then collected by trypsin-EDTA, washed, and then supplemented with 1X PBS completed with 1% FBS. The fibroblasts were filtered through a nylon net filter 41 µm pore size (Millipore, Burlington, MA, USA). The cellular ROS was measured in filtered cells by fluorescence-activated cell sorting (FACS) Aria III (BD Biosciences, Franklin Lakes, NJ, USA) at Ex/Em: 492/517 nm. FACS data were analyzed by FlowJo software v10 (FlowJo LLC, Ashland, OR, USA).

4.4. Mitochondrial membrane potential measurement in juvenile HD fibroblasts

We performed two assays to evaluate mitochondrial membrane potential ($\Delta\Psi m$) in juvenile HD fibroblasts and healthy control.

4.4.1. Mitotracker red CMXRos

In the first assay, we used Mitotracker Red CMXRos (MTR) (Thermo Fisher, Waltham, MA, USA). MTR is a red fluorescent dye and used for mitochondria staining in live cells. We seeded 10^5 cells in each well of 6 well plates. On the following day, we incubated the fibroblasts in serum-free media of MEM completed with a 50 nM MTR probe at 37 °C and 5% CO_2 for 30 min. MTR diffuses through the cell membrane and accumulates in the active mitochondria. Then, we washed the cells, harvested them by trypsin-EDTA, and resuspended the cells in 100 µl of 1X PBS contains 1% FBS v/v. To avoid cell clumps or cell debris that could interfere with our measurement, we filtered the cells through a 41 µm nylon net. In each experiment, 20000 events of filtered cells were evaluated by FACS Aria III (BD Biosciences, Franklin Lakes, NJ, USA) at Ex/Em: 579⁄599 nm. The obtained results were analyzed by FlowJo v10 software (FlowJo LLC, Ashland, OR, USA).

4.4.2. Tetramethylrhodamine ethyl ester

In the second assay, we used Tetramethylrhodamine ethyl ester (TMRE) (Abcam, Cambridge, UK). TMRE is a red-orange, fluorescent dye that rapidly stains the mitochondria, which accumulates upon increasing ΔΨm. Fibroblast cells were cultured in 6 well plates at 10^5 cells/well. On the day of the experiment, we performed negative control by treating one sample of each cell type with 20 µM carbonyl cyanide 4-(trifluoromethoxy) phenylhydrazone (FCCP) for 10 min. The negative control and our test samples were incubated in CMEM with 100 nM TMRE for 10 min at normal growth conditions. The positively charged TMRE was permeated to cells led red-orange dye accumulated in active mitochondria. Cells were harvested and 20000 events were analyzed by FACS as previously described using Ex/Em: 549/575 nm.

4.5. Measurement of bioenergetic profiles of juvenile HD fibroblasts

Bioenergetic profile refers to the measurement of mitochondrial respiration and glycolysis under basal conditions and maximal capacities.

4.5.1. Mitochondrial respiration

The XFe96 extracellular flux analyzer enables the real-time measurement of extracellular flux changes of oxygen in media surrounding the adherent cells in 96 well format. This measurement provides a readout in terms of oxygen consumption rate (OCR). To evaluate the OCR, we seeded cells at the density of 2×10^4 cells/well in the XF96 cell culture plate (Seahorse Bioscience, Billerica, MA, USA) in CMEM overnight. At the same time, the sensor cartridge (Seahorse Bioscience, Billerica, MA, USA) was incubated with Seahorse calibrant buffer pH 7.4 (Seahorse Bioscience, Billerica, MA, USA) overnight at 37 °C, in free CO_2 condition. On the day of the experiment, the culture media was replaced with 180 µl of Seahorse DMEM free glucose (Seahorse Bioscience, Billerica, MA, USA), which was adjusted at pH 7.4. This media was supplemented with 2 mM L-glutamine and 1 g/L glucose. Cells with Seahorse media were equilibrated in a non-CO_2 incubator for 1 hr before OCR analysis. The OCR real-time reading was obtained every 6 min (1 min mixing and 5 min measurement) for five loops under basal condition, and after each injection of mitochondria inhibitors 1 µM oligomycin (O), 1 µM FCCP (F), and 1 µM antimycin-A with 1 µM rotenone (A+R)). These inhibitors specifically modulate the mitochondrial function to be quantified. Each inhibitor prevents a specific stage during ETC. For example, oligomycin inhibits ATP synthase by blocking the proton channel (FO subunit), which is necessary for energy production through the phosphorylation of ADP to ATP. FCCP is a potent uncoupler of mitochondrial membrane by transporting protons across the mitochondrial inner membrane and disrupted ATP synthases. To stop the electron transfer

in the mitochondria membrane, rotenone is used to inhibit complex I, and antimycin A to inhibit complex III.

4.5.2. Glycolysis

The XFe96 extracellular flux analyzer also allows measuring the extracellular flux changes of protons as extracellular acidification rate (ECAR). Fibroblasts were cultured as previously described. CMEM was replaced with 180 µL of Seahorse DMEM free glucose media, pH 7.4, and supplemented with 2 mM L-glutamine. ECAR was measured every 9 min (1 min mixing, 5 min measure, and 3 min wait) for five loops in basal condition, and after the injections of 10 mM glucose (G), 1 µM oligomycin (O), and 50 mM 2-deoxy-D-glucose (2DG). 2-DG inhibits glycolysis through competitive binding to glucose hexokinase (the first enzyme in the glycolytic pathway).

The data obtained from each well of OCR or ECAR analysis were normalized to the protein account of cells in the same well. Therefore, cells were lysed by 1 M NaOH, and protein concentrations were measured by Bradford assay. Data were analyzed by Wave 2.3 software (Agilent Technologies, Santa Clara, CA, USA).

4.6. Cell cycle analysis of juvenile HD fibroblasts

Fibroblasts were seeded at cell number 10^5 per well of 6 well plates in CMEM media. On the next day, the cell cycle was analyzed based on the general protocol from Abcam (www.abcam.com) with small changes. Briefly, the cells were harvested and fixed with 70% ethanol for 30 min on the ice. Fixed cells were collected by centrifugation at 2000 rpm for 5 min at 4 °C, then, the cells were washed two times with ice-cold 1X PBS. To exclude the potential background from RNA, we treat the fixed cells with 100 µg/ml of RNAse for 30 min at room temperature (RT). We stained the DNA with 10 µg/ml propidium iodide (PI), followed by analysis with FACS Aria III flow cytometer (BD Biosciences, Franklin Lakes, NJ, USA) at Ex/Em maxima of 493/636 nm. The data were analyzed by FlowJo v10 software (FlowJo LLC, Ashland, OR, USA).

4.7. Cell death analysis of juvenile HD fibroblasts

Cell death was identified based on FITC Annexin V and PI apoptosis detection kit I (BD Pharmingen™, Franklin Lakes, NJ, USA). Where the cells are positively stained with FITC Annexin V only that means the cells are in the early apoptosis. While FITC Annexin V and PI are positively stained the cells that mean the cells are in the late stage of apoptosis or necrosis. In our experiment, approximately 10^5 cells from each sample were stained by FITC Annexin

V/PI kite according to the manufacturer's protocol. Briefly, fibroblasts were collected by trypsinization, washed twice by 1X PBS. Then, cells were stained with PI using 2.5 µl and FITC Annexin V using 2.5 µl in a total volume of 50 µl of 1X binding buffer (0.01 M HEPES/NaOH, pH 7.4, 0.14 M NaCl, 2,5 mM $CaCl_2$). The cells with dye were incubated for 15 min in dark at RT. Data were obtained by FACS Aria III flow cytometer and analyzed by FlowJo v10.

4.8. Mitochondria staining and immunocytochemistry

The coverslips were coated with gelatin before culturing the cells. The coverslips were incubated with 1% w/v gelatin in 1X PBS for 4 hr at 37 °C in a normal cell culture incubator. Then, the coverslips were washed with 1X PBS. Then, the cells were cultured in a suitable cell culture medium.

4.8.1. Mitochondria staining

For mitochondria staining, living cells were incubated in serum-free media containing 50 nM MTR for 20 min at 37 °C and 5% CO_2 condition. MTR has diffused through the plasma membrane and stained the mitochondria with red-fluorescent dye. Cells were washed and then proceed with the immunostaining if require double staining with mitochondrial proteins.

4.8.2. Immunocytochemistry

Cells were fixed by 4% paraformaldehyde (PFA) for 15 min at RT. The fixed cells were carefully washed two times by 1X PBS. The cells were permeabilized with 0.1% v/v Triton X-100 for 35 min at RT. Then, the cells were blocked with 3% bovine serum albumin (BSA) in 1X PBS for 60 min. The primary antibody, which is listed in **Table 6,** was diluted in blocking buffer and incubated for 90 min at RT. Cells were washed three times with 1X PBS. After that, the cells were incubated for 90 min with the secondary antibody (**Table 6),** and 1 µg/ml DAPI (Life Technologies, Carlsbad, CA, USA) in (1% BSA, 1X PBS). The cells were washed three times with 1X PBS contains 0.01% v/v Triton X-100. The coverslips were mounted on microscope slides using a mounting medium (Dabco 33-LV, Mowiol 4-88, 1:50), followed by image acquisition using confocal microscopy.

Table 6. A list of primary and secondary antibodies was used for immunocytochemistry.

Primary antibody	Source	Host	Dilution
Drp1	BD Biosciences, CA, USA	Mouse	1:1000
Anti-HA-tag	Cell Signaling Technology, Leiden, The Netherlands	Rabbit	1:1000
Anti-HA-tag	Cell Signaling Technology, Leiden, The Netherlands	Mouse	1:500
PA200	Novus Biologicals, Littleton, CO, USA	Rabbit	1:1000

Secondary antibody	Source	Host	Dilution
Alexa fluor 594	Thermo Fisher Scientific, Waltham, MA, USA	Mouse Rabbit	1:1000
Alexa fluor 488	Thermo Fisher Scientific, Waltham, MA, USA	Mouse Rabbit	1:1000

Confocal images were obtained using the Leica TCS SP8 confocal microscope (Leica Microsystems, Wetzlar, Germany), HC PL APO CS2 63x/1.40 OIL immersion objective was applied for image acquisition. The images were processed by LAS-X small v3.7.1 (Leica Microsystems, Wetzlar, Germany).

In case to quantify aggregates size and number that formed in the cells upon mutant N terminal huntingtin expression. We analyzed approximately 1000 cells that contain aggregates only. This quantification was performed based on analysis of confocal images by ImageJ software (imagej.nih.gov).

4.9. Quantification of the mitochondrial populations in juvenile HD fibroblasts

Cells were seeded in ultra-microplate 96-carrier cells at a density of 2,000 cells per well. On the next day, the cells were incubated with 50 nM of MTR and 10 µM of Hoechst in serum-free MEM for 30 min in normal cell culture conditions. After that, the cells were rinsed, and then covered with 100 µl FluoroBrite DMEM phenol-red-free (Thermo Fisher, Waltham, MA, USA) supplemented with 2 mM L-glutamine and 1% FBS for live-cell imaging. The confocal mode of Opera Phenix high content screening (HCS) (Perkin Elmer, Waltham, MA, USA) was used to quantify mitochondrial species. Z stacked images with 1 µm distance between 4 stacks were taken by 40× water objective (Na 1.1). Channels for Hoechst and Mitotracker orange were used. First, the nuclei were detected with the Hoechst channel, then the mitochondria with the construction block (Find Spots) were analyzed. The readout parameters were spots/nuclei and the average spot length.

4.10. Cell size estimation in juvenile HD fibroblasts

The cell size of fibroblasts was estimated by Opera Phenix high content screening (Perkin Elmer, Waltham, MA, USA). 1000 cells/well were cultured for 48 hr with CMEM in cell carrier-96 ultra microplates (Perkin Elmer, Waltham, MA, USA). The cells were washed with 1X PBS, fixed with 4% PFA for 15 min, permeabilized with 0.1% Triton X-100 for 15 min at RT, and the cells were incubated with blocking buffer (1% BSA in 1X PBS) for 30 min at RT to avoid the non-specific staining. Then, the cells were incubated with 2 U/ml Texas Red™-X Phalloidin (Thermo Fisher, Waltham, MA, USA) and 1 µg/ml DAPI in blocking buffer for 1 hr in dark at RT. The X Phalloidin selectively labeled F-actin and DAPI stained the nucleus. After that, the cells were washed and covered with 100 µl of 1X PBS for image acquisition. The objective 10× air (Na 0.3) was applied in non-confocal mode using the Alexa 568 (561/570-630) and DAPI (405/435-480) channels. Images were analyzed with Harmony software (Perkin Elmer, Waltham, MA, USA). Images were segmented according to the channels of DAPI and Alexa 568 to detect the nucleus and cytoplasm, respectively of the cell. The cell area was calculated after removing the border touching objects.

4.11. Differential interference contrast imaging

The imaging by differential interference contrast (DIC) microscopy was accomplished by Olympus BX61 microscope (Olympus Corporation, Tokyo, Japan). These images were obtained by a cooled CCD camera (Sensicam QE, MI, USA) using IP lab 4.0 software (BD Biosciences, Franklin Lakes, CA, USA).

4.12. Total RNA isolation and cDNA synthesis

Total RNA was isolated by the TRIzol reagent (Molecular Research Centre, Cincinnati, OH, USA) based on the manufacturer's instructions. The quality and quantity of RNA were estimated by the NanoDrop spectrophotometer (NanoDrop Technologies, Wilmington, DE, USA). Complementary DNA (cDNA) synthesis was accomplished by PCR (Applied Biosystems, Foster City, CA, USA) from a template of 1 µg total RNA. cDNA was performed based on reverse transcription kit instructions (Applied Biosystems, Foster City, CA, USA).

4.13. Real-time quantitative PCR for gene expression analysis

The gene expression is based on mRNA level, which was analyzed from cDNA by real-time quantitative polymerase chain reaction (RT-qPCR) (Roche, Basel, Switzerland). In our experiments, cDNA was diluted 50 times with NFW, and the appropriate volume of diluted cDNA was mixed with a specific primer of the target gene, and together with a 2X SYBR Green

master mix (IAB, Strašnice, Czech Republic). The primers used in our study are summarized in **Table 7.** While, the qPCR cycling conditions were applied to obtain cycle threshold (Ct) as follows: Phase 1/pre-incubation (95 °C 10 min, 1 cycle), phase 2/amplification (95 °C; 15 sec, 60 °C; 30 sec, for 40 cycles), phase 3/melt curve analysis (95 °C; 0.05 sec, 65 °C; 1 min, 97 °C; 0 sec, 1 cycle), and phase 4/cooling (40 °C; 30 sec, 1 cycle). Relative quantification of gene expression was compared between different samples based on the ΔΔCt approach. The data output was determined as fold change of gene expression, which calculated based following formula: Relative gene expression = $2^{-\Delta\Delta Ct}$

ΔΔ Ct = [(Ct gene of interest - Ct internal control) control cells] - [(Ct gene of interest - Ct internal control) target cells].

Table 7. Primers' list was used for RT-qPCR analysis in this study, *to determine the gene expression of the target gene.*

Gene name	Forward primer (5'-3')	Reverse primer (5'-3')
FIS1	AGCTGGTGTCTGTGGAGGAC	ACGATGCCTTTACGGATGTC
MFN1	CGGAACTTGATCGAATAGCC	AGAGCTCTTCCCACTGCTTG
MFN2	ATGCATCCCCACTTAAGCAC	AGCACCTCACTGATGCCTCT
DNM1L	AGATCTCATCCCGCTGGTC	CAGATCCTCGAGGCAAGAAG
MIEF2	GCAGAGTTCTCCCAGAAACG	GTCTGCCTTGGTGTCATCCT
MIEF1	GCAAAGGCAAGAAGGATGAC	CTTCATGTCCCTGTTCAGCA
OPA1	CACTTCCTGGGTCATTCCTG	TGCTTCGTGAAACCAGATGT
MFF	AAACGCTGACCTGGAACAAG	TTTTCAGTGCCAGGGGTTTA
PRKN	CAGCAGTATGGTGCAGAGGA	TCCTGAGGCTTCAAATACGG
PMSE4	ATGGAGAGTGCCTGAACTATTG	GTAGGTCAGCACACTTCCTATTC
GAPDH	GAGTCAACGGATTTGGTCGT	GATCTCGCTCCTGGAAGATG

4.14. SDS-PAGE and immunoblot

To prepare the samples for SDS-PAGE, cells were rinsed by 1X PBS and then lysed on the ice using lysis buffer RIPA (50 mM Tris-HCl, 150 mM NaCl, 0.5% Na-deoxycholate, 2 mM EDTA, 1% NP-40, and 50 mM NaF), supplemented with several protease inhibitors (1 mM PMSF, 1 mM benzamidine, and 1X EDTA-free protease inhibitor cocktail (Roche, Basel, Switzerland)). The homogenized cells were completely lysed by sonication (1 sec, with frequency 20 kHz, 3 times with 10-sec breaks). The cell lysates were cleared by centrifugation (13000 rpm, 10 min at 4 C°). The protein concentration of the upper layer was determined by Bradford assay (Bio-Rad Laboratories, CA, USA) based on the manufacturer's protocol. Each sample with 20 µg protein amount was mixed with sample buffer (60 mM Tris-Cl pH 6.8, 2% SDS, 10% glycerol, 0.01% bromophenol blue, and freshly added 140 mM DTT). Then the

protein sample was boiled for 5 min at 95 °C. After that, the proteins were separated by SDS-PAGE. The separated proteins were transferred onto a 0.45 µm nitrocellulose membrane (GE Healthcare Life Sciences, Marlborough, MA, USA). The blot was probed with primary and secondary antibodies, these antibodies are listed in **Table 8.** The signals of bands were augmented using a chemiluminescent substrate (Santa Cruz Biotechnology, Dallas, TX, USA). This signal was captured by ChemiDoc Imager (Bio-Rad Laboratories, Hercules, CA, USA). The densitometry of the signals was analyzed by Image Lab software 6.0.1 (Bio-Rad Laboratories, Hercules, CA, USA).

Table 8. The list of primary and secondary antibodies used in this study.

Primary antibody	Source	Host	Dilution
Drp1	BD Biosciences, NJ, USA	Mouse	1:1000
Mfn1	Abnova, Taipei, Taiwan	Mouse	1:1000
Mfn2	Sigma Aldrich, MO, USA	Mouse	1:800
Opa1	Novus Biologicals, CO, USA	Rabbit	1:1000
MFF	Proteintech, IL, USA	Rabbit	1:1000
Proteasome 20S β1 (human) subunit	Enzo Biochem, NY, USA	Mouse	1:1000
Proteasome 20S (Yeast) core subunits	Enzo Biochem, NY, USA	Rabbit	1:1000
Ubiquitin	Covance, NJ, USA	Mouse	1:800
p62	Novus Biologicals, CO, USA	Rabbit	1:3000
LC3I, LC3II	Novus Biologicals, CO, USA	Rabbit	1:1000
Parkin	Invitrogen, MA, USA	Rabbit	1:1000
Anti-HA-tag	Cell Signaling Technology, Danvers, MA, USA	Rabbit	1:1000
Anti-HA-tag	Cell Signaling Technology, Danvers, MA, USA	Mouse	1:1000
PSME4/PA200	Novus Biologicals, Littleton, CO, USA	Rabbit	1:2000
Anti-GFP	Clontech, Mountain View, CA, USA	Rabbit	1:1000
Anti-GST-tag	Upstate Biotechnology, Lake Placid, NY, USA	Mouse	1:1000
β1 subunit of Proteasome 20S (human)	Enzo Biochem, Farmingdale, NY, USA	Mouse	1:1000
Proteasome 20S (Yeast) core subunits	Enzo Biochem, Farmingdale, NY, USA	Rabbit	1:1000
Actin	Santa Cruz Biotechnology, Dallas, TX, USA	Goat	1:10000

Secondary antibody	Source	Host	Dilution
Anti-mouse IgG antibody, HRP conjugate	Sigma	Goat	1:3000
Anti-rabbit IgG antibody, HRP conjugate	Sigma	Goat	1:3000
Anti-goat IgG antibody, HRP conjugate	Sigma	Rabbit	1:3000
Anti-rabbit IgG IRDye 800 CW	LI-COR, NE, USA	Monkey	1:10000
Anti-mouse IgG IRDye 680RD	LI-COR, NE, USA	Goat	1:5000

4.15. Cycloheximide chase analysis of protein degradation in fibroblast model

To analysis the half-life of a specific protein, we performed the cycloheximide (CHX) chase assay. The cells were cultured in two groups of 6 well plates with cells number 2×10^5 per well. On the following day, the first group of the cells was treated with 10 μM of MG132 the proteasomal inhibitor for one hour before CHX treatment. However, both cell groups were exposed to 300 μg/ml of CHX for the particular time points. Cycloheximide is an inhibitor for protein synthesis by inhibiting translational elongation in treated cells. Then, the cells were collected immediately at specific time points 0, 1, 2, 4, 6, and 18 hr after inhibiting the protein synthesis. The collected cells were lysate, and the changes of protein levels were analyzed by typical SDS-PAGE and Western blot. The primary and secondary antibodies were used in this assay, are listed in **Table 8.**

4.16. Bacterial expression of recombinant N-Htt, protein purification, and GST Pull-down assay

For *in vitro* studies, *Escherichia coli (E. coli)* BL21 (DE3) bacteria were transformed with pGEX-4T-2 contains either GST-N-Htt18Q encoding pGEX-5' construct or mutant GST-N-Htt51Q encoding pGEX-5' construct. Protein expression was induced by 1 mM isopropyl-β-D-1-thiogalactopyranoside (IPTG), which triggers transcription of the lac operon, and is used to induce protein expression. DE3 bacteria grew for 3 hr with shaking 180 rpm at RT. Then, the bacteria were collected by centrifugation, followed by cell lysis by sonication in an appropriate volume of lysis buffer (50 mM Tris–HCl; pH 7.5, 0.1% Tween 20, 0.2% 2-mercaptoethanol supplemented with protease inhibitors). Proteins with GST-tag were isolated using affinity chromatography on glutathione Sepharose 4B (GE Healthcare Life Sciences, Chicago, IL, USA) in accordance with the instructions provided by the manufacturer.

For pull-down assay, SH-SY5Y neuroblastoma cell line was grown in a 100 mm dish. Then it was washed with ice-cold 1X PBS and lysed in 600 μl of lysis buffer. The SH-SY5Y lysate was incubated with GST, GST-N-Htt18Q, and GST-N-Htt51Q fragments coupled to glutathione Sepharose beads for 16 hr at 4 °C with gentle rotation. After that, the beads were washed with 1X TBST three times. The GST tagged proteins were eluted by direct boil the beads with 2X SDS sample buffer. The eluted proteins were tested for the PA200 and β1 subunit of the 20S-CP proteasome **(Table 8)** by a typical Western blot.

4.17. Filter retardation analysis for detecting and quantifying polyglutamine aggregates in an HD yeast model

The filter retardation method was used to detect and quantify mutant N-Htt aggregates. In this method, SDS insoluble protein aggregates can be retained in a cellulose acetate membrane after filtration. Therefore, the retained protein aggregates are recognized by antibodies and assign for quantification. In our study, the samples were prepared as reported by Ocampo and Barrientos [255] with slight modifications. Briefly, wild-type strain (WT), and *BLM10* deleted strain (*blm10Δ*) strains, which are carrying either pYES2-25Q-CFP or pYES2-103Q-CFP as listed in **Table 5** used in our study. The strains were incubated overnight in synthetic complete media, this media contains 2% v/v raffinose with low amino acids for cell selection that harboring the plasmid. To trigger the expression of N-Htt fragments containing specific polyQ length, the media was completed with 2% v/v galactose, and cells were harvested at different time points (10, 14, and 18 hr) of induction. Then, the cells were collected by centrifugation at 1,500 g for 10 min and washed with 1.2 M sorbitol. The cell wall of the yeast strains was removed by incubating the cells with an appropriate volume of cell wall digestion buffer (20 mM K_3PO_4, pH 7.4, 1.2 M sorbitol, and 0.6 mg/ml zymolase-100T) at 30 °C for 0.5-1 hr with mild shaking. After approximately 80% of yeast was converted into spheroplasts, the yeast strain was diluted by wash buffer (20 mM KPO_4 pH 7.5, 1.2 M sorbitol), collected by centrifugation at 5,500 g for 10 min, and washed two more times with the wash buffer. The spheroplasts were lysed by lysis buffer (40 mM HEPES, pH 7.5, 1% v/v Triton X-100, 50 mM KCl, 2 mM DTT, 5 mM EDTA, and protease inhibitor 1 mM PMSF). The lysates were kept on the ice for 1 hr. The upper layer was transferred into a new tube as total lysate (T), and the remaining were fractionated by centrifugation at 2,000 g for 10 min into supernatant (S) and pellet (P). The pellet was washed with lysis buffer and resuspended with distilled water for further analysis. The SDS insoluble aggregates were determined based on the described method by Alberti et al., [256] with slight modification. Briefly, protein amounts 10 µg of (T, S, P), besides, 2 µg, 5 µg, 7 µg of the pellet were diluted with TBS buffer contains 0.1% SDS. Then, the samples were loaded onto 0.2 µm cellulose acetate membrane (Whatman GmbH, Maidstone, UK), filtered through Whatman Vacuum Minifold I apparatus (Whatman GmbH, Maidstone, UK). The wells were washed twice with TBS, the membrane removed from the apparatus. The membrane followed by typical immunoblot steps. The anti-GFP and secondary antibodies were used, are listed in **Table 8**. The signals were determined by ImageQuant LAS4000 mini system (GE Healthcare Life Sciences, Chicago, IL, USA).

4.18. Gradient gel analysis of soluble and insoluble fractions of toxic N-Htt in an HD yeast model

The samples were prepared like a filter retardation assay sample preparation. The T, S, and P with 10 µg protein amount were loaded onto a NuPAGE 3-8% Tris-Acetate gel (Thermo Fisher, Waltham, MA, USA). The upper part of the gel containing insoluble fractions and the bottom part of the gel containing soluble fractions of the sample. The separated fractions were transferred onto a nitrocellulose membrane. The transferred fractions on the blot were detected by anti-GFP as primary antibody **Table 8**, followed by typical immunoblotting analysis. The signals were determined by ImageQuant LAS4000 mini system (GE Healthcare Life Sciences, Chicago, IL, USA).

4.19. Filter trap analysis for detecting and quantifying toxic N-Htt aggregates formed in human cells

shPA200 cells and their respective control were transiently transfected with plasmids pHM6-Q23 and pHM6-Q74 for 48 hr. Cells were raised with 1X PBS and lysed on the ice with lysis buffer (40 mM HEPES, pH 7.5, 1% v/v Triton X-100, 50 mM KCl, 2 mM DTT, 5 mM EDTA, and protease inhibitor cocktail). Each lysate was fractionated into supernatant (S) and pellet (P) by centrifugation (16,000 rpm for 20 min, at 4 °C). To avoid DNA and RNA interfering the analysis, the pellet was suspended with 75 µl DNA digestion buffer (40 mM Tris-HCl, pH 8.0, 10 mM NaCl, 6 mM $MgCl_2$, 10 mM $CaCl_2$) supplemented with 100 µg/ml RNase, 30 U DNase I (Zymo, Irvine, CA, USA), and incubated for 1 hr at 37 °C. The reaction was stopped with 2X termination buffer (4% SDS, 100 mM DTT, 40 mM EDTA,). Samples with a protein amount of 10 µg were resuspended with 200 µl buffer for filter trap contains TBS (50 mM Tris-Cl, pH 7.5, 150 mM NaCl) and, 2% SDS. The samples were then loaded onto 0.2 µm nitrocellulose membrane (Bio-Rad Laboratories, Hercules, CA, USA) using Minifold I-96 well dot-blot system (GE Healthcare Life Sciences, Chicago, IL, USA). The dotes were washed two times with (TBS, 0.1% SDS). The membrane was incubated with shaking for 1 hr at RT with Odyssey blocking buffer (LI-COR, Lincoln, NE, USA). Specific antibodies for PA200 and HA-tag **(Table 8)** were diluted by Odyssey blocking buffer contains 0.1% Tween and shaken overnight in the cooled room. The membrane was washed with (TBS, 0.05% Tween), and then probed with secondary antibody **(Table 8)** in Odyssey blocking buffer also contains 0.1% Tween for 1.5 hr at RT. The secondary antibody used in this assay conjugates with infrared fluorescent dyes (IRDye® 800 CW, IRDye® 680 RD). The dotes blots were visualized by the LI-COR

Odyssey imaging system (LI-COR, Lincoln, NE, USA). The signals were quantified by Image studio v 5.2 (LI-COR, Lincoln, NE, USA).

4.20. Purification of proteasomal complexes

The proteasomes 20S-CP, Blm10-CP, and 26S were purified as previously described [219, 257]. The core particles were purified from the yMS476 yeast strain **(Table 5)**. The yeast yMS476 was grown in medium containing a 2% glucose to reach OD_{600nm} = 4-5. The proteasomal complexes Blm10-CP and 26S were purified from the yMS122 yeast strain **(Table 5)**. First, the yMS122 was grown in a 2% glucose to reach OD_{600nm} = 2. The cells then were switched to a medium containing 2% galactose for 8 hr to reach cell density OD_{600nm} = 4-5. Then, the cells were collected by centrifugation. The cells pellet was lysed by cryogenic disruption with a Retsch MM301 grinder mill in one pellet volume using the buffer (50 mM Tris, pH 8.0, 5 mM MgCl, 50 mM NaCl, and 1 mM DTT) in order to purify core particles. Where, the same buffer, but supplemented with (1X ATP-regenerating mix (ARS), and 10% glycerol, 5mM ATP) was used in order to purify the 26S proteasomes. The thawed cell lysate was cleared by centrifugation at 13,000 rpm for 30 min. The cleared supernatant was batch-incubated with IgG affinity gel (Cappel) for 1.5 hr at 4 °C. The beads were collected and washed with the buffer consist of (50 mM Tris, pH 7.5, 5 mM MgCl, 100 mM NaCl, and 0.5 mM DTT). Proteasomal complexes were eluted after using TEV protease (Invitrogen, Carlsbad, CA, USA), and then concentrated in a Vivaspin 6 Centrifugal Concentrator of 100 kDa proteins (GE Healthcare, Chicago, IL, USA). The concentrated proteasomal complexes were loaded into a Superose 6 10/300 GL column. The same protocol was followed to purify the Blm10-CP proteasomal complexes. Where the doubly capped complexes come out first when a size-exclusion column is used during the proteasome's purification. The samples were separated by SDS-PAGE, followed by Coomassie blue staining to assess the complex composition and purity of the sample.

4.21. Proteasomal activity assays

The proteasomal activity assays were assessed based on the hydrolysis of fluorogenic substrate by chymotrypsin-like proteases activities of the proteasomes. The fluorogenic Suc-LLVY-AMC substrates were obtained from (Enzo Life Sciences, Farmingdale, NY, USA). We investigated the proteasomal activity in the total cell lysates of fibroblasts and the purified proteasomes *in vitro*.

4.21.1. In total cell lysates

Fibroblasts were used in this assay. Healthy and HD fibroblasts were seeded with cell density 2×10^6 in a T150 flask. On the next day, one flask of each cell type was treated with 10 μM of MG132 for 1 hr before the experiment to use it as a negative control. Then, the cells were collected and lysed on ice with lysis buffer (20 mM HEPES, 320 mM sucrose, 5 mM $MgCl_2$, 1 mM ATP, 0.2% NP-40, 2 mM EDTA, and protease inhibitor cocktail). Cell lysates were cleared by centrifugation for 10 min at 16,000× g and 4 °C. The protein amount of 50 μg from cleared supernatant was mixed with loading buffer (50 mM Tris-HCl, pH 7.4, 12 ng/ml xylene cyanol, 5 mM $MgCl_2$, 6% glycerol). The samples were loaded into 3-8% Tris-acetate native gel (Thermo Fisher, Waltham, MA, USA). Electrophoresis was performed by running buffer (90 mM Tris, 90 mM boric acid, pH 8.3, 5 mM $MgCl_2$, 0.5-mM ATP, 0.5 mM EDTA) applying voltage 60 V for 12 hr. The gel with separated proteasomes was incubated with 20 ml of reaction buffer (50 mM Tris-HCl, pH 7.4, 1 mM ATP, 5 mM $MgCl_2$, 100 μM Suc-LLVY-AMC in DMF, and 0.02% SDS) for 30 min at 30 °C in dark. Fluorescent bands were analyzed using ChemiDoc imager, and band densitometry was quantified by Image Lab software 6.0.1 (Bio-Rad Laboratories, Hercules, CA, USA). The proteasomal activity was normalized to 1 μg protein in each sample. In this experiment, all buffers were filtered sterilized with a 0.2 μm filter, and all steps were performed at 4 °C unless stated otherwise. In parallel, to confirm the equal quantity of core particles loaded for proteasomal activity assay, equal protein 50 μg amounts were loaded into typical SDS-PAGE and performed Western blot. We determined the β1 subunit as representative of 20S-CP. The primary and secondary antibodies are listed in **Table 8**.

4.21.2. Purified proteasomes *in vitro*

To assess the activity of purified proteasomes, an in-gel activity assay was performed based on fluorogenic substrate Suc-LLVY-AMC as previously published [223, 258] and as we discussed before. Briefly, equal molar amounts of purified 20S-CP and Blm10-CP complexes were separated on a 3.5% polyacrylamide native gel, followed by an in-gel activity assay. Subsequently, the same samples were analyzed by SDS-PAGE, followed by Coomassie blue staining to confirm the equal core particles are present for this assay. The images were taken by the Kodak gel logic 100 Imaging System.

4.22. *In vitro* degradation assay of soluble N-Htt fragments

The soluble fragments that were used for the *in vitro* degradation assay are the purified GST-Htt18Q and GST-Htt51Q. Each fragment with concentration 40 nM was incubated with 12 nM of selected proteasome in reaction buffer (50 mM Tris pH7.5, 2.5 mM MgCl2, 25 mM NaCl,

1mM DTT, 0.5mM EDTA). The interactions were performed in a final volume of 15 µL at 30 °C for indicated time points. The reactions were terminated at each time point by addition 4X loading buffer followed by boiling for 3 min. Then the samples were tested by typical SDS-PAGE and followed by Western blotting. The degradation products were determined by anti-GST primary antibody (**Table 8).** The proteasomes in the reactions were determined by the anti-CP primary antibody (**Table 8).** The protein signals were visualized using ImageQuant LAS 4000 (GE Healthcare Life Sciences, Chicago, IL, USA). The strength of the protein bands was quantified using ImageQuant software.

4.23. Peptidomics analysis of the degradation of N-Htt fragments *in vitro*

The purified GST-Htt18Q and GST-Htt51Q were degraded into short peptides by 20S-CP or Blm10-CP proteasomal complexes *in vitro*. The peptides were cleaned up by using a stage-tip microcolumn [259]. The cleaned peptides were resuspended with 0.1% formic acid (Merk, Darmstadt, Germany) in distilled water (dH_2O). The samples were measured by a Q-Exactive mass spectrometer (MS) system (Thermo-Fisher, Waltham, MA, USA), which is coupled to a Proxeon nano-liquid chromatography (LC) system (Thermo-Fisher, Waltham, MA, USA) in data-dependent acquisition mode. Where the top 10 peaks were selected for higher-energy collisional dissociation (HCD) fragmentation. Each sample with 5 µl was injected and applied for 3 hr gradient solvent A (0.1% formic acid, 5% acetonitrile), and solvent B (0.1% formic acid, 80% acetonitrile). We used an in-house prepared nano-LC column (0.075 mm × 250 mm, 3 µm Reprosil C_{18}), this column was obtained from Maisch GmbH, Germany. The samples were eluted 3 hr with gradients of 4-76% acetonitrile and 0.1% formic acid in dH_2O at flow rates of 0.25 µl/min. The acquisition of MS was carried out at a resolution of 70,000 m/z in the scan range from 300 to 1700 m/z. Dynamic exclusion was set at the 30s and normalized collision energy at 26eV. The mass window for precursor ion selection was adjusted to 2.0 m/z. Data were analyzed using the MaxQuant software. The internal Andromeda search engine was used to search MS/MS spectra against the *S. cerevisiae* proteome database and the recombinant huntingtin protein sequences of N-Htt fragments that forward and reverse sequences. The search included the variable modification of methionine oxidation and fixed modification of carbamidomethyl cysteine. The smallest peptide length for analysis was adjusted to seven amino acids without any selection for the digestion pattern. The false discovery rate (FDR) was set to 0.01 for peptide identification. The data was further analyzed using the R program (www.r-project.org) and the tidyverse assessment package [260].

4.24. Statistical data analysis

The data were obtained from each experiment, are presented as mean value ± standard deviation (SD) of equal or more than three independent experiments ($n \geq 3$). Statistical analysis was performed by ANOVA test followed by Tukey test for multiple comparisons, or to compare the parameters of three cell lines. While Student t-test was used to compare the values of two cell types. All analyses were performed by Graphpad Prism 8.2.1 software. Statistical significances were determined as * indicates $p < 0.05$, ** indicates $p < 0.01$, *** indicates $p < 0.001$, and **** indicates $p < 0.0001$.

5. Results

5.1. Increased ROS production and ΔΨm indicate changes in mitochondrial function of juvenile HD fibroblasts

Many studies have been demonstrated that HD is associated with increased production of ROS. Increased ROS leads to cell death in the striatum and the cerebral cortex of the HD patient's brain [261-264]. To date, the cellular dysfunction in HD peripheral tissues has not been completely clarified. Therefore, we determined ROS production in juvenile HD fibroblasts (68Q and 86Q) using carboxy-H_2DCFDA dye. Interestingly, we found a significant increase of cytosolic ROS in HD fibroblast- containing 86Q compared to healthy control (16Q), which indicates oxidative stress in the juvenile HD model **(Figure 9A)**.

The intracellular ROS production is mainly generated from mitochondria dysfunction in HD neuron cells [115]. Consequently, we measured ΔΨm by two methods. First, we stained the mitochondria with MTR, and second, we stained the mitochondria with TMRE. Mitotracker CXMRos is a sensitive indicator for ΔΨm changes and oxidative stress, while tetramethylrhodamine ethyl ester is an indicator for the polarization of the mitochondrial membrane. In the case of TMRE, we used a negative control to confirm the specificity of TMRE. Our negative control was generated by treating cells with uncoupler 20 µM FCCP to depolarize the mitochondrial membrane **(Figure 9C)**. FCCP disrupts ATP synthesis by transporting protons across the mitochondrial inner membrane, which leads to a loss of mitochondrial membrane potential, and eliminates TMRE staining. In both MTR and TMRE staining assays, we detected a significant increase in ΔΨm of HD fibroblasts containing- 68Q and 86Q compared to healthy control containing-16Q **(Figure 9B, C)**.

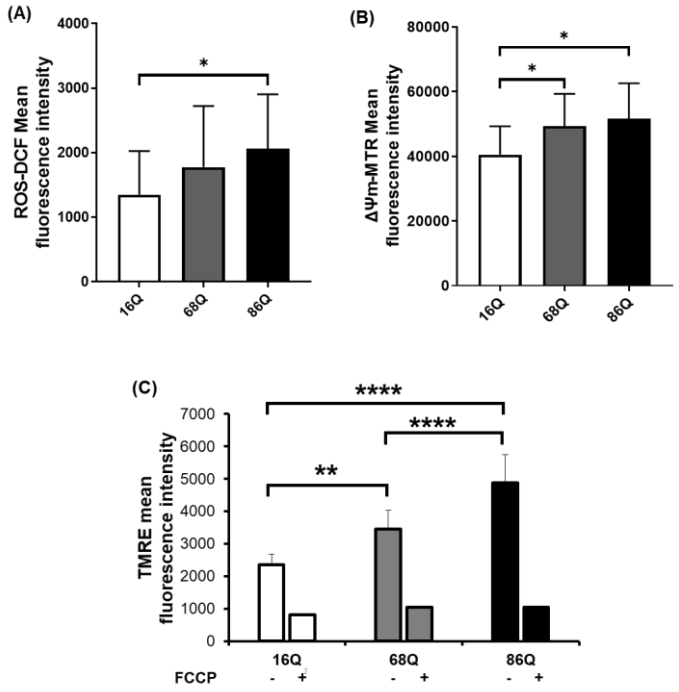

Figure 9. Elevated ROS production and ΔΨm in juvenile HD fibroblasts. *(**A**) Compared ROS levels between juvenile HD fibroblasts 68Q, 86Q, and 16Q. Cells were stained using 1 µM of Carboxy-H_2DCFDA for 30 min. Results are shown as mean ± SD of n = 5. (**B**) ΔΨm was indicated by staining the mitochondria with 50 nM of MTR, data are presented as mean ± SD for n = 4. (**C**) The second method to assess ΔΨm is by using 100 nM TMRE. For negative control, cells were treated with 20 µM FCCP for 10 min before staining. Results are shown as mean values ± SD of n = 4. These experiments were obtained by FACS, and the data were analyzed using FlowJo. Statistical analysis was carried out by ANOVA test using GraphPad Prism 8.2.1 (* indicates p < 0.05; ** indicates p < 0.01, **** indicates p < 0.0001).*

5.2. Juvenile HD fibroblasts show maintained mitochondrial ATP production, suppressed glycolysis, and disturbed cell cycle

It was previously reported that adult-onset HD fibroblasts tend to show slower cell proliferation compared to healthy counterparts. This observation is caused by disturbances in the OXPHOS machinery in HD cells [67]. We studied the OXPHOS in juvenile HD fibroblasts, and we analyzed mitochondria respiration by Seahorse XF. In our study, we normalized the mitochondrial respiration measurements data to the protein amount in each well. Our data revealed that HD fibroblasts exhibited slightly reduced ATP generation, basal, and maximal mitochondrial respiration **(Figure 10A, B)**.

Glycolysis is another energy source in the cells. To determine glycolysis in HD cells, we measured the extracellular acidification rate by Seahorse XF [265]. We detected a significant

decrease of glycolysis in HD fibroblasts containing-68Q compared to healthy control containing-16Q. While this decrease was not significant in 86Q cells **(Figure 10C, D)**. In summary, these data suggest that mitochondrial OXPHOS is maintained, while glycolysis is suppressed in juvenile HD fibroblasts.

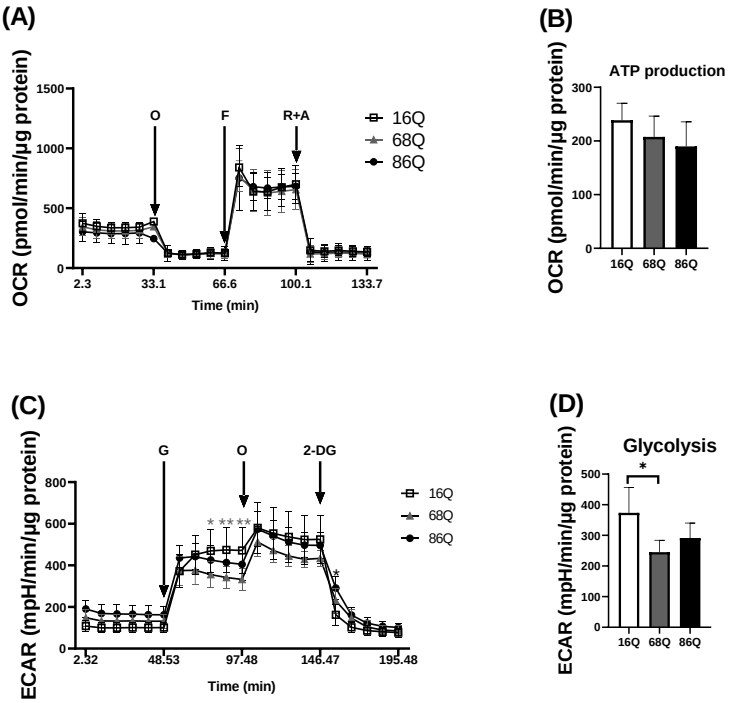

Figure 10. Juvenile HD fibroblasts show maintained ATP production and reduced glycolytic activity. *The bioenergetic profile of mitochondria respiration and glycolysis was analyzed by Seahorse XF96. (**A**, **B**) Juvenile HD fibroblasts with different polyQ lengths 68Q and 86Q, where healthy control containing-16Q were seeded in an XF96 microplate at 20,000 cells/well. In the following day, the basal respiration was examined for 30 min before the injection of 1 µM Oligomycin (O); 1 µM FCCP (F), and 1 µM Rotenone (R) with 1 µM Antimycin A (A). (**A**) Mitochondrial respiration was measured based on OCR in 68Q, 86Q and 16Q. (**B**) ATP production is generated from OXPHOS. Data are presented as mean ± SD for n = 3. Mitochondria respiration was normalized to protein amount (µg protein). (**C**, **D**) Glycolysis was determined by measuring the extracellular acidification rate in fibroblasts. The basal ECAR was determined for 30 min in the glucose-free medium before the injection of 10 mM glucose (G), 1 µM oligomycin (O), and 50 mM 2-deoxy-D-glucose (2-DG). (**C**) Glycolysis profile of juvenile HD and healthy fibroblasts. (**D**) The measurement of glycolysis is based on the ECAR after the addition of saturating amounts of glucose. Data are presented as mean ± SD for n = 4. Data were normalized to protein amount (µg protein) in each well of Seahorse 96 well plate. OCR and ECAR data were analyzed using Wave Desktop software. Statistical analysis was carried out by ANOVA test using GraphPad Prism 8.2.1 software, compared to healthy control (* p < 0.05, ** p < 0.01).*

Increased generation of intracellular ROS, suppressed glycolysis lead to reduce cell viability in neurodegenerative diseases [266]. Therefore, we analyzed the cell death/viability in HD fibroblasts by flow cytometry analysis. The analyzed data showed that juvenile HD fibroblasts are viable and both apoptosis and necrosis are relatively low like healthy control **(Figure 11A).** During our daily care of fibroblasts, we observed low cell proliferation in 86Q compared to 16Q cells. Therefore, we analyzed the cell cycle to determine whether the cell cycle disturbance is a possible reason for decreased cell proliferation in juvenile HD fibroblasts. We assessed the percentage of cells in G0/G1, S, and G2/M phases. Data showed that the percentage of HD cells in S and G2/M phases are significantly lower compared to healthy cells, while the percentage of 68Q and 86Q cells in the G0/G1 phase is significantly higher compared to 16Q. These data indicate that HD cells are accumulated in G0/G1 before proceeding to the S phase, which might lead to reduced mitosis in juvenile HD fibroblasts compared to heathy fibroblasts **(Figure 11B).** During daily monitoring of fibroblasts HD model, we observed also that HD fibroblasts containing-86Q are larger than healthy cells containing-16Q. Therefore, we analyzed the cell area by high content screening confocal microscopy, where the cells F-actin was stained by Texas Red staining. Data analysis showed that the average cell size of 68Q and 86Q juvenile HD fibroblasts are significantly larger compared to 16Q healthy cells **(Figure 11C, D).** We suggest that increased cell area might be related to the cell cycle disturbance in juvenile HD fibroblasts.

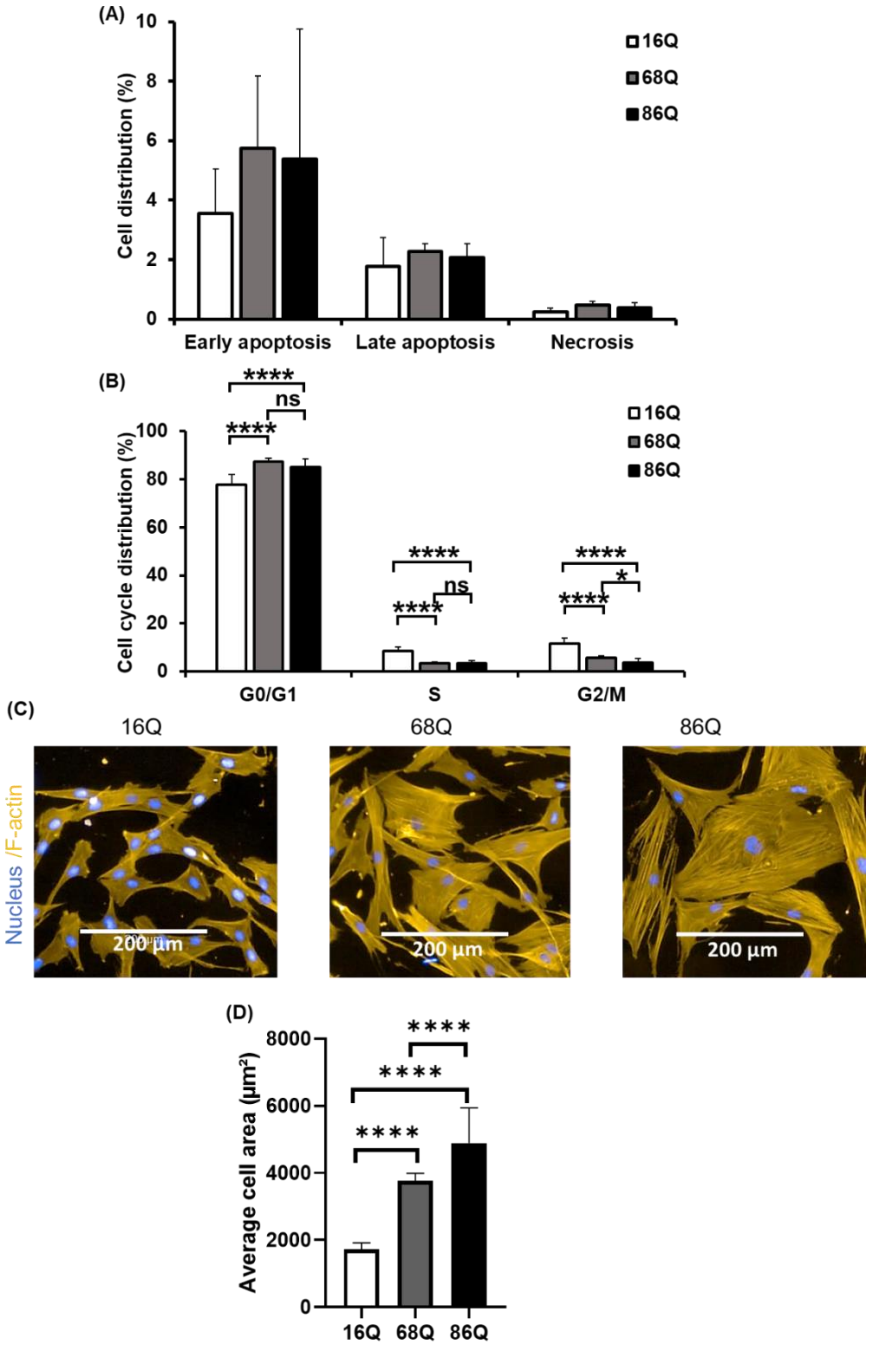

Figure 11. Juvenile HD fibroblasts are viable, with decreased mitotic rate, and increased cell size. *(**A**) Cell viability was determined by FACS analysis using double staining of Annexin-V-FITC and propidium-iodide staining. The results are presented as the mean ± SD of n = 3. (**B**) Cell cycle distributions were measured by FACS after staining with 10 µg/ml of PI. (**C, D**) The cell area was determined by staining the juvenile fibroblasts with Texas-Red Phalloidin for F-actin, and DAPI was used to stain the nuclei of the cells. Cell area quantification was performed by high content screening analysis using the Opera Phenix HCS. Data are shown as mean ± SD of n = 5. The Statistical analysis was calculated by ANOVA test using GraphPad Prism 8.2.1 software. (ns indicates not significant, * indicates p < 0.05; **** indicates p < 0.0001).*

5.3. Juvenile HD fibroblasts demonstrate alterations in mitochondrial fission-fusion protein levels

Mitochondria function is regulated by the fission-fusion machinery. The increase of ΔΨm might be associated with the disturbed mitochondrial fission-fusion process [267-270]. We performed qPCR analysis to investigate the gene expression of several mitochondrial fission and fusion genes. We determined fission genes such as *DNM1L* (Drp1), *FIS1* (Fis1), *MIEF1* (Mid51), *MIEF2* (Mid49), and *MFF* (Mff). The fusion genes were *MFN1* (Mfn1), *MFN2* (Mfn2), and *OPA1* (Opa 1). We found that the gene expression of *DNM1L* for mitochondrial fission protein Drp1 was significantly decreased in 86Q cells compared to 16Q cells **(Figure 12A)**. The gene expressions of mitochondria fusion proteins did not change significantly in HD cells compared to healthy control cells.

We also evaluated the protein levels for a number of mitochondrial fission-fusion proteins by Western blot and by confocal microscopy for Drp1. Our results revealed that the Drp1 protein level is decreased in HD fibroblasts containing-68Q and 86Q with a significant decrease in 86Q compared to healthy control 16Q **(Figure 12B, C)**. The decrease in the Drp1 protein level is compatible with the decrease of *DNM1L* gene expression in HD fibroblasts. Mff did not change significantly in both gene and protein levels in both 68Q and 86Q compared to 16Q **(Figure 12D)**. The protein levels of mitochondrial fusion proteins such as Opa1 and Mfn1 were significantly decreased in juvenile HD fibroblasts, but the protein level of Mfn2 did not show a significant decrease in diseased cells compared to healthy control **(Figure 12E–G)**. Our data suggest that the alteration in fission-fusion proteins could lead to changes in mitochondrial morphology.

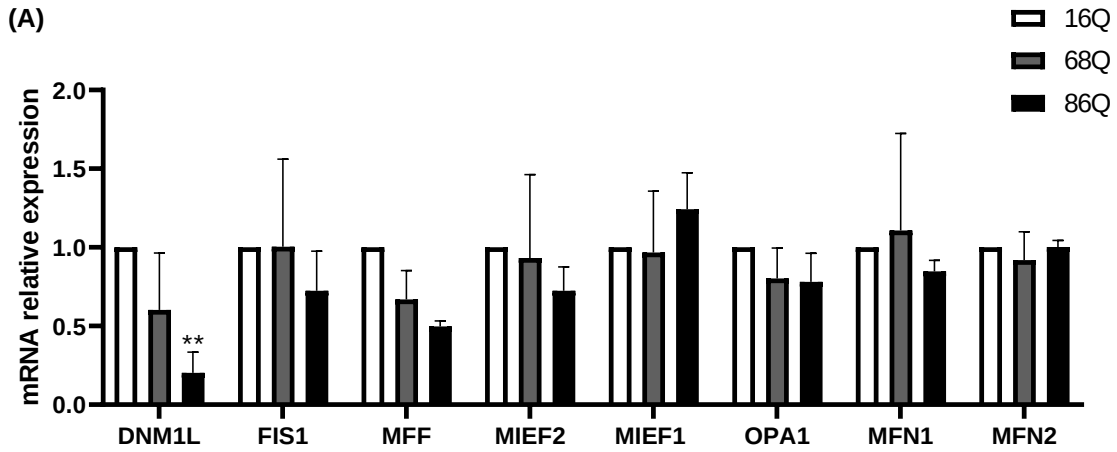

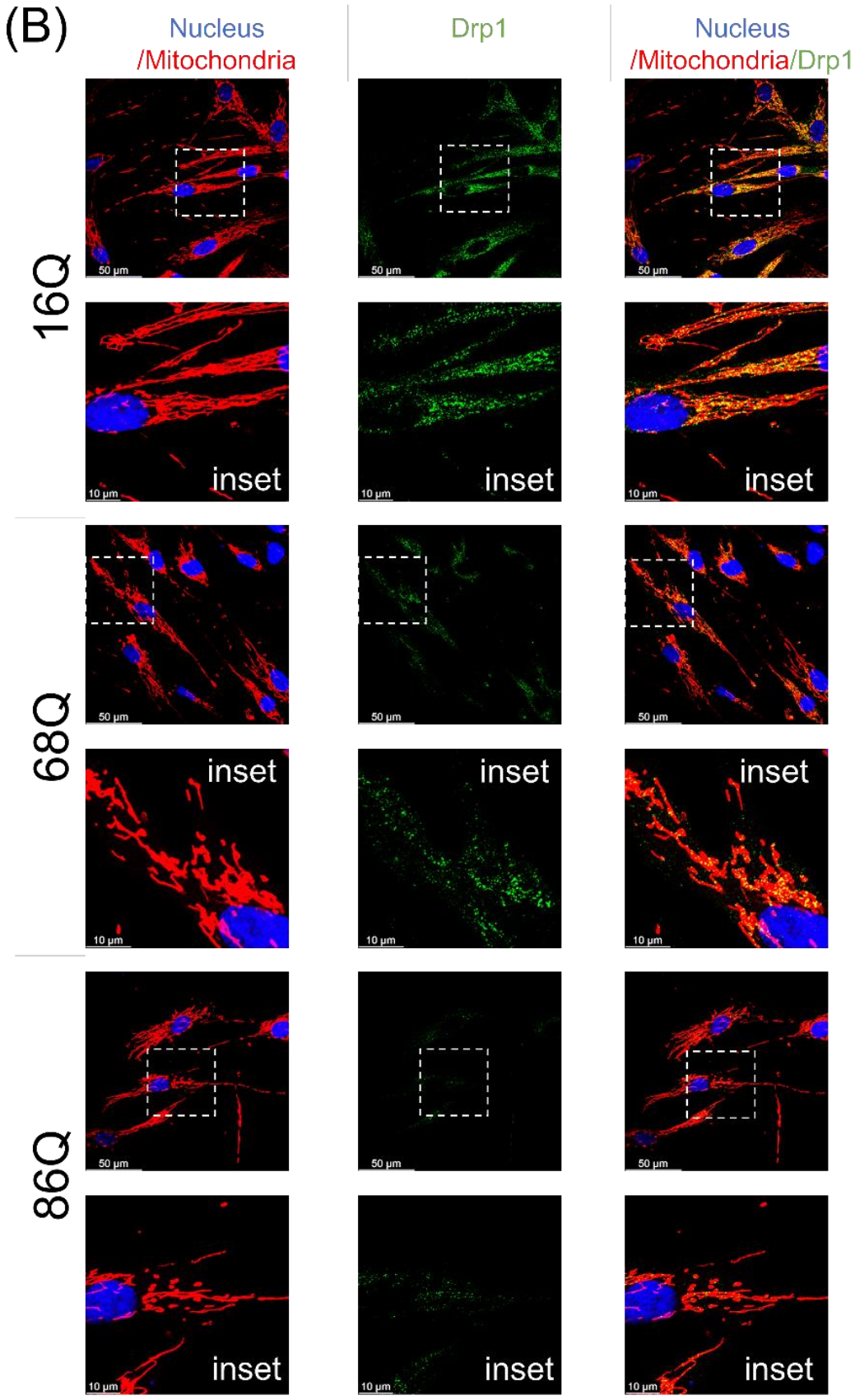
(B)
Nucleus /Mitochondria
Drp1
Nucleus /Mitochondria/Drp1
16Q
68Q
86Q
50 μm
10 μm
inset

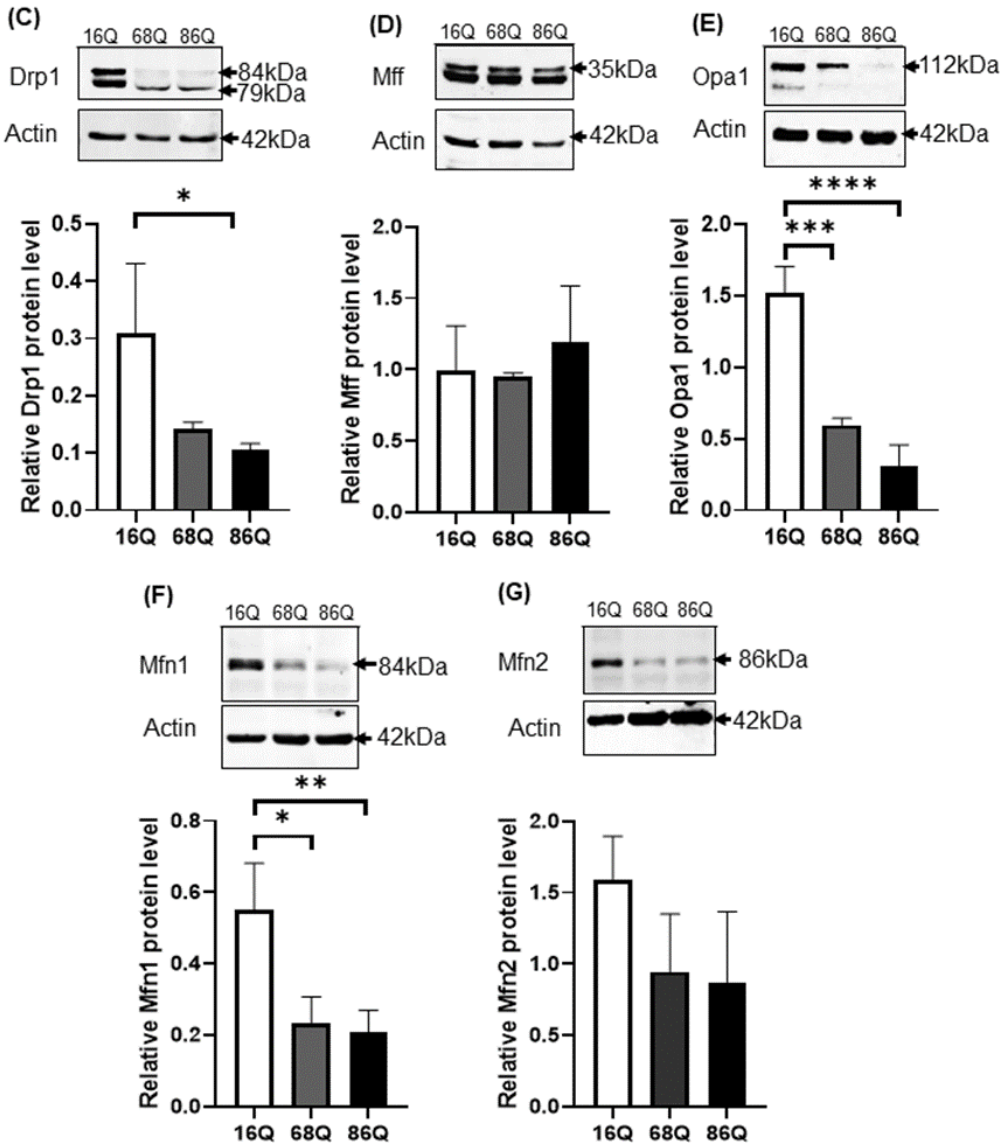

Figure 12. Alterations the profile of gene expressions and protein levels of the mitochondrial fission-fusion machinery in juvenile HD fibroblasts. (A) *The mRNA levels of mitochondrial fission-fusion genes were determined by qPCR. The mRNA levels of 68Q, and 86Q containing cells were normalized to the 16Q containing cells. Data are shown as mean ± SD of n = 3.* ***(B)*** *Representative confocal microscopy images show Drp1 protein levels of mitochondrial based on fluorescence in healthy and HD fibroblasts. The mitochondria were stained by 50 nM MTR, Drp1 protein was detected with an anti-Drp1 antibody/Alexa Fluor 488, and nuclei were stained by DAPI. (**C-G**). Mitochondrial fission-fusion protein levels profile was determined by SDS-PAGE and Western blot. The total cell lysates amount with 20 µg were loaded into SDS-PAGE and transferred onto nitrocellulose membrane for Immunoblot. Band's intensity was normalized to actin internal loading control. Data are presented as mean ± SD of n = 3. Statistical analysis was carried out by ANOVA test using GraphPad Prism 8.2.1 software, significance compared to healthy control 16Q are (* indicates p < 0.05; ** indicates p < 0.01, *** indicates p < 0.001 **** p indicates < 0.0001).*

Therefore, we studied mitochondrial morphology by HCS **(Figure 13A)**. The live-cell confocal images were analyzed based on a quantitative evaluation of mitochondrial morphology. We found a significant decrease of mitochondrial branching in both juvenile HD fibroblasts 68Q and 86Q compared to the healthy control 16Q, which was determined by an increased mitochondria fragmentation score **(Figure 13B).** Simultaneously, we also found that mitochondrial length was significantly shorter in 68Q and 86Q-containing HD cells compared to the 16Q-containing control cells **(Figure 13C),** which is suggesting mitochondrial fragmentation in juvenile HD fibroblasts.

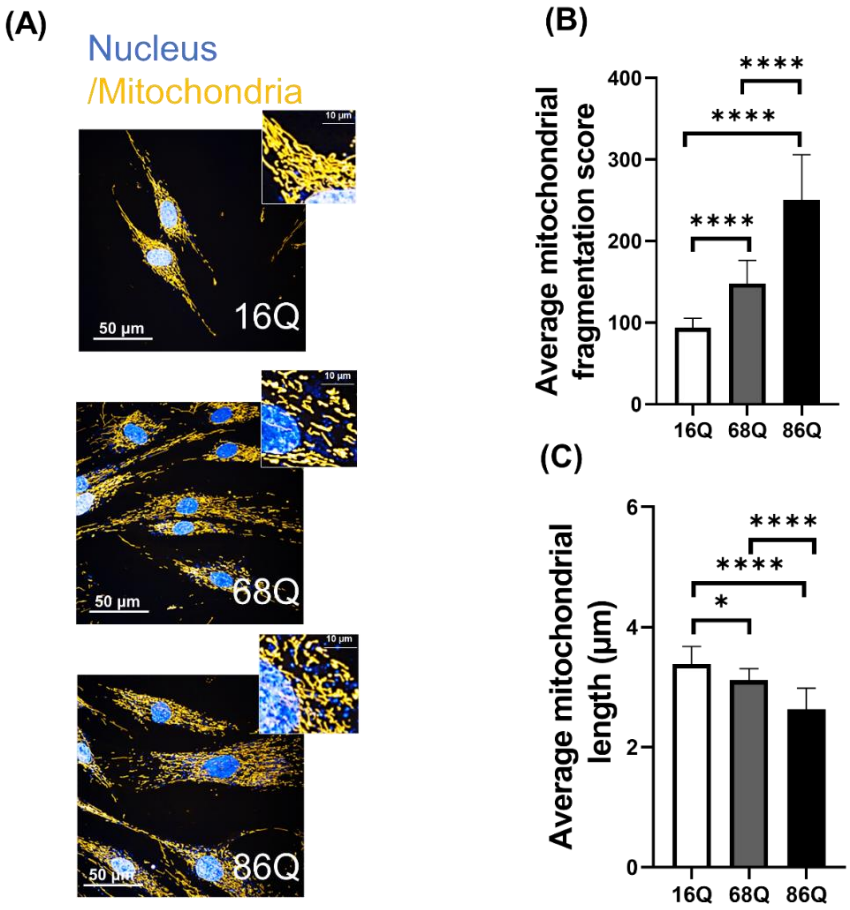

Figure 13. Mitochondrial branching and length are decreased in HD fibroblasts. *(**A**) Representative images from HCS confocal microscopy show the mitochondrial morphology in juvenile healthy and HD fibroblasts. The cells were stained by 50 nM MTR. The images were analyzed by Harmony software. We performed our analysis using 2000 cells per condition. (**B**) Quantification of mitochondrial population and (**C**) measurement and comparison of mitochondrial length in healthy and HD fibroblasts. Data are shown as mean ± SD of n = 5. Statistical analysis was carried out by ANOVA test using GraphPad Prism 8.2.1 software. (* indicates $p < 0.05$; ** indicates $p < 0.01$, *** indicates $p < 0.001$ **** indicates $p < 0.0001$).*

5.4. Increased the proteasomal activity accompanied by a normal rate of autophagy in juvenile HD fibroblasts

The deficit of the UPS has been well-studied in neuronal HD cell models [92, 177, 253]. But our knowledge about the activity of the UPS and its implication in HD pathogenesis of peripheral tissues is still limited. We hypothesized that juvenile HD fibroblasts counterbalance the mitochondrial morphology changes with altered proteasomal activity to promote cell survival. We studied the relative distribution of the proteasomal complexes using total cell lysates by in-gel activity assay. We performed this assay in two groups of cells. In the first group, the cells were treated with the proteasomal inhibitor MG132 (Carbobenzoxy-Leu-Leu-leucinal). MG132 is a peptide aldehyde, which potently blocks the proteolytic activity of the 20S-CP proteasome [271]. In the second group, the cells grew without treatment. Then, we loaded the cell lysates into the native gel to fractionate the proteasomes based on their molecular weights, followed by an in-gel activity assay. In this experiment, the 20S-CP, PA700-20S, and PA700-20S-PA700 are fractioned in the gel as reported before [258, 272]. To visualize the activity of the core particle of these complexes, the native gel was incubated with the specific fluorogenic substrate Suc-LLVY-AMC. This substrate is hydrolyzed by the chymotrypsin-like activity of the proteasome. Both doubly PA700-20S-PA700 and singly PA700-20S capped proteasomal complexes showed increased activity in HD fibroblasts compared to healthy control **(Figure 14A upper and lower panel)**. To confirm the exact amount of core particle was loaded for each sample, we determined the protein level of the β1 subunits of 20S-CP by Western blot. We found that the β1 subunits protein levels were similar in all samples **(Figure 14B upper and lower panels)**.

The singly and doubly capped proteasomes with PA700 mediate protein degradation in an ATP and ubiquitin-dependent manner. We also determined the higher chymotryptic-like activity of the PA700-20S and PA700-20S-PA700 proteasomes in HD fibroblasts **(Figure 14A)**. To show the effects of this activity on the degradation of ubiquitinated proteins, we investigated the accumulation of ubiquitinated proteins in the total cell lysates after inhibition of the proteasomal activities by MG132. We found that the level of ubiquitinated proteins was significantly higher in 68Q- and 86Q-containing HD fibroblasts compared to 16Q-containing healthy control after MG132 treatment **(Figure 14C right and left panels)**. Our results suggested that the proteolytic activity of the proteasomal complexes was higher in juvenile HD fibroblasts compared to healthy cells.

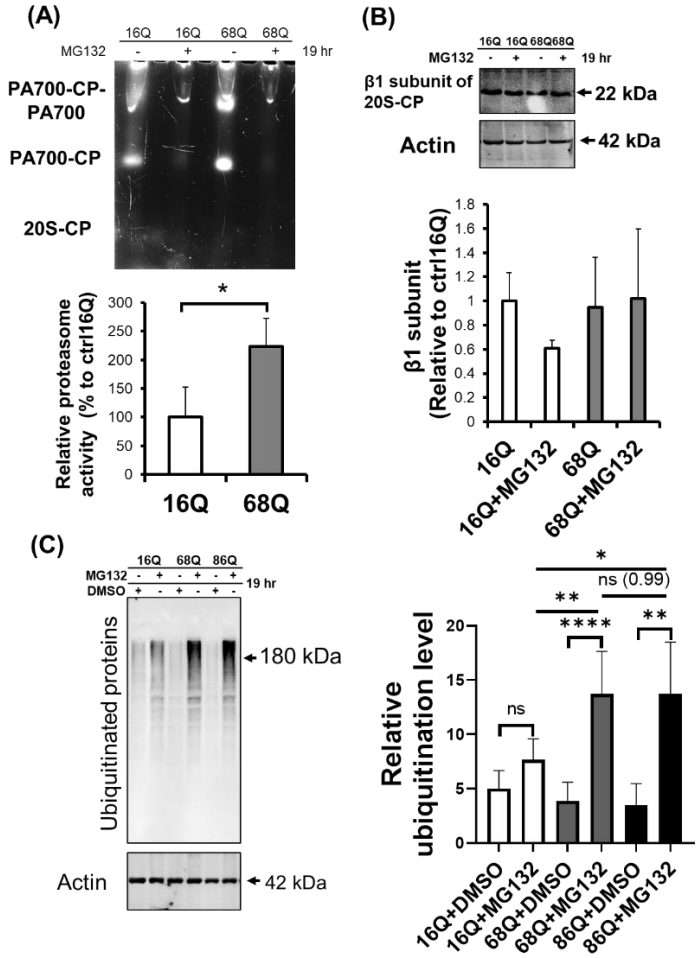

Figure 14. Proteasomal activity and its effect on ubiquitinated proteins in juvenile HD fibroblasts. *(**A**) For the in-gel proteasomal activity assay, fibroblasts were incubated in the absence and presence of a 10 µM MG132 proteasomal inhibitor. The cells were lysed in native condition, and 50 µg protein amount of each sample was loaded onto 3-8% native gel. The activities of separated proteasomes were assayed by incubating the gel with fluorogenic substrate Suc-LLVY-AMC, shows in the upper panel. The proteasomal activity of HD fibroblasts was normalized to healthy fibroblasts. Data represented as mean value ± SD of n = 3, shows in the lower panel. (**B**) Total cell lysates with 50 µg protein amount from each sample were used for SDS-PAGE and immunoblot using a specific anti-β1 subunit of the core particle, shows in the upper panel. Actin was used as an internal loading control. The protein levels of HD fibroblasts were normalized to healthy fibroblasts. Data represented as mean value ± SD from n = 3, shows in the lower panel. (**C**) Determination of the ubiquitinated proteins in the presence and absence of 10 µM of MG132 proteasomal inhibitor. The equal protein amounts of 10 µg from each sample were loaded onto SDS-PAGE, followed by a normal Western blot to assess the ubiquitinated proteins, shows in the left panel. Protein levels of HD fibroblasts were normalized to actin loading control. Data present as mean ± SD of n = 3, shows in the right panel. Data present as mean ± SD of n = 3. Statistical analysis was performed using the ANOVA test by GraphPad Prism 8.2.1. (ns indicates not significant, * indicates p < 0.05; ** indicates p < 0.01, **** indicates p < 0.0001).*

Autophagy is the other protein degradation pathway to remove dysfunctional or long-lived proteins. To determine the efficiency of autophagy in HD fibroblasts, we treated cells with bafilomycin A1 (BMA1) the autophagy inhibitor. BMA1 inhibits vacuolar H^+ ATPase in the lysosome, which leads to preventing the fusion between autophagosomes and lysosomes [273]. We found that ubiquitinated proteins are slightly increased upon autophagy inhibition in HD cell lysates compared to control cells **(Figure 15A right and left panels)**. Furthermore, we compared the protein levels of the autophagy markers such as LC3I, LC3II, and p62 in the presence and absence of the autophagy inhibitor BMA1. LC3I converts to LC3II, which requires the formation of autophagosomes [274]. We found that the ratio of LC3II/LC3I is significantly increased in HD and healthy fibroblasts after treatment with BMA1 compared to its corresponding vehicle-treated cells **(Figure 15B upper and lower panels)**. We used p62, an autophagy substrate, and marker for autophagy activity [275]. Western blot analysis of p62 showed that autophagy is active in HD fibroblasts **(Figure 15C upper and lower panels)**. The accumulation of p62 after autophagy inhibition in 68Q-containing HD fibroblasts was similar compared to the 16Q-containing healthy fibroblasts, while the accumulation of p62 in 86Q-containing HD fibroblasts following autophagy inhibition was significantly lower compared to 16Q-containing healthy control **(Figure 15C lower panel)**. Decreased p62 in 86Q cells could be a preliminary indicator of the impairment of autophagy in the later progression of the disease. Taken together, our observations reveal that juvenile HD fibroblasts show a higher capacity of 26S proteasomes but not autophagy. These findings were confirmed by increased proteasomal activity and elevated levels of ubiquitinated proteins after proteasomal inhibition.

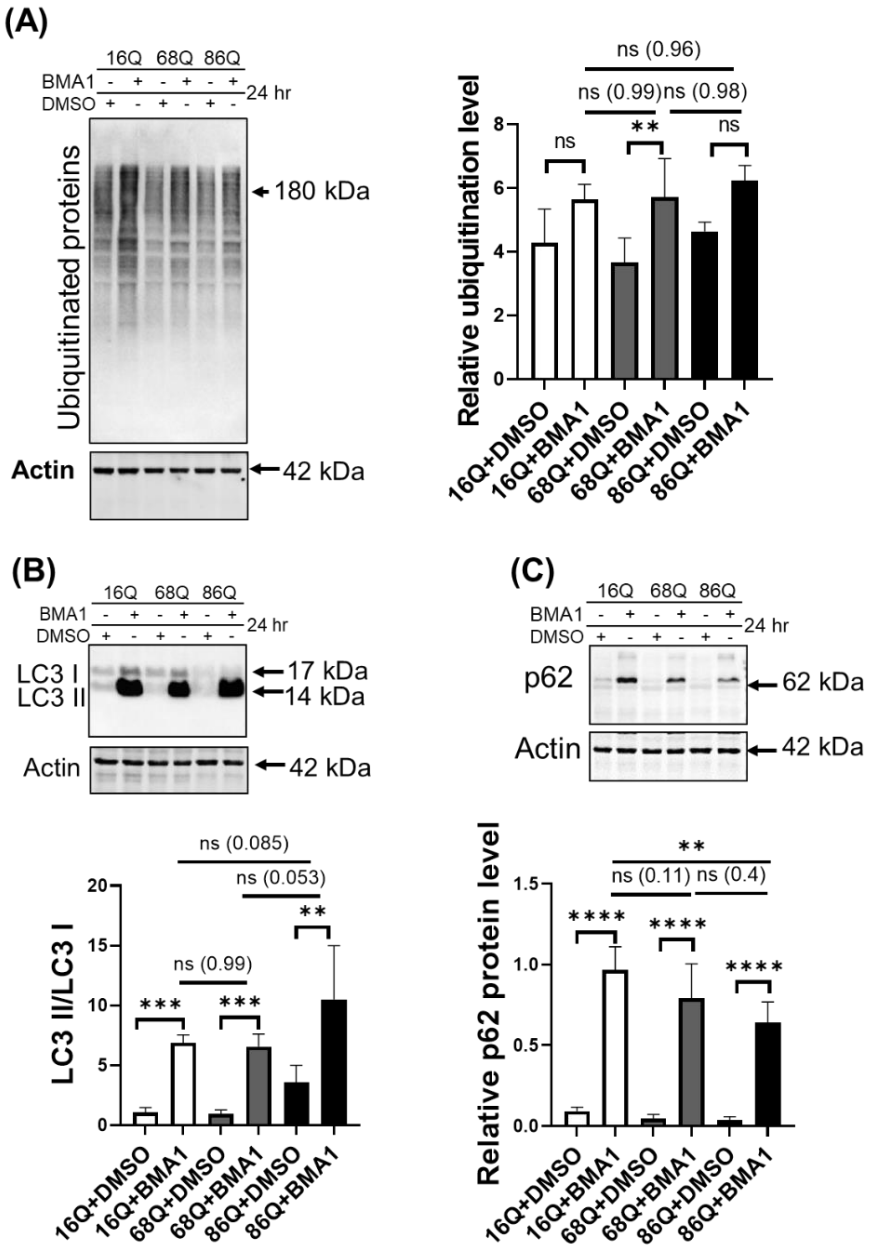

Figure 15. Proteolytic efficiency of autophagy in juvenile HD fibroblasts. *(**A**) Determination of the ubiquitinated proteins in the presence and absence of 100 nM of BMA1 the autophagy inhibitor. Equal protein amounts of 10 µg of total cell lysates were used for SDS-PAGE and then performed normal Western blot analyses to determine the proteins' ubiquitination, shows in the left panel. Protein levels were normalized to actin loading control. Data present as mean value ± SD of n = 3, shows in the right panel. (**B, C**) Determine the autophagy efficiency using autophagy markers LC3I, LC3II, and p62 in healthy and HD fibroblasts by SDS-PAGE and Western blotting in 10 µg protein amount, which shows in upper panels. Data represent as the mean value ± SD of n = 3, shows in lower panels. Statistical analysis was performed by ANOVA test using GraphPad Prism 8.2.1 software. (ns indicates not significant, ** indicates p < 0.01, *** indicates p < 0.001 **** indicates p < 0.0001).*

5.5. Accelerated turnover of Mfn1 might be associated with increased Parkin levels in juvenile HD fibroblasts

Parkin is an E3 ubiquitin ligase, this protein has multiple protective functions in the cell. Parkin is also participating in proteasomal-mediated protein degradation, mitochondrial function, and cell survival [276-278]. We hypothesized that the elevated levels of ubiquitinated proteins after proteasomal inhibition, and the preserved cell viability in juvenile HD fibroblasts, might be associated with elevated Parkin levels. We investigated the *PRKN* gene expression and Parkin protein levels in healthy and HD fibroblasts. Our results showed that mRNA levels of *PRKN* gene expression are increased in juvenile HD fibroblasts with a significant increase in 86Q-containing cells **(Figure 16A)**. Moreover, Parkin protein level increased significantly in 68Q-, and 86Q-containing cells compared to 16Q healthy cells **(Figure 16B).**

We detected a decreased level of mitochondrial fission-fusion proteins including Mfn1 in juvenile HD fibroblasts **(Figure 12)**. Mfn1 is a substrate for Parkin for ubiquitination and degradation by the 26S proteasome [279]. We performed a CHX chase assay to determine the Mfn1 half-life in healthy and HD cells. Cycloheximide inhibits the translation elongation by binding to the ribosomal E-site [280, 281]. We used 300 µg/ml of CHX to block new protein synthesis in the presence and absence of the proteasomal inhibitor MG132. Hence, the degradation of a protein by the proteasomes can be monitored in cells. We determined an increased turnover of Mfn1 protein over 18 hr in juvenile HD fibroblasts **(Figure 16C left and right panels)**. We propose that elevated Parkin level promotes the ubiquitination of proteins and together with increased 26S proteasomal activities leading to an increase in the turnover of Mfn1. This finding confirms our previous results, which was shown in **Figure 12F.** Then, we tested if these activates could explain the decreased protein levels of Drp1 and Opa1. Therefore, we performed CHX chase assay for Drp1 **(Figure 16D left panels)** and Opa1 **(Figure 16D right panels)**. We found that protein levels for both Drp1 and Opa1 did not show a difference in the presence or absence of MG132. These results suggest, that increased UPS activity in juvenile HD fibroblasts influences the degradation of Mfn1 protein but neither Drp1 nor Opa1.

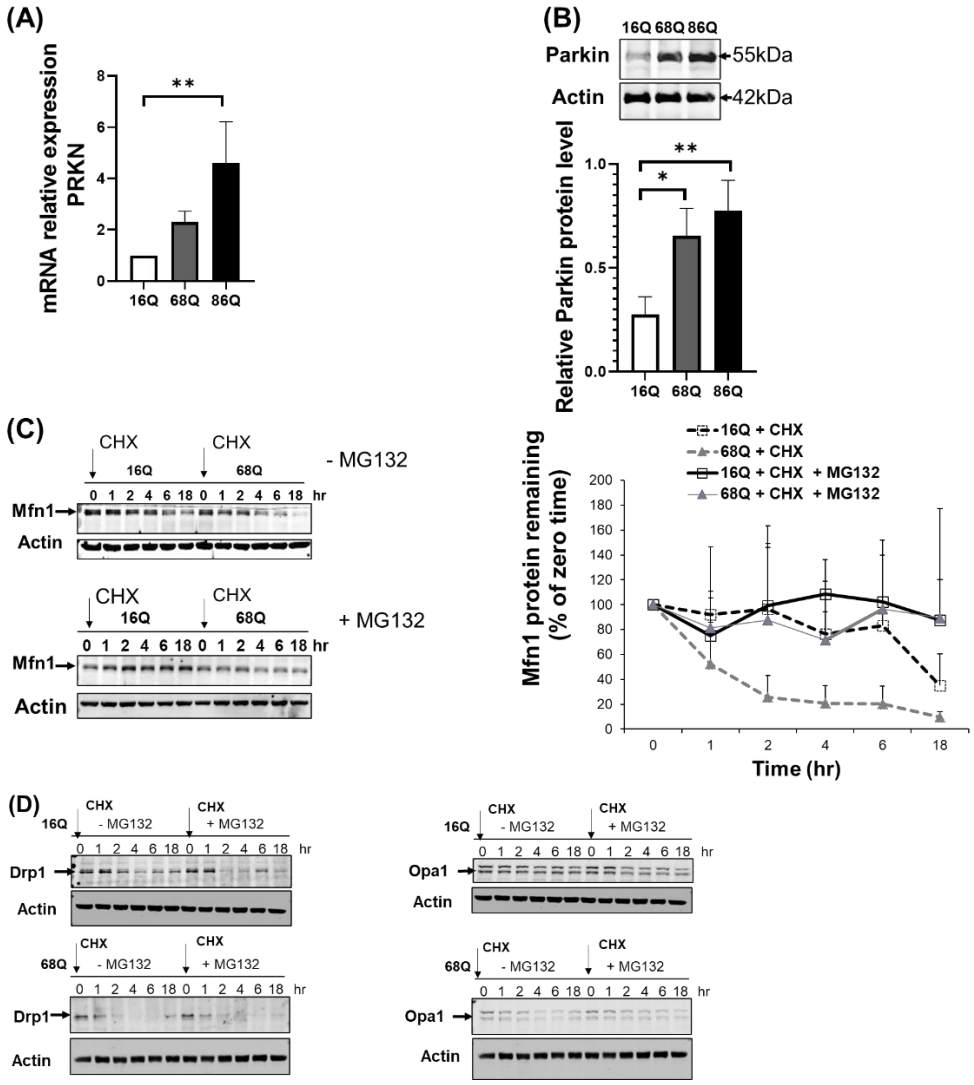

Figure 16. The elevated gene expressions and protein levels of Parkin in juvenile HD fibroblasts promote Mfn1 degradation. *(**A**) Relative mRNA expression of PRKN was determined using RT-qPCR analysis. The relative mRNA levels for PRKN of 68Q-, and 86Q-containing HD fibroblasts were normalized to 16Q-containing healthy control. Data are shown as mean ± SD of n = 3. (**B**) Parkin protein levels in 68Q, 86Q, and 16Q were determined by Western blotting. Actin was used as a loading control. Data present as mean value ± SD of n = 3. Statistical analysis was performed by ANOVA test using GraphPad Prism 8.2.1 (* indicates p < 0.05, ** indicates p < 0.01). (**C, D**) Cycloheximide chase assay. Each cell type was cultured in two flasks. The cells in the first flask were treated with 10 µM of MG132 for 1 hr before CHX treatment. The synthesis of proteins was blocked by 300 µg/ml of CHX in both flasks. At each time point indicated, the cells were collected, lysed, and then equal protein quantities of 20 µg protein amount were loaded onto SDS-PAGE followed by Western blotting. (**C**) Mfn1 Western blot (left panel), and data analysis for Mfn1 presented as mean value ± SD of n = 4 (right panel). Band's intensities were detected based on chemiluminescence detection, and different band quantifications were determined by Image Lab software. (**D**) Western blots of cycloheximide chase assay for Drp1 (left panel), and Opa1 (right panel).*

5.6. Blm10-CP complexes antagonize the toxic effects of mutant N-Htt in the yeast HD model

HD is an age-related disease. Thus, the cells that expressing mutant polyQ show severe cytotoxicity when the patient's age reaches more than 40 years old [282, 283]. In the same manner, the HD yeast model does not show immediate cell death upon expression of toxic polyQ, but the expression of toxic polyQ in yeast causes disability of cell growth. Therefore, yeast is an ideal model to study cytotoxicity in neurodegenerative diseases [77, 284, 285]. A recent study reported that knockdown of mammalian *PSME4* (PA200) or deletion of its yeast ortholog *BLM10* (Blm10) accelerates cellular aging [286]. The loss of the PA200/Blm10 family leads to a decrease in proteasomal activity during aging [287]. Both findings provide a solid idea that the PA200/Blm10 family might have a significant role in age-related diseases. We examined whether the *BLM10* deletion (*blm10Δ*) affects the viability of yeast cells expressing the mutant N terminal Htt fragments containing extended polyQ. We induced the expression of the N-Htt103Q as mutant fragments and the N-Htt25Q as wild-type fragments. Then, we determined the viability of the HD yeast model by a serial dilution assay. Hence, we found that deletion of *BLM10* causes impaired yeast growth in the presence of toxic fragments compared to wild-type yeast (WT) or *RPN4* deletion strain (*rpn4Δ*) **(Figure 17A upper right panel)**. Rpn4 protein is a transcription factor that catalyzes the transcription of various genes of proteasomal subunits [288]. Rpn4 protein is rapidly degraded by the 26S proteasome, where the Rpn4 level provides a negative feedback cycle to control the proteasome abundance in *S. cerevisiae*. We found that inducing the expression of the nontoxic fragments contains 25Q did not affect yeast viability after deletion of *BLM10* or *RPN4* genes in yeast strains **(Figure 17A lower right panel).** However, all uninduced strains were grown normally **(Figure 17A left panels).**

Next, we examined the effect of delete *BLM10* on the formation of insoluble aggregates from mutant N-Htt by filter retardation assay. The cells were induced by galactose to express the mutant N-Htt and collected at different time points of induction. We found that the accumulation of aggregates from mutant N-Htt was increased in both WT and *blm10Δ* strains during the time of induction **(Figure 17B)**. We determined the accumulation of mutant N-Htt aggregates based on chemiluminescent intensities of 10 μg protein amount of samples. We normalized the values of the total lysate (T), supernatant (S), and pellet (P) fractions to the WT counterpart. Statistical analysis showed a slight increase in the aggregates containing T and P fractions after 18 hr of galactose induction of *blm10Δ* strain compared to WT. However, these changes did not reach to significant difference **(Figure 17C)**.

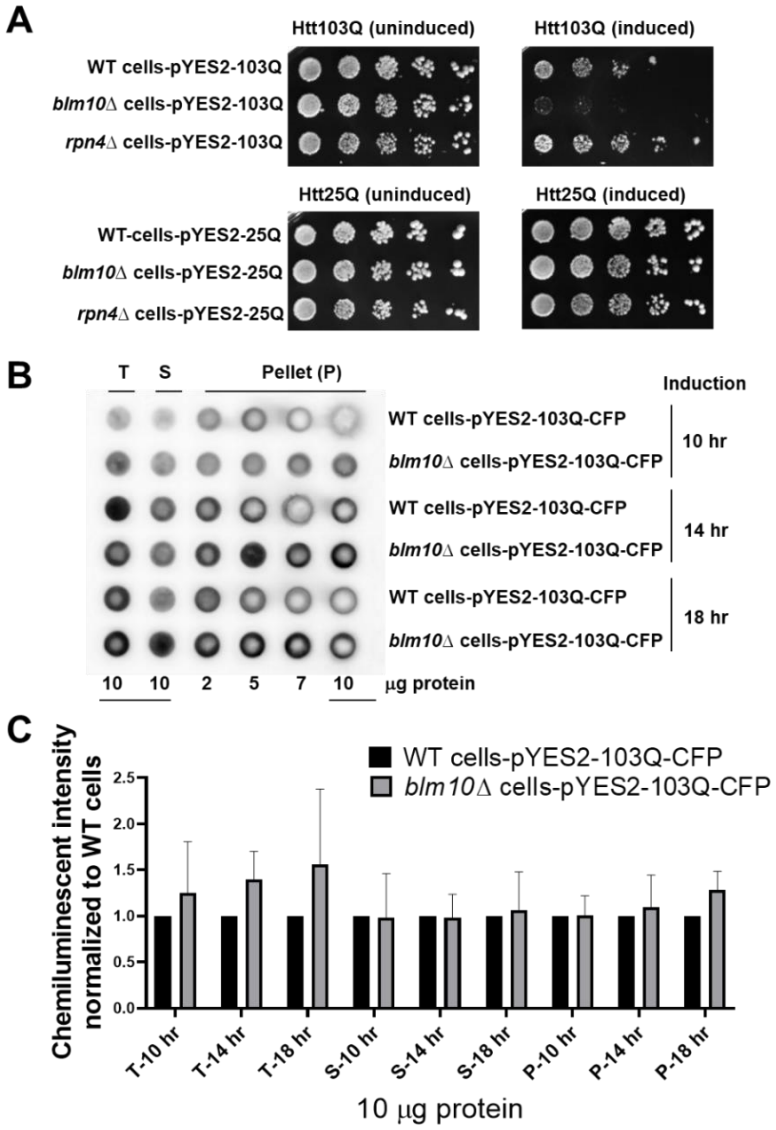

Figure 17. Cytotoxicity and aggregation of toxic N-Htt fragments in WT and blm10Δ strains. (**A**) *Mutant N-Htt fragments impair yeast growth in the blm10Δ strain. The strains WT, blm10Δ, and rpn4Δ were transformed to express the CFP-N-Htt103Q are shown in upper panels, while the strains expressing CFP-N-Htt25Q shown in lower panels. The cells were grown in galactose (termed as induced) or raffinose (termed as uninduced) containing media for 18 hr, after that the cells were spotted on the plates containing synthetic media. (**B**) Comparison of insoluble aggregates from N-Htt103Q in WT and blm10Δ cells by filter retardation assay. The cells were induced by 2% galactose for the 10, 14, and 18 hr to expressing N-Htt103Q fragments. Total lysate (T, 10 µg), supernatant (S, 10 µg), and pellet (P, 2; 5; 7; 10 µg) were loaded onto cellulose acetate membrane (0.2 µm pore size) using a vacuum Minifold I System. CFP-N-Htt103Q was determined by an anti-GFP antibody. (**C**) Dote blots analysis of SDS-insoluble aggregates were normalized to the WT counterpart samples. Dote blot intensities were quantified and analyzed using Image Studio Lite version 5.2 software. Data present as mean values ± SD of n = 4. ANOVA test by GraphPad Prism 8.2.1 was used for statistical analysis.*

To determine the insoluble and soluble fractions of mutant N-Htt in WT and *blm10Δ*, we induced the expression of N-Htt103Q for different time points. The samples (T, S, P) were loaded onto gradient gel under native conditions. The insoluble aggregates are stuck in the upper part of the gel, while the soluble fraction runs into the separating gel **(Figure 18A, B)**. These data were normalized to the values of their corresponding 10 hr of induction (The first value was obtained after galactose induction) of each strain **(Figure 18C)**. Data analysis indicated that the trend of toxic N-Htt aggregation is increased in both strains WT and *blm10Δ* over the time of induction. The formation of aggregates is more evident but not significant in *blm10Δ* cells **(Figure 18C right panel)** compared to WT **(Figure 18C left panel)**. We analyzed these data again using the main effects ANOVA (Statistica V. 13.6). This type of analysis determines the effects of multiple categorical independent variables. In our case, the categorical variables were the fractions of the cells, time, and the strains we used. We found that the formation of the aggregates in WT and *blm10Δ* strains changes significantly over time ($p < 0.001$). Due to the methodological difficulties to determine and quantify the accumulation of aggregates in our model by native gel and immunoblotting, we also wanted to find another approach for more accurate quantification. Therefore, we used live-cell fluorescent microscopy to determine the wild-type **(Figure 18D)** or toxic **(Figure 18E)** fragments expressing in yeast cells. These fragments are fused with a cyan fluorescent protein (CFP). The live-cell imaging of CFP showed that the CFP-Htt25Q is distributed equally in the cytosol in all strains **(Figure 18D)**. The deletion of *BLM10* drives a larger aggregates formation from CFP-Htt103Q in *blm10Δ* compared to WT and *rpn4Δ* strains **(Figure 18E)**. Data analysis confirmed that the number of *blm10Δ* cells with larger aggregates of toxic N-Htt is significantly higher compared to WT and *rpn4Δ* cells **(Figure 18F, G).**

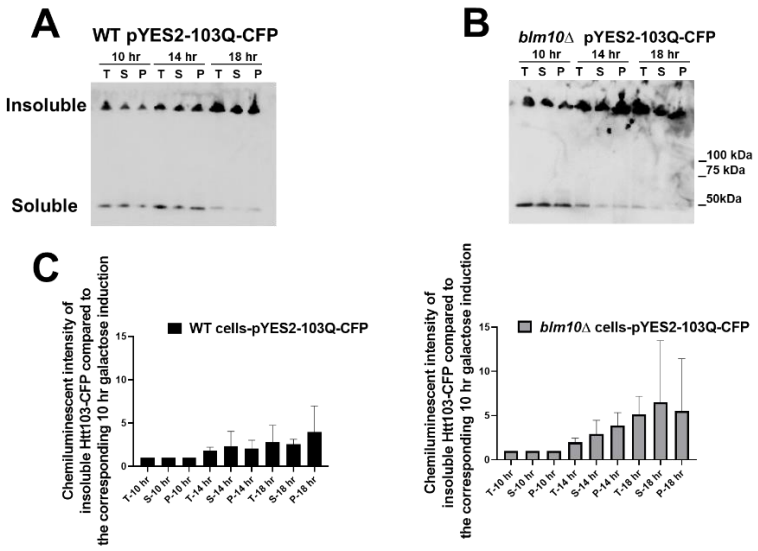

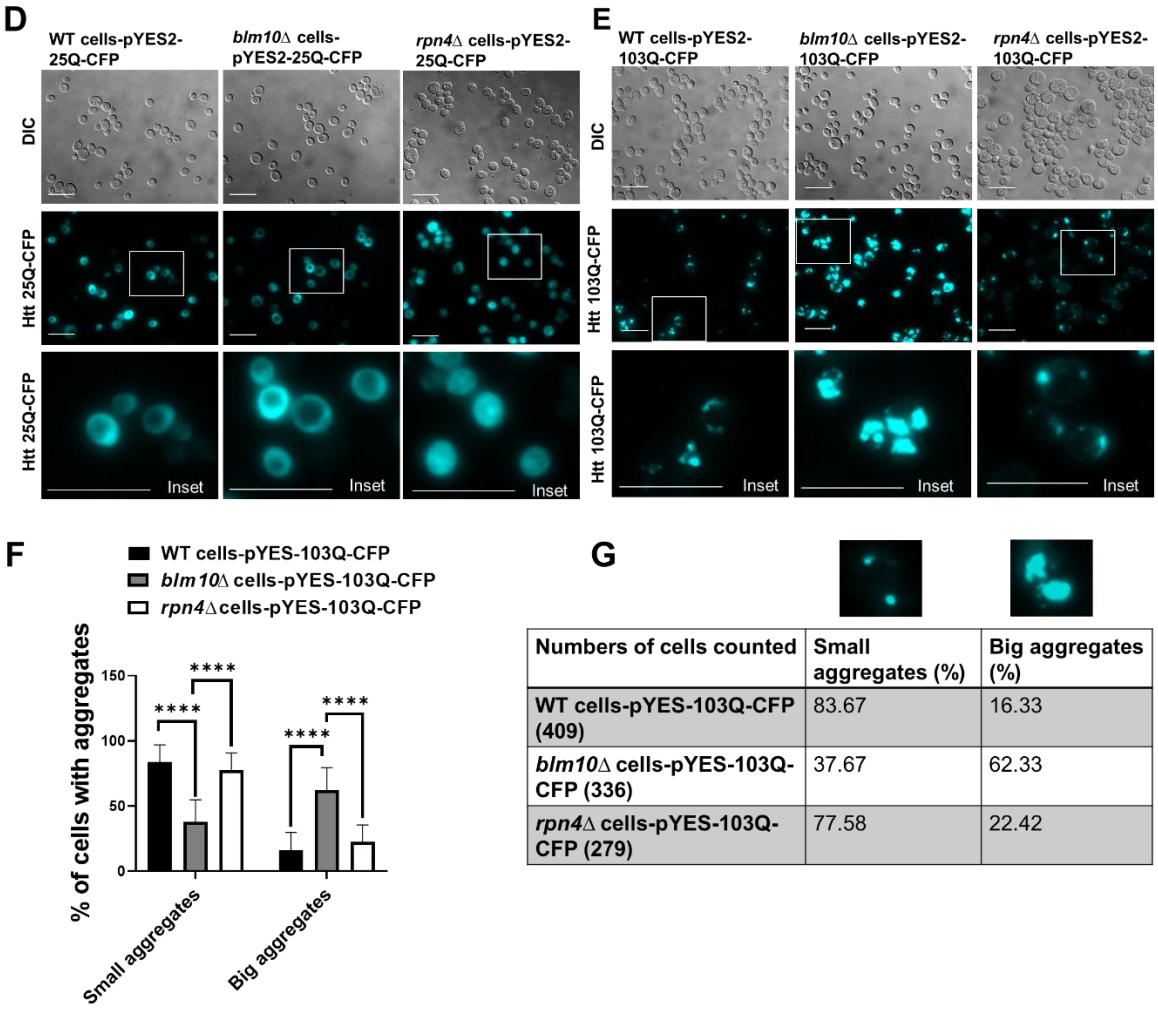

Numbers of cells counted	Small aggregates (%)	Big aggregates (%)
WT cells-pYES-103Q-CFP (409)	83.67	16.33
*blm10*Δ cells-pYES-103Q-CFP (336)	37.67	62.33
*rpn4*Δ cells-pYES-103Q-CFP (279)	77.58	22.42

Figure 18. Expression of toxic N-Htt leads to the formation of insoluble aggregates in WT and blm10Δ strains following galactose induction. *(**A, B**) CFP-N-Htt103Q expressions were induced by 2% galactose for the 10, 14, and 18 hr in both WT and blm10Δ strains. The protein amounts of total lysates (T, 10 µg), supernatant (S, 10 µg), and the pellet containing aggregates (P, 10 µg) were loaded into the native gel. The anti-GFP antibody was used to determine CFP-N-Htt103Q in the different samples. (**C**) Quantifications of the insoluble aggregates from N-Htt103Q expressing in either WT or blm10Δ were normalized to 10 hr induction counterpart of each strain. Bands' intensities were determined and analyzed using Image Lab software v5.2.1. Data are shown as mean ± SD of three independent experiments. (**D, E**) Visualization of N-Htt in cells expressing 25Q or 103Q is based on CFP fused with N-Htt fragments using live-cell microscopy. Differential interference contrast (DIC) images are presented in the upper panel. Scale bars are 25 µm and the insets are 10 µm. (**F-G**) Cells' classification and counting are based on CFP-N-Htt103Q aggregates size in the indicated strains. Data present as mean value ± SD of n = 3. The cells that were counted and analyzed in this experiment are 409 cells from the WT strain, 336 cells from the blm10Δ strain, and 279 cells from the rpnΔ strain. Statistical evaluations were accomplished by the ANOVA test using GraphPad Prism 8.2.1 (**** indicates p < 0.0001).*

5.7. Endogenous PA200 colocalizes with wild-type and mutant N-Htt in the SH-SY5Y

To determine whether PA200, the human ortholog of Blm10 has any physiological relevance in HD. We transiently transfected the SH-SY5Y cells with specific plasmids to express the wild-type and mutant N-Htt fragments. These fragments are tagged with hemagglutinin (HA). We transfected the SH-SY5Y cells for 48 hr, and then we performed immunostaining using a specific antibody for HA-tag to detect N-Htt fragments. We performed immunostaining to indicate the PA200 localization in the SH-SY5Y. We showed that the endogenous PA200 is distributed in both the nucleus and cytosol **(Figure 19A, C left panels)**. The wild-type N-Htt with a normal length of polyQ was evenly distributed in the cytosol of the cells **(Figure 19A middle panel)**, while mutant N-Htt with an expanded length of polyQ formed aggregates in the nucleus and/or cytoplasm of the cells **(Figure 19C middle panel).** We then merged the confocal images at superposition **(Figure 19A, C right panels).** Then, we analyzed the colocalization between N-Htt and PA200 via the JaCoP plugin tool using ImageJ software (imagej.nih.gov). The JaCop plugin combines several overlap determinations methods, including Pearson's colocalization coefficient (PCC), and Manders' colocalization coefficient (MCC). PCC indicates linear regression between two continuous variables, whereas, MCC determines the percentage of overlap between two variables [289]. The overlap is a co-occurrence between two variables such as the simple spatial overlap of two probes. In our case the variables are proteins. The values we obtained for PCC are $r = 0.659 \pm 0.093$ for PA200 overlap N-Htt23Q **(Figure 19B),** and $r = 0.72 \pm 0.097$ for PA200 overlap N-Htt74Q **(Figure 19D)**. The positive r-value indicates the positive colocalization between two proteins [290, 291]. MCC was also calculated using JaCoP plugin. MCC is very sensitive to the background. Therefore, we deduct the background when we estimated M1 and M2 values. The value of M1 (or M2) shows the proportion of the green signal concurrent with the red signal over its total intensities. M1 indicates the fraction of N-Htt overlapping PA200, and M2 indicates the fraction of PA200 overlapping N-Htt. The M1 value = 0.35 for N-HttQ23 and PA200, which means that the two pixels overlap by 35% **(Figure 19B).** The M2 value = 0.34 for PA200 and N-HttQ23, which means that the two pixels overlap by 34% **(Figure 19B)**. In the same manner, M1 for N-HttQ74 and PA200 refers to the two pixels overlap by 30%, and M2 refers to overlap 44.8% for PA200 and N-HttQ74 **(Figure 19D).**

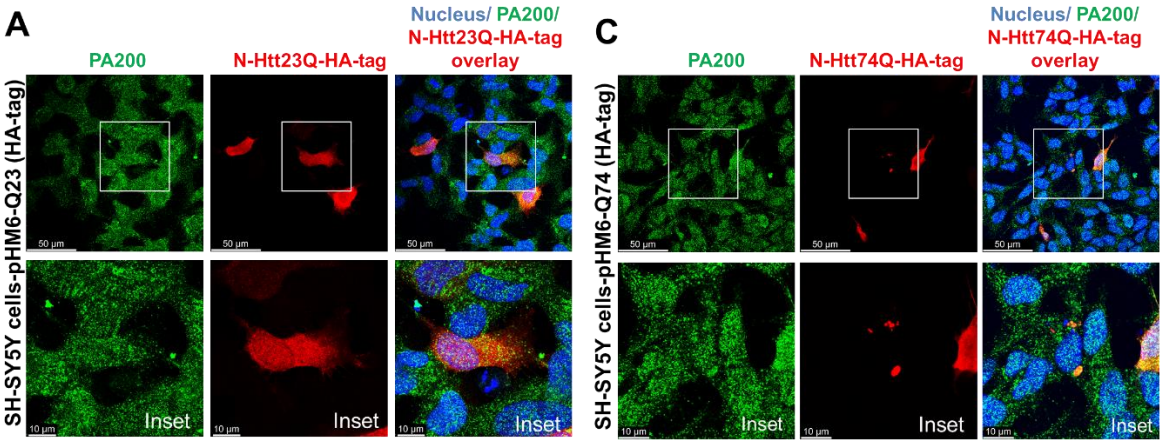

B

Pearson's coefficient	Manders' coefficients	
r	M1	M2
0.659 ± 0.093	0.35 ± 0.1	0.34 ± 0.1

D

Pearson's coefficient	Manders' coefficients	
r	M1	M2
0.72 ± 0.097	0.303 ± 0.146	0.448 ± 0.159

Figure 19. Endogenous PA200 displays colocalization with N terminal Htt in SH-SY5Y cells. (A, C) *The merged confocal images show that PA200 overlaps with N-Htt. The SH-SY5Y cells were transfected with pHM6-Q23 and pHM6-Q74 transient plasmids for 48 hr. The overexpressed N-Htt fragments with HA-tag were determined by anti-HA/Alexa Fluor 594 shown in red. Endogenous PA200 was detected with a specific antibody for PA200/Alexa Fluor 488 shown in green. Cell nuclei were stained by DAPI.* ***(B, D)*** *The tables show PCC as r-values, and MCC as M1 and M2 values. The evaluated values were determined by the JACoP plugin using ImageJ software. The r-value indicates the colocalization between N-Htt and PA200. The positive M1 value implies the fraction of N-Htt overlap with PA200, where the positive M2 implies the fraction of PA200 overlap with N-Htt. The data are shown as mean value ± SD. These data were generated using 28 images contained cells expressing N-Htt23Q-HA, and 24 images contained cells expressing N-Htt74Q-HA.*

5.8. PA200 interacts with wild-type and soluble mutant N-huntingtin fragments *in vitro*

Since PA200 overlap with wild-type and mutant N-Htt, we sought to detect whether PA200 might interact with N-Htt fragments. We performed a pull-down assay to show the potential interaction between the recombinant N-Htt18Q tagged GST and N-Htt51Q tagged with GST endogenous PA200 *in vitro*. We used two constructs expressing N-Htt fragments with GST. These constructs were modified by the addition of a tobacco etch virus (TEV) protease cleavage site between the GST sequence and *HTT*-exon1 coding regions. The presence of the GST-tag preserves the mutant fragments in a soluble form. Once the GST is cleaved by TEV protease,

the fragments with the 51Q length rapidly form insoluble aggregates [180, 253]. Both proteins GST-Htt18Q and GST-Htt51Q were produced in bacteria and purified by glutathione Sepharose 4B beads. The purified samples were loaded onto SDS-PAGE and examined by Coomassie blue staining **(Figure 20A)**. The GST-Htt18Q band was detected at the approximate size of 45 kDa and the GST-Htt51Q at 55 kDa. The purified GST tagged proteins were incubated with total cell lysate of SH-SY5Y. The interactions between GST-Htt18Q and GST-Htt51Q with PA200 were determined by immunoblot using a specific anti-PA200 antibody **(Figure 20B)**. In the same experimental setting, we also examined whether the GST-N-Htt protein may interact with the β1 subunit of the 20S-CP. We did not detect any interaction between the soluble N-Htt and the β1 subunit of the 20S-CP **(Figure 20C)**.

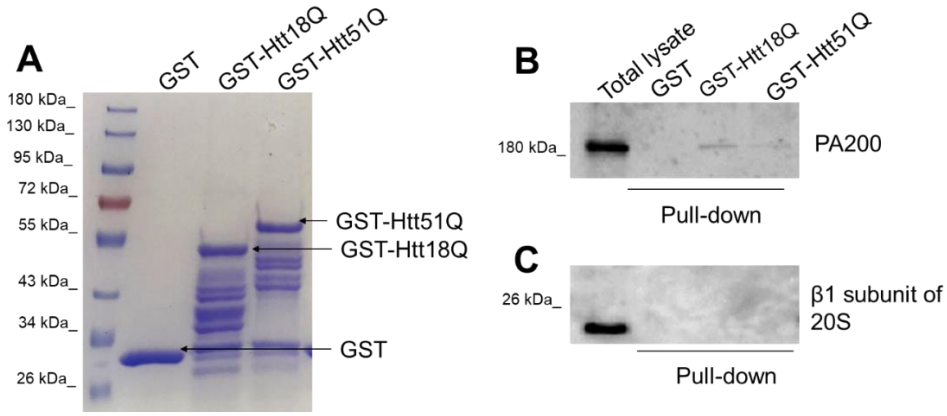

Figure 20. PA200 binds to wild-type and soluble mutant N-Htt fragments in vitro. *(**A**) The GST, Htt18Q tagged GST, and Htt51Q tagged GST were bacterially expressed. The purified proteins with GST-tag were loaded onto SDS-PAGE, and the proteins were stained by Coomassie blue staining. (**B, C**) The soluble proteins of GST, Htt18Q tagged with GST, and Htt51Q tagged with GST were incubated with total cell lysate of SH-SY5Y. The proteins after elution were analyzed by Western blot using (**B**) anti-PA200 antibody and (**C**) anti-β1 subunit of 20S-CP specific antibody.*

5.9. Depletion of PA200 leads to increased size and number of the mutant N-Htt aggregates in SH-SY5Y cells

To examine the possible role of PA200 (gene: *PMSE4*) on the formation of the aggregates from mutant N-Htt, we used the formerly established stably PA200 depleted cell line (shPA200 cells) and its corresponding control, which is expressing the pGIPZ-GFP [245]. We validated again the knockdown efficiency of the *PMSE4* gene by RT-qPCR, Western blot, and confocal microscopy. Our results confirm the successful knockdown of *PMSE4* in shPA200 cells

(Figure 21A-C). These findings also indicate the specificity of the anti-PA200 antibody that was used in this study **(Figure 21B, C)**. We also validated the overexpression of wild-type (N-Htt25Q-HA-tag) and mutant (N-Htt74Q-HA-tag) fragments in control and shPA200 cell lines by Western blot **(Figure 21D).**

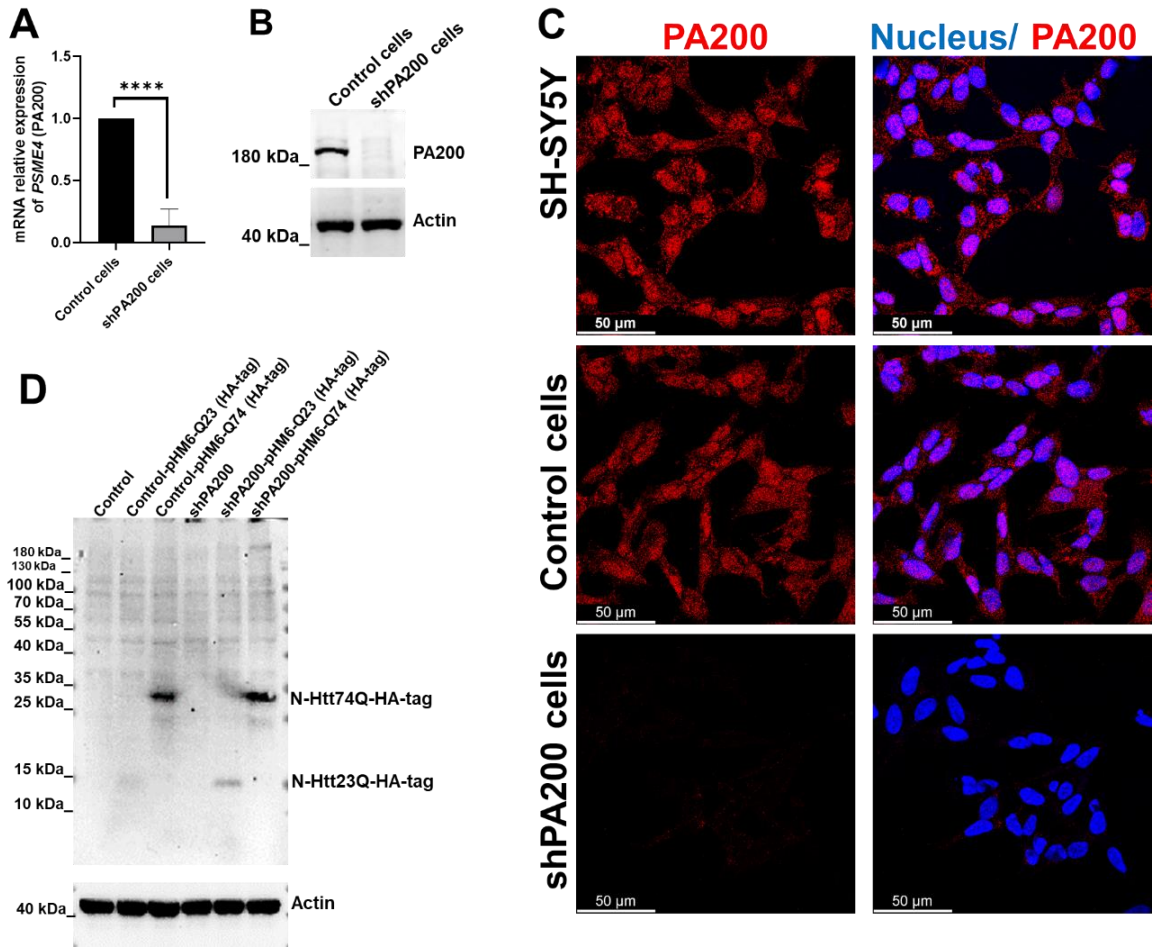

Figure 21. Validating the depletion of PA200 and the overexpression of wild-type and mutant N-Htt fragments. *(**A**) Comparing the gene expression of PSME4 in control and shPA200 cell lines, the data are shown as the mean value ± SD of three independent experiments. The statistical evaluation was obtained using unpaired student's t-test by GraphPad Prism v. 8.2.1 (**** indicates p < 0.0001). (**B**) Representative Western blot using a specific antibody for human PA200. Equal protein amounts 30 µg of shPA200 and control were loaded onto SDS-PAGE, followed by the normal immunoblot detection method. (**C**) Representative confocal microscope images of PA200 protein in shPA200 and control cells. Immunocytochemistry was performed with anti-PA200/Alexa Fluor594 (Red). (**D**) Validation of the wild-type and mutant N-Htt expression in both control and shPA200 cells after 48 hr of plasmid transfections. Equal protein amounts 30 µg from transfected and non-transfected total cell lysates were loaded into SDS-PAGE and followed by normal Western blotting. The blots were detected by antibody specific for HA-tag, and actin was used as a loading control.*

We performed immunocytochemistry for shPA200 and control cells after overexpression of wild-type and mutant N-Htt fragments for 48 hr. The confocal microscopy images showed that wild-type fragments are evenly distributed in the cytosol in both shPA200 and control cells **(Figure 22A)**. We also analyzed the formation of aggregates from mutant fragments in shPA200 and control cells **(Figure 22B)**. The data showed that the stable depletion of PA200 leads to a significant increase of aggregates size **(Figure 22C)** and the number **(Figure 22D)** of mutant N-Htt compared to the control cells.

Next, we performed a filter trap assay to determine the SDS-insoluble aggregates of mutant N-Htt. The cells were transfected with plasmids containing normal or expanded CAG repeats for 48 hr. Cell lysates were fractionated by centrifugation into supernatant (S) and the pellet (P) containing aggregates. Our results demonstrate that the SDS-insoluble aggregates of mutant N-Htt are significantly higher in the pellet fraction of shPA200 compared to the control pellet **(Figure 22E left panel, F)**. Furthermore, when we applied an anti-PA200 antibody, we found that PA200 is present in the aggregates of the pellet fraction of control cells **(Figure 22E right panel)**. Thus, we propose that PA200 may be recruited into mutant huntingtin aggregates in HD neuronal cells.

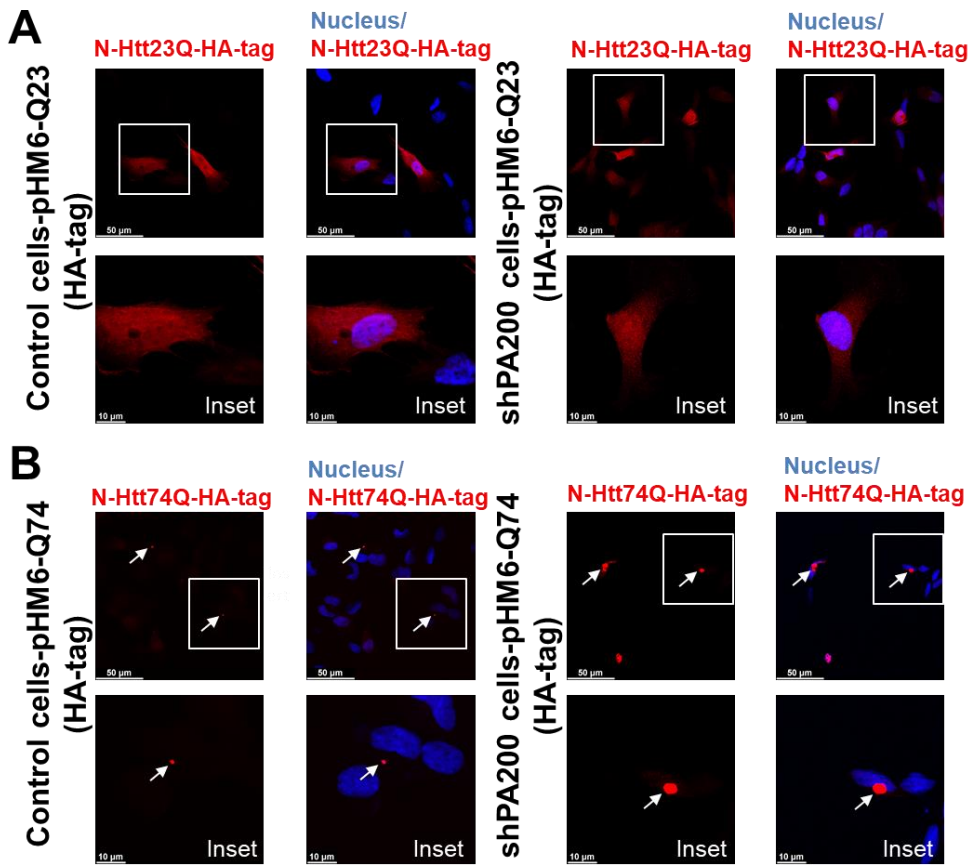

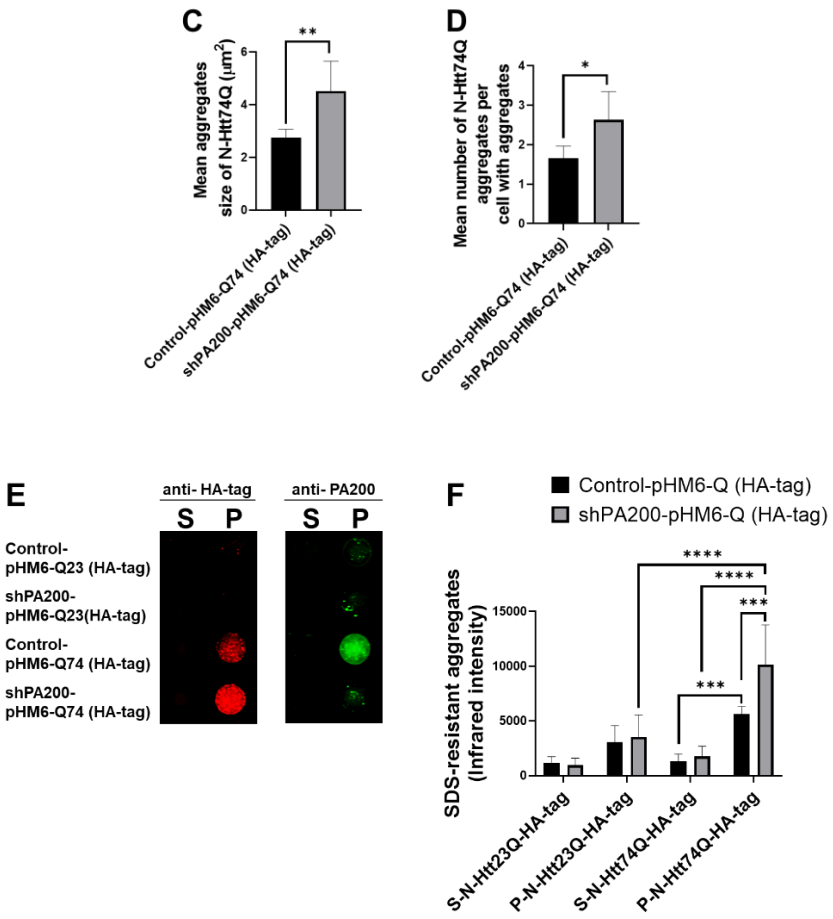

Figure 22. PA200 depletion drives to increased size and number of mutant N-Htt aggregates. ***(A, B)*** *The behavior of wild-type and mutant N-Htt in control and shPA200 cells. The cells were transfected with pHM6-Q23 and pHM6-Q74 plasmids for 48 hr, these plasmids contain the sequence of HA. The HA-tag was immunodetected with anti-HA-tag/Alexa Fluor 594 (Red). DAPI stained the nuclei of the cells.* ***(C, D)*** *Analysis of size and number of the mutant N-Htt aggregates generated in control and shPA200 cells. Confocal microscopy images were analyzed by ImageJ software (imagej.nih.gov). The data are presented as mean value ± SD, which is accomplished from 1207 shPA200 cells and 1057 control cells, which are obtained from n = 5. Statistical evaluation was performed using student's t-test (unpaired) using GraphPad Prism v. 8.2.1 (* indicates p < 0.05; ** indicates p < 0.01).* ***(E)*** *Filter trap of SDS-insoluble aggregates. Cell lysates of control and shPA200 cells after transaction were fractionated into (S, supernatant) and (P, pellet). Equal protein amounts of 10 µg of each fraction were loaded onto a nitrocellulose membrane with 0.2 µm pore size, then applied vacuum filtration. The stuck proteins on the membrane were probed with anti-HA-tag and specific anti-PA200 antibodies. The secondary antibodies were detected using infrared fluorescent dyes (anti-HA-tag/IRDye700 (Red), and anti-PA200/IRDye800 (Green)). The dote blots were detected by LI-COR Odyssey infrared approach.* ***(F)*** *Quantitative analysis of blot signals was obtained by image studio v 5.2. Data present as the mean value ± SD of n=4. ANOVA test using GraphPad Prism v. 8.2.1 was used for statistical analysis (*** indicates p < 0.001, **** indicates p < 0.0001).*

5.10. The Blm10/PA200 family promotes the degradation of wild-type and mutant N-terminal Htt fragments *in vitro*

We hypothesized that the Blm10/PA200 family might be involved in the proteasomal degradation of wild-type and mutant N-Htt. To examine this hypothesis, we performed *in vitro* degradation assay purified GST-Htt18Q as wild-type and GST-Htt51Q as mutant proteins. The equal molar amounts of a purified CP-20S or CP-Blm10 complexes were incubated with GST-Htt18Q and GST-Htt51Q over different time points. We found that both wild-type and mutant GST-N-Htt are degraded by CP or CP-Blm10 proteasomes **(Figure 23A and B left panels)**. Data analysis showed that both soluble N-Htt fragments with different polyQ lengths are significantly degraded by the proteasomes in the presence of Blm10 over time **(Figure 23A and B right panels)**. While the soluble fragments remain stable in the absence of the catalytically active proteasomes **(Figure 23C)**. Moreover, the GST protein was not degraded by either CP or CP-Blm10 **(Figure 23D upper panels)**, and the GST remained stable without the presence of active proteasomes **(Figure 23D lower left panel)**, which indicates the specificity of CP and CP-Blm10 complexes toward soluble N-Htt with different polyQ lengths. We also determined that the incubation of Blm10 alone with GST-Htt18Q or GST-Htt51Q does not result in the degradation of protein indicating that Blm10 is a catalytically inactive protein **(Figure 23D lower right penal)**. To confirm that Blm10 specifically promotes the degradation of soluble N-Htt in a ubiquitin-independent manner, we also performed *in vitro* degradation assay for GST-H51Q soluble protein using the 26S proteasome. Our results showed that GST-Htt51Q remains stable over time in the presence of the 26S **(Figure 23E).** Taken together, Blm10 the ortholog of human PA200 enhances the activity of 20S-CP to degrade the soluble non-ubiquitinated N-Htt fragments.

These proteasomal complexes were purified by affinity purification and then subjected to size-exclusion chromatography. To confirm the purity of CP and Blm10-CP complexes and detect whether the purified proteasomes are catalytically active, the purified proteasomes were first subjected to Coomassie staining. The degradation products are labeled with an asterisk in **Figure 23F**. We performed a native gel analysis followed by an in-gel activity assay and native gel protein staining, as previously reported [219, 223]. We demonstrate that all purified proteasomes CP, CP with singly, and doubly capped by the proteasomal activator Blm10 are all fully active **(Figure 23G upper panel),** moreover, we confirmed the presence of proteasomes in the native gel by protein staining **(Figure 23G lower panel).**

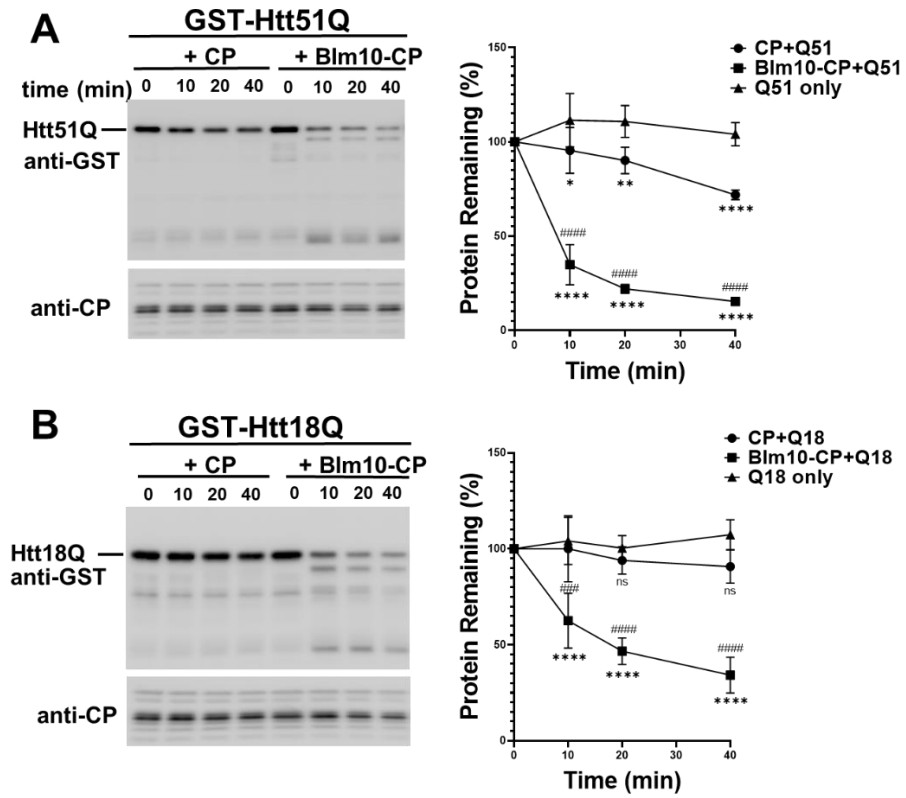
A
GST-Htt51Q
+ CP
+ Blm10-CP
time (min)
0 10 20 40 0 10 20 40
Htt51Q
anti-GST
anti-CP
CP+Q51
Blm10-CP+Q51
Q51 only
Protein Remaining (%)
Time (min)
B
GST-Htt18Q
+ CP
+ Blm10-CP
Htt18Q
anti-GST
anti-CP
CP+Q18
Blm10-CP+Q18
Q18 only
Protein Remaining (%)
Time (min)

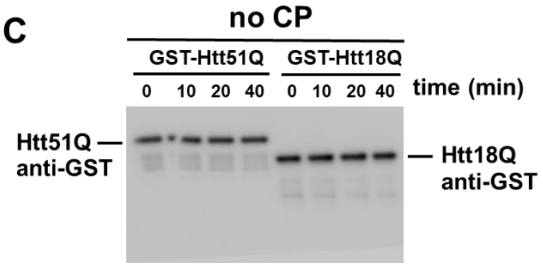
C
no CP
GST-Htt51Q
GST-Htt18Q
0 10 20 40 0 10 20 40
time (min)
Htt51Q
anti-GST
Htt18Q
anti-GST

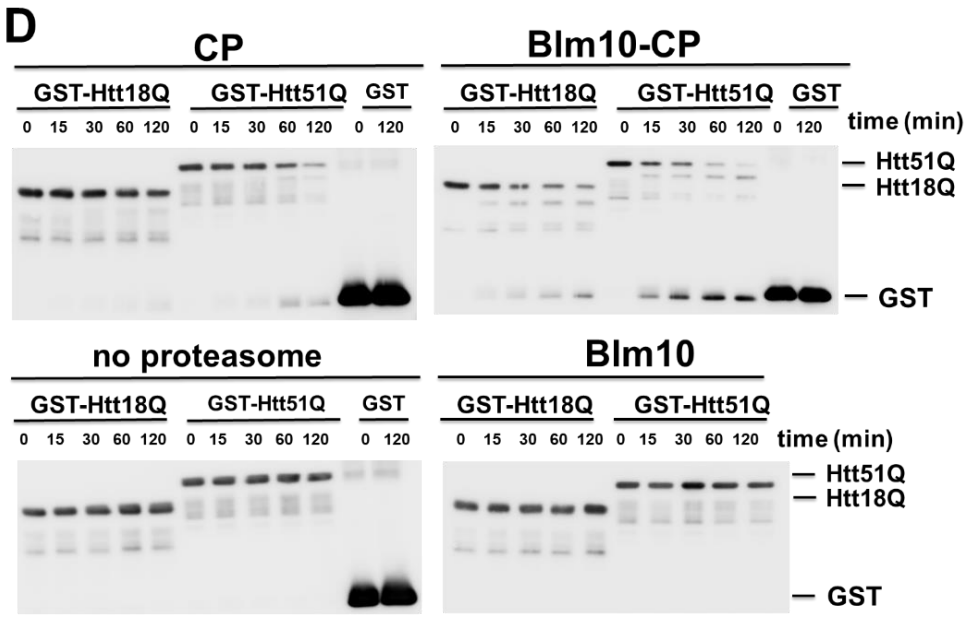
D
CP
Blm10-CP
GST-Htt18Q
GST-Htt51Q
GST
0 15 30 60 120 0 15 30 60 120 0 120
time (min)
Htt51Q
Htt18Q
GST
no proteasome
Blm10

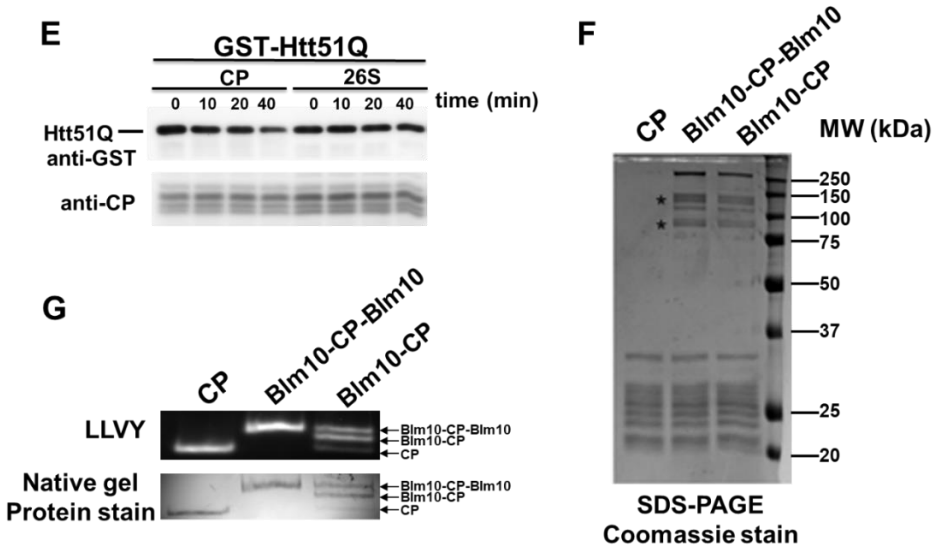

Figure 23. Blm10 accelerates the degradation of soluble mutant and wild-type of N-Htt fragments by the proteasome in vitro. *(**A, B**) GST-Htt51Q (mutant) and GST-Htt18Q (wild-type) were incubated in vitro with purified 20S-CP and Blm10-CP proteasomes for 0, 10, 20, 40 min. The remaining protein was analyzed by SDS-PAGE and Western blotting. The GST-Htt51Q and GST-Htt18Q proteins were detected by anti-GST antibody, shown in left panels. The assessments of the degradation processes of soluble N-Htt51Q and N-Htt18Q tagged with GST in the presence of purified proteasomes show in the right panels. Data are shown as the mean value ± SD of n = 3. Statistical evaluation was determined by ANOVA test using GraphPad Prism (* indicators $p < 0.05$, ** indicates $p < 0.01$, indicates **** $p < 0.0001$). * is termed when the statistical compare and contrast of proteasomes with Q18 or Q51 to the counterpart of polyQ only without proteasome complexes, and ns indicates to not significant. (### $p < 0.001$, #### $p < 0.0001$), # indicates the statistical comparison between the degradation by proteasomes, CP with either Q18 or Q51 compares to Blm10-CP with the corresponding polyQ lengths. (**C**) The mutant and wild type of GST-Htt fragments are not affected in the absence of proteasomal complexes during the indicated time points. (**D**) GST is not degraded by CP, Blm10-CP complexes, and GST also remains stable in the solution, the GST was incubated at the indicated times with or without proteasomes. (**E**) The soluble GST-N-Htt51Q is not degraded by the 26S proteasomal complex and remains stable in vitro. Soluble GST-N-Htt51Q was incubated for 0, 10, 20, 40 min with the presence of 26S proteasomes. Samples were taken at the indicated times and SDS-PAGE and Western blot were performed. The blots were determined by using an anti-GST antibody and a suitable secondary antibody. (**F**) Blm10-CP or CP was loaded into SDS-PAGE, the separated proteins were stained by Coomassie staining to confirm the identical amounts of CP were loaded for in-gel activity assay. The degradation products are marked with an asterisk. (**G**) The 20S-CP and proteasomal complexes (Blm10-CP singly and doubly capped) were determined by native gel and in-gel activity assay (upper panel), and native gel protein staining (lower panel).*

5.11. Blm10 increases the capacity of the proteasomes to cut within mutant N terminal Htt fragments *in vitro*

It was previously reported that Blm10 induces the trypsin-like and caspase-like protease activities without changing the chymotrypsin-like activity of the proteasome [223]. Thus, we studied the proteasomal degradation of soluble N-Htt51Q and N-Htt18Q by mass spectrometry (MS) based peptidomics. The purified GST-Htt18Q and GST-Htt51Q proteins were incubated with purified 20S-CP and Blm10-CP proteasomes. The degradation products were subjected to MS. The MS analysis identified 2417 peptides, and 461 peptides were derived from the N-Htt fragments **(Figure 24B)**. Peptide analysis showed that without 20S-CP, one peptide was detected, which was derived from the N-Htt51Q. The addition of the 20S-CP to the reaction led to generate a significant number of peptides from the N-Htt18Q and N-Htt51Q as shown in the second column of the heat map **(Figure 24A)**. Moreover, adding Blm10 to the 20S-CP led to generate more peptides such as (SLKSFQQ). Blm10 also triggered the production of other types of peptides generated from 20S-CP alone such as (KASFESLKSFQQ), which show in the third column of the heat map by an increase of the peptides' intensity **(Figure 24A)**. Double cuts in the polyQ stretch are not triggered by Blm10 as seen in the column of 51Q of the heat map **(Figure 24A).** The addition of Blm10 to the 20S-CP led to an elevated degradation of wild type with 18Q and mutant with 51Q of N-Htt fragments **(Figure 24C)**, while the lengths of peptides were unchanged **(Figure 24D).**

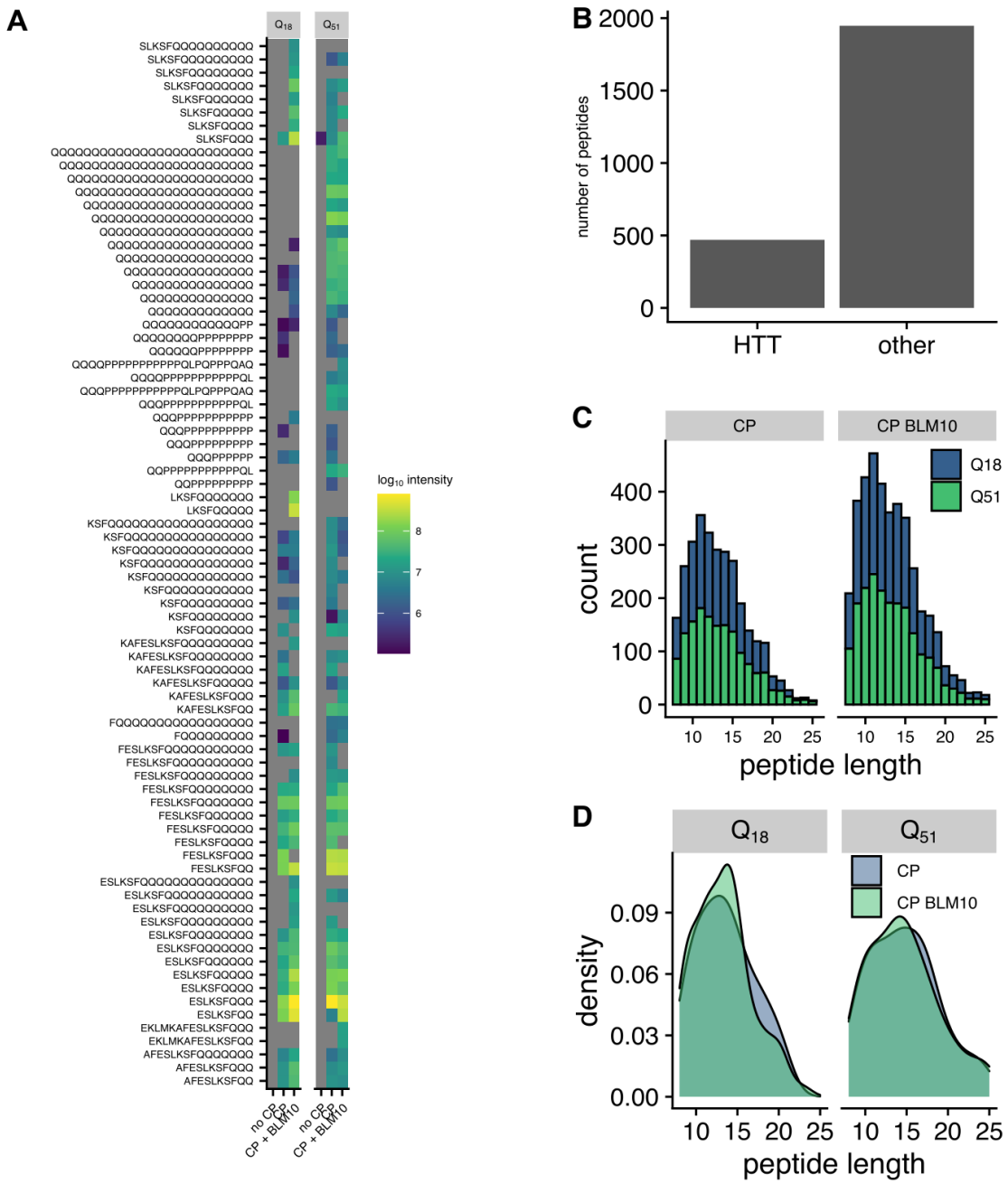

Figure 24. Peptidomics analysis of peptides generated by the 20S and Blm10-CP proteasomes. *(**A**) Heatmap of the generated peptides from proteasomal degradation of soluble N-Htt fragments. The purified GST-Htt51Q and GST-Htt18Q were incubated with no proteasome (fragments only), 20S-CP, and Blm10-CP complexes. The color refers to the detected peptides intensities, while the grey color refers to the no peptides were detected. (**B**) Approximately 20% of the overall number of generated peptides found in the degradation experiment are derived from N-Htt fragments. (**C**) The histogram represents the distribution of the peptides lengths, which were generated by the presence of the 20S-CP versus Blm10-CP proteasomes. (**D**) The density plot of the peptides from proteasomal degradation of N-Htt-18Q and N-Htt-51Q fragments in the presence of 20S-CP versus Blm10-CP proteasomes.*

To determine the specific cutting patterns by 20S-CP and Blm10-CP proteasomes, we probed our peptides data and analyzed the differences between the detected peptides from the *in vitro* degradation assays. The peptides generated by the 20S-CP have 71% similarity with peptides produced from Blm10-CP proteasomal degradation **(Figure 25A)**. The number of peptides generated from the degradation experiment with Blm10-CP complexes was considerably higher compared to peptides generated by the 20S-CP proteasomes or without active proteasomes **(Figure 25B)**. To look deeply and investigate the cleavage site of the recognized peptides, we investigated the peptides sequences upstream of the cleavage sites of the recognized peptides. To explain the cleavage specificity, we applied the Berger and Schechter nomenclature [292]. The proteolytic cleavage sites are distinguished based on protease recognition of a substrate [293, 294]. We found the amino acid residues around the protease-binding pocket are denoted as P4-P3-P2-P1↓P1′-P2′-P3′-P4′. The arrow demonstrates that the cleavage happens between amino acid residues of P1 and P1′ **(Figure 25C).** Then, we analyzed the peptides sequence of cleavage site according to amino acids logos **(Figure 25D)**, and by positional enrichment of the amino acids **(Figure 25E)**. We found that the cleavage specificity by the 20S-CP proteasome is not altered in the presence of the Blm10 activator for the degradation of N terminal Htt fragments. We found also that both proteasomes demonstrate a preference for hydrophobic and charged amino acids in positions P1, P2, and P5 **(Figure 25E)**. This finding is in line with that cleavage preference of both proteasomes in position P1 is the chymotryptic-like activity of the β5 subunit in the core particle. This specificity is not the same as previously described, which was shown that PA200 stimulates the trypsin-like and caspase-like protease activities [202, 220]. This might be because we used N terminal Htt fragments in our study, but other studies used peptides as reported by Rêgo, et al., [202], and chromatin extracts as reported by Blickwedehl, et al., [220]. N terminal Htt fragments have a specific amino acid composition, which let the 20S-CP or Blm10-CP proteasomes be biased to utilize the specific cleavage site for degradation of N-Htt fragments.

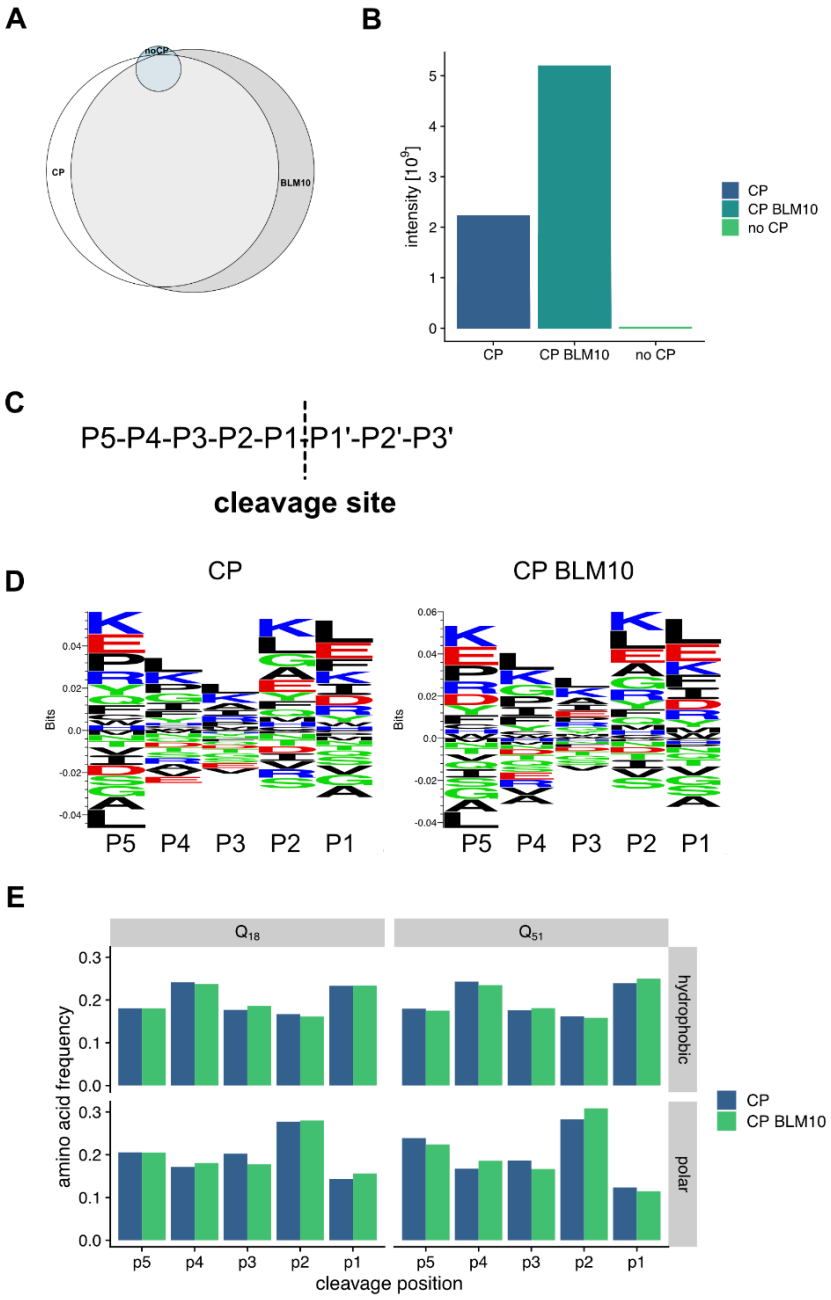

Figure 25. Characterization of the generated peptides from 20S-CP and Blm10-CP proteasomal degradation of N-Htt fragments. *(**A**) The Venn diagram shows the similarity of peptides detected in the proteasomal degradation experiments of N-Htt fragments in vitro. (**B**) Blm10 leads to an increase in the generation of peptides by the proteasome. Blm10-CP generates more peptides at the same time of degradation experiment with 20S-CP. (**C**) The scheme describes the cleavage site in the fragments. (**D**) The sequences of the peptides using amino acids logos, these peptides are generated by the 20S-CP and Blm10-CP proteasomes. (**E**) The bar chart shows the hydrophobic and polar amino acid frequencies of the cleavage sites.*

6. Discussion

Several neurodegenerative disorders are characterized by the impairment of proteasomal complexes in neuronal cells. This impairment leads to the dysregulation of protein turnover and insufficient clearance of misfolded proteins. A wild range of proteins can be ubiquitinated and degraded by a ubiquitin and ATP-dependent manner. This process regulates numerous cellular mechanisms including mitochondrial function and removal of the misfolded proteins. Small proteins and unfolded peptides can be directly degraded by the proteasomes in a ubiquitin and ATP-independent manner. The hallmarks of HD are mitochondria dysfunction and the accumulation of toxic oligomers and aggregates in neurons. Therefore, we investigated the role of proteasomal complexes in HD neurodegeneration. HD is a neurodegenerative disorder, and most HD studies have been accomplished by using post-mortem brains, neuronal and non-neuronal relevant cell lines, and mice HD models. Huntington's disease is caused by mutant Htt. This protein is ubiquitously expressed throughout the patient body. Thus, studying HD in peripheral tissues might add more details to develop biomarkers for HD, and might emphasize the use of these cells as model systems.

In recent years, many studies have been made to investigate the connection between proteolytic machinery and mitochondrial quality control [114, 295, 296]. In the first project, we determined the role of the ubiquitin-proteasome system in the alteration of mitochondria function in juvenile HD fibroblasts, and investigated the impact of full-length mutant Htt on cellular homeostasis. Various studies on adult-onset HD fibroblasts showed that oxidative stress usually occurs with metabolic alterations in the cells [67, 297]. Oxidative stress is stimulated by the overproduction of mitochondrial ROS in the cytosol. Increasing ROS production tightly correlates with elevated mitochondrial membrane potential [298-301]. On the other hand, the mitochondrial membrane potential decreases in certain diseases, this decrease is accompanied by dysfunction of the mitochondrial respiratory complexes, and the production of ROS increases in these diseased cells [302]. Our results demonstrate that ROS production is higher in juvenile HD fibroblasts indicating cellular stress. This increase is also accompanied by elevated mitochondrial membrane potential. Many studies using different HD models demonstrate that the mitochondria produce low ATP at low mitochondrial membrane potential [104, 303]. It is well known that ATP synthesis is precisely regulated by mitochondrial membrane potential and the enzymatic activities of the mitochondrial respiratory chain. Mitochondria studies in adult-onset HD fibroblasts showed impairment of catalase activity in cells [297]. The importance of catalase is protecting cells from ROS. However, the activity of

the enzyme complexes of the mitochondrial respiratory chain remains active in adult-onset HD fibroblasts [297]. We show in our study that mitochondria generate slightly less ATP in juvenile HD fibroblasts compared to healthy control. Therefore, the maintenance of energy production alongside elevated mitochondrial membrane potential may be one of the earliest compensatory responses against mutant Htt in juvenile HD fibroblasts.

The alterations in mitochondria morphology are usually associated with dysregulation of the mitochondrial fission-fusion machinery. Numerous studies provide evidence that the link between ATP generation and mitochondrial morphology is bidirectional, which suggests the important role of fission-fusion machinery in the regulation of mitochondria function [304-306]. Mitochondria is a highly dynamic organelle that undergoes frequent cycles of fission and fusion processes. According to Twig et al., [136], fusion is a shortened process and induces fission. The mitochondria with high membrane potential subsequently drive fusion. On the contrary, mitochondria with low membrane potential have a low possibility for fusion. We found that the levels of fusion proteins such as Opa1, Mfn1, and Mfn2 are lower in juvenile HD fibroblasts. While both gene expression and protein level of the fission protein Drp1 decrease in diseased cells. Mff levels unaltered in HD cells compared to healthy cells. It is tempting to speculate that mutant Htt triggers oxidative stress in juvenile HD fibroblasts, which goes together with elevated mitochondrial membrane potential. This increase of the mitochondrial membrane potential maintains ATP synthesis to provide enough energy for cell survival and promotes the degradation of misfolded proteins by UPS. However, with elevated mitochondrial membrane potential in juvenile HD fibroblasts, the mitochondria would initiate the fusion process. But, due to the decrease of the fusion proteins, this process, however, fails to proceed and would leave the mitochondria in small sizes and higher populations. Moreover, the low level of Drp1 means that the mitochondrial fission process is also limited. The transcriptional function of huntingtin suggests that mutant Htt is implicated in the changes of the expression of many genes in juvenile patients [46, 96]. Our results show that the gene expression of *DNM1L* is downregulated and the Drp1 protein level is significantly decreased in juvenile HD fibroblasts. While gene expressions of the fusion proteins are not changed or affected significantly in juvenile HD fibroblasts. Therefore, we suggest that HD fibroblasts trigger the proteasomal degradation of the fusion proteins to counterbalance the low level of Drp1. This process inhibits the mitochondria fusion and drives to a significant alteration in mitochondrial branching and morphology in juvenile HD fibroblasts.

We measured a significant increase in chymotryptic-like activity of the 26S proteasomes in juvenile HD fibroblasts. Recent studies demonstrated that overexpression of PA28γ proteasomal activator in neuronal HD models leads to improved proteasomal function and enhanced cell survival [93, 210]. We propose here that misfolded proteins can induce the activity of the proteasomes and boost their capacity for the turnover of specific proteasomal substrates. We found in our study that after inhibition of the proteasomal activity but not autophagy, the ubiquitinated proteins were increased in juvenile HD fibroblast compared to healthy cells. The mitochondrial fusion protein Mfn1 can be ubiquitinated and is a substrate for proteasomal degradation [279]. Parkin is a ubiquitin ligase, and a number of studies suggested that Parkin can regulate mitochondrial dynamic through enhancing Mfn1 ubiquitination for potential degradation by the 26S [279, 307, 308]. We demonstrated that Mfn1 but not Opa1 or Drp1 requires Parkin for ubiquitination. Parkin induces the ubiquitination of Mfn1 for degradation by the 26S proteasomes [279]. In juvenile HD fibroblasts, Parkin shows a higher gene expression and protein level compared to healthy fibroblasts, and this increase might promote the turnover of Mfn1. Parkin also promotes the activity of the 26S proteasomal complexes by inducing the interaction between the subunits of the 19S-PA700 regulatory particle [277]. Therefore, we propose that Parkin could regulate the activity of the 26S in juvenile HD fibroblasts, leading to increased 26S proteasomal activity. However, more studies are needed to investigate how increased Parkin might affect the mitophagy pathway in juvenile HD fibroblasts.

Taken together, our data suggest that mitochondrial dynamics are altered in juvenile HD fibroblasts. The expression of mutant Htt influences the mitochondria fission-fusion machinery. The role of Htt in the transcription of various genes could implicate the mutant Htt in reducing gene expression and protein level of Drp1 in juvenile HD fibroblasts. To counterbalance this manifestation in the cell, the HD fibroblast accelerates the turnover of Mfn1 by triggering the activity of the 26S proteasome, which is supported by the high level of Parkin. The energy requirements for UPS activities are obtained from mitochondria. Mitochondrial energy production is often correlated with mitochondrial fusion. However, the accelerated degradation of mitochondrial fusion protein Mfn1 leads to limitations in mitochondrial fusion. The elevated mitochondrial membrane potential in juvenile HD fibroblasts acts back on the homeostasis of mitochondria and cellular function **(Figure 26)**. Glycolysis is another source of ATP in cells and provides the carbon fuel for mitochondrial function. In tumor studies, the suppression of the glycolytic pathway in cancer cells leads to reprogramming the intracellular energy metabolism toward mitochondrial function in an autophagy-dependent manner. This drives to

upregulate OXPHOS to generate ATP that is sufficient for cell survival [309]. In our study, we determined a decrease in glycolysis in juvenile HD fibroblasts, which may lead to reprogrammed ATP production in cells to provide enough energy for cell survival. Our findings discuss numerous events that are significantly altered in juvenile HD fibroblasts. These events confirm that mitochondrial dynamics are changed, which are caused by increased Parkin level, and elevated proteasomal activity in HD cells. These findings might lay a foundation stone to better understand the pathogenesis of HD in juvenile fibroblasts. Thus, a critical direction for future research is to find a mechanism that induces the UPS activity and recovers the mitochondrial network. These processes would be a promising strategy to eliminate the detrimental effects of mutant Htt in neuronal cells of adult patients.

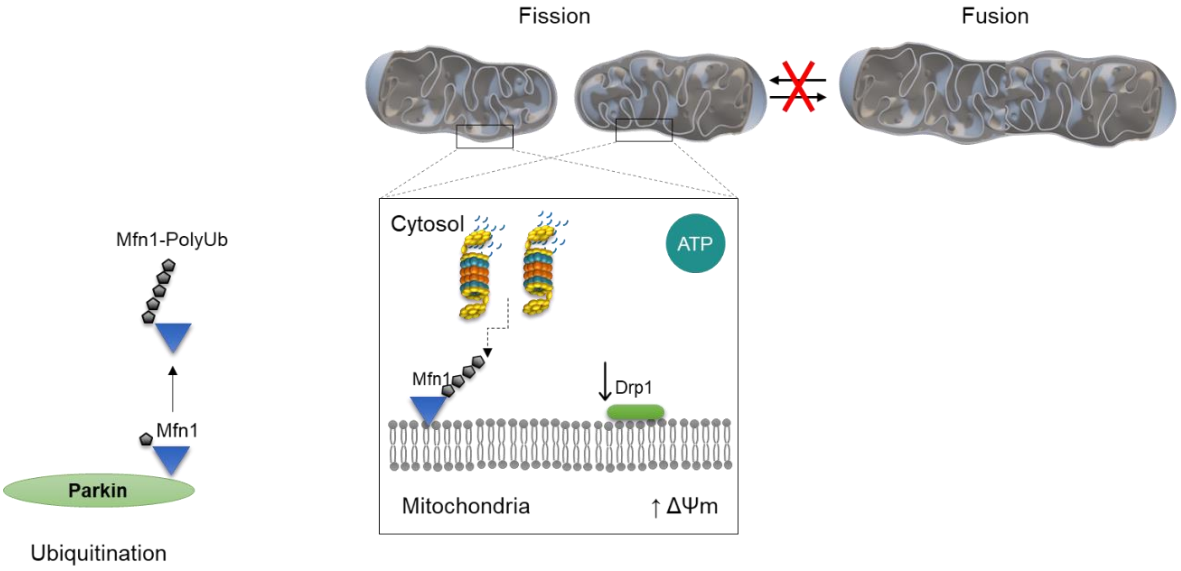

Figure 26. The crosstalk between mitochondria and the ubiquitin-proteasome system in juvenile HD fibroblasts. *Increased Parkin level leads to elevated the ubiquitination of Parkin's substrates such as Mfn1, this process drives to decreased the branching of the functional mitochondria.*

Various studies have been used *S. cerevisiae* as a successful model to investigate misfolding proteins in neurodegenerative diseases including HD [77, 220]. The main advantages of using yeast as a model to study HD are: First, there is no Htt ortholog present in yeast. Therefore, the alteration of the yeast phenotype upon expression of mutant N-Htt fragments is independent of wild-type Htt. Second, there are many consequences of mutant N-Htt expression on cellular toxicity, proteolysis, and mitochondria dysfunctions. All these manifestations are observed in HD yeast models, are similar to the effects of mutant Htt are shown in human HD models [254,

284, 285]. These observations put the yeast model of HD as a valuable model to study the disease.

The role of the proteasomal complexes in the degradation of Htt has been widely investigated. Proteasomal activators provide a strategy to enhance gate opening of 20S-CP. This strategy may expedite the degradation of polyQ stretches in HD and reduces the possibility of the accumulation of toxic oligomers and aggregates. In the second project, we investigated the role of the Blm10/PA200 proteasomal activator family in the degradation of N-Htt fragments in a ubiquitin and ATP-independent manner. We performed our experiments using an HD yeast model, then we confirmed our findings using a human cell line. The HD yeast model used in our study was developed by Meriin et. al, [254]. The transformed yeast expresses N terminal Htt fragments under galactose-induction. These fragments contain the first 17 amino acids of the Htt followed by 25 or 103 glutamines. Our data confirm that N-Htt103Q can form insoluble aggregates in the yeast model of HD, and the accumulation of the aggregates causes cytotoxicity.

Tar et al., [250] reported that the *BLM10* deletion leads to an increase in cell death when cells were exposed to acetic acid. We studied the deletion of *BLM10* on the formation of toxic aggregates from N-Htt103Q in a galactose-inducible HD yeast model. We found that N-Htt103Q provokes cytotoxicity in the absence of Blm10 more than WT and *Rpn4Δ* strains. The absence of Blm10 drives the cells to reach the solubility threshold of mutant N-Htt earlier than in control cells. Thus, we propose that Blm10 could play an essential role in the degradation of polyQ stretches and reduce the formation of toxic aggregates in cells. We determined an increasing number and size of insoluble aggregates in the *blm10Δ* compared to WT of HD yeast models. We suggest that the efficiency of the proteasome is reduced in the absence of Blm10 leading to the accumulation of N-Htt103Q aggregates, which propels cellular toxicity in the HD yeast model.

We demonstrated that the Blm10/PA200 family promotes the proteasomal degradation of soluble toxic and wild-type N-Htt. *In vitro* degradation assay confirms that both 20S-CP and Blm10-CP proteasomes can degrade non-ubiquitinated N-Htt fragments. The degradation efficiency of the soluble fragments is higher in the presence of Blm10. Our results are in accordance with previously reported data, which show that the soluble form of N-Htt fragments does not inhibit the CP-20S proteasomes, hence, the core particle can cleave within polyQ stretches and generate short peptides [180, 185, 253]. We verified the activity of the purified 20S-CP and Blm10-CP complexes, and we confirmed that the proteasomes are fully active. Therefore, we speculate that non-ubiquitinated N-Htt fragments are targets for the

Blm10/PA200 family for degradation by Blm10/PA200-CP proteasomal complexes. Mass spectrometry-based peptidomics analysis demonstrated that the 20S-CP proteasome is not clogged by the mutant N-Htt, and the 20S-CP cuts within the N-Htt fragments, which contain the polyQ stretches. This activity is increased by capping the proteasome with Blm10. Thus, we consider that the Blm10/PA200 activator family targets soluble non-ubiquitinated N-Htt fragments for degradation by the proteasomes **(Figure 27A, B)**, which might help to delay to reach the solubility threshold of mutant N-Htt in the cells, thus, postpone the formation of the toxic aggregates **(Figure 27A)**.

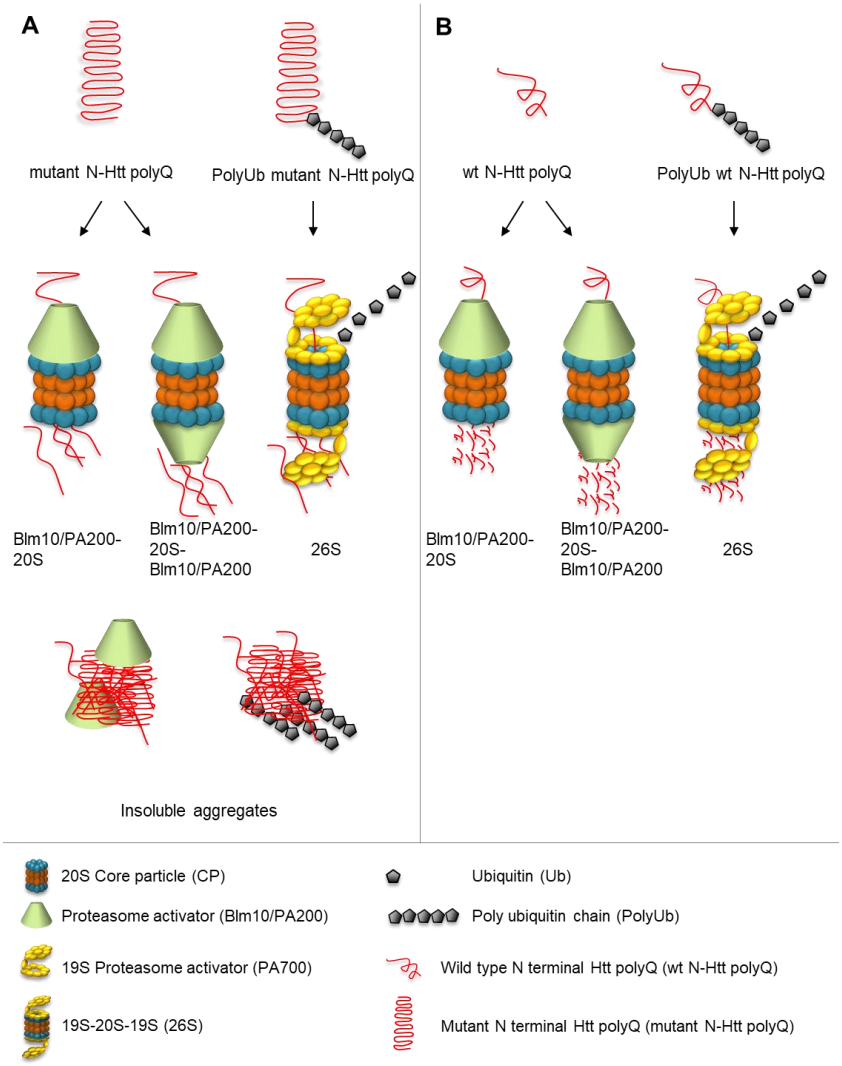

Figure 27. Proposed model for the role of the proteasomal activator Blm10/PA200 family in the degradation of (A) mutant N-Htt, and (B) wild-type N-Htt fragments. *Both ubiquitin-dependent and -independent pathways are active in the cells. However, the ubiquitinated unfolded fragments are recognized by 26S proteasomes for degradation. Whereas the non-ubiquitinated soluble fragments can be directly sent to Blm10/PA200-CP complexes for degradation.*

To investigate the role of PA200 the human ortholog of Blm10 in the proteasomal degradation of N-Htt fragments, we studied the relationship between PA200 and N-Htt fragments in a human HD model. Interestingly, PA200 shows spatial colocalization with wild-type and mutant N-Htt fragments in the SH-SY5Y cells. Moreover, the pull-down assay showed that PA200 also interacts with soluble N-Htt fragments *in vitro*. In parallel with our results in the HD yeast model, we found a significant increase in size and number of mutant N-Htt aggregates in the PA200 depleted cell line compared to control cells. We also detected PA200 in SDS insoluble aggregates of mutant N-Htt by filter trap assay. Therefore, we propose that PA200 is recruited to insoluble aggregates. Consequently, the accumulation of PA200 in the aggregates leads to an impairment of the degradation of toxic N-Htt fragments in HD neurons and drives to increase the formation of toxic aggregates.

Many HD studies documented that Htt can be polyubiquitinated and ubiquitins are found in the insoluble aggregates of mutant Htt. Other studies demonstrated that Htt is often non-ubiquitinated and insoluble aggregates lacking Ubs [27, 181, 253]. We show in our study that the 20S-CP degrades soluble N-Htt fragments by a ubiquitin-independent pathway, and this degradation is enhanced by the Blm10/PA200 activator family. The Blm10/PA200 activators are unable to recognize globular proteins, but they usually recognize peptides and facilitates the degradation of the peptides without ubiquitination and ATP energy [223, 310]. Blm10 triggers the caspase-like and trypsin-like activities of the core particle, while the recombinant PA200 triggers the trypsin-like and chymotrypsin-like peptidase activities of the proteasomes [218, 223]. The addition of the endogenous PA200 that isolated from bovine testes to the purified 20S-CP leads to activation of the caspase-like peptidase activity of the proteasomes [211]. The Blm10/PA200 activator family is involved in the degradation of soluble and unstructured small proteins like Tau [223]. Many HD studies demonstrated that the first 17 amino acids followed by a specific number of glutamines in N terminal Htt are typically disordered in solution [20, 21]. Therefore, we suggest that these disordered peptides are substrates for Blm10/PA200-CP proteasomal complexes.

The variety of proteasome species present in the cell are based on the different proteasomal activators that are assembled to the 20S-CP. For instance, Blm10/PA200-CP complexes can be present as singly or doubly capped proteasomes. Furthermore, Blm10/PA200 can form hybrid proteasomal complexes with PA700 [186, 222]. In the cellular context, the Htt and unfolded fragments can be ubiquitinated and recognized by the PA700 for potential degradation by the 26S proteasomes. At the same time, Blm10/PA200-CP proteasomes are active and able to degrade the unstructured fragments including mutant N-Htt in a ubiquitin-independent manner

with high efficiency **(Figure 27A)**. Thus, the soluble non-ubiquitinated polyQ monomers and oligomers can be degraded by the 20S-CP capped with a single or double Blm10/PA200 proteasomal activator. Our study is a step in a critical orientation for future research to find upstream mechanisms, which regulate the degradation of mutant N-Htt fragments in a ubiquitin-independent manner.

Collectively, we investigated the roles of proteasomal complexes in HD neurodegeneration in two different manners. We used juvenile HD fibroblasts as a cellular model for demonstrating the ubiquitin and ATP-dependent degradation of proteins by the 26S. We found that cells respond to polyQ expansion of mutant Htt by enhancing the 26S proteasomal activity and faster degradation of specific UPS substrates to protect cells. In a ubiquitin and ATP-independent manner, we performed our study using a combination of yeast and human HD models. Our data identify that the soluble N-Htt fragments are a substrate for Blm10/PA200-CP complexes for degradation. We suggest the potential value of enhancing the activity of proteasomes by proteasomal activators. This process would be a promising strategy to restore the mitochondrial function and reduce the toxic Htt accumulation in HD neuronal cells of the patients.

7. Summary

Huntington's disease is characterized by ineffective degradation of mutant Htt, which leads to the accumulation of mutant N-Htt fragments, oligomers, and aggregates in neuronal cells. The toxic species of mutant Htt influence multiple intracellular pathways including proteasomal degradation. Mutant huntingtin widely expresses throughout patient tissues from early life. Many studies have determined the impairment of ATP synthesis and proteolytic function, which are the hallmarks of the disease in HD neuronal cells. But no hypothesis clearly describes the crosstalk between mitochondria and ubiquitin-proteasome system in HD peripheral tissues. In the first study, we investigated the role of the ubiquitin-proteasome system in mitochondrial function using juvenile HD fibroblasts. We found elevated ROS levels, accompanied by an increase of mitochondrial membrane potential in diseased cells. The analysis of mitochondrial respiration does not show a significant difference in HD cells compared to healthy cells. Numerous mitochondrial fission-fusion protein levels were significantly decreased in HD fibroblasts. This decrease led to reduced mitochondria branching. On the other hand, the function of the ubiquitin-proteasome system was increased by an elevated proteasomal activity and a high level of Parkin. We examined the proteasomal degradation of Mfn1 a specific substrate for Parkin in healthy and diseased cells by chase assay. We found the turnover of Mfn1 was faster in diseased cells compared to healthy ones. Moreover, we demonstrated that juvenile HD fibroblasts are viable with a low rate of mitosis. We suggest that juvenile HD fibroblasts were responded to mutant Htt by triggering the activity of the 26S. This activity promotes the turnover of specific substrates by the ubiquitin-proteasome system to protect cells, and the mitochondria provide sufficient energy for cell survival.

The 26S proteasomes degrade ubiquitinated Htt. While the 20S-CP cleaves within polyQ in a ubiquitin-independent manner. Moreover, the proteasomal activator Blm10/PA200 family controls the gate opening of the 20S core particle in the ubiquitin and ATP independent pathway. The Blm10/PA200-CP proteasomal complexes participate in the degradation of Dnm1, acetylated histones, and unstructured proteins such as Tau. In the second study, we demonstrated the role of the Blm10/PA200 family in the degradation of N terminal Htt fragments in a ubiquitin-independent manner. We showed that PA200 interacts with N terminal Htt fragments. The deletion of *BLM10* in yeast and the silencing of *PSME4* (PA200) in human cells leads to the accumulation of mutant N-Htt aggregates in the cells. *In vitro* degradation analysis confirms the potent role of Blm10 in the proteasomal degradation of soluble N-Htt

fragments. Our finding indicates that the Blm10/PA200 activator family promotes the proteasomal degradation of N terminal Htt fragments.

8. References

1. Thibaudeau, T.A., R.T. Anderson, and D.M. Smith, *A common mechanism of proteasome impairment by neurodegenerative disease-associated oligomers.* Nature communications, 2018. **9**(1): p. 1-14.
2. Rubinsztein, D.C. and J. Carmichael, *Huntington's disease: molecular basis of neurodegeneration.* Expert reviews in molecular medicine, 2003. **5**(20): p. 1-21.
3. Fisher, E.R. and M.R. Hayden, *Multisource ascertainment of Huntington disease in Canada: prevalence and population at risk.* Movement Disorders, 2014. **29**(1): p. 105-114.
4. van der Burg, J.M., M. Björkqvist, and P. Brundin, *Beyond the brain: widespread pathology in Huntington's disease.* The Lancet Neurology, 2009. **8**(8): p. 765-774.
5. Morrison, P., S. Harding-Lester, and A. Bradley, *Uptake of Huntington disease predictive testing in a complete population.* Clinical genetics, 2011. **80**(3): p. 281-286.
6. Evans, S.J., et al., *Prevalence of adult Huntington's disease in the UK based on diagnoses recorded in general practice records.* J Neurol Neurosurg Psychiatry, 2013. **84**(10): p. 1156-1160.
7. MacDonald, M.E., et al., *A novel gene containing a trinucleotide repeat that is expanded and unstable on Huntington's disease chromosomes.* Cell, 1993. **72**(6): p. 971-983.
8. Orr, H.T. and H.Y. Zoghbi, *Trinucleotide repeat disorders.* Annu. Rev. Neurosci., 2007. **30**: p. 575-621.
9. Koyuncu, S., et al., *Proteostasis of huntingtin in health and disease.* International journal of molecular sciences, 2017. **18**(7): p. 1568.
10. Potter, N.T., E.B. Spector, and T.W. Prior, *Technical standards and guidelines for Huntington disease testing.* Genetics in Medicine, 2004. **6**(1): p. 61.
11. Orth, M. and C. Schwenke, *Age-at-onset in Huntington disease.* PLoS Curr, 2011. **3**: p. Rrn1258.
12. Myers, R.H., *Huntington's disease genetics.* NeuroRx : the journal of the American Society for Experimental NeuroTherapeutics, 2004. **1**(2): p. 255-262.
13. Squitieri, F., et al., *Juvenile Huntington's disease: does a dosage-effect pathogenic mechanism differ from the classical adult disease?* Mechanisms of ageing and development, 2006. **127**(2): p. 208-212.
14. Rosenblatt, A., et al., *The association of CAG repeat length with clinical progression in Huntington disease.* Neurology, 2006. **66**(7): p. 1016-1020.
15. Carroll, J.B., et al., *Treating the whole body in Huntington's disease.* The Lancet Neurology, 2015. **14**(11): p. 1135-1142.
16. Li, S.-H. and X.-J. Li, *Huntington and its role in neuronal degeneration.* The Neuroscientist, 2004. **10**(5): p. 467-475.
17. Steffan, J.S., et al., *SUMO modification of Huntingtin and Huntington's disease pathology.* Science, 2004. **304**(5667): p. 100-104.
18. Atwal, R.S., et al., *Huntingtin has a membrane association signal that can modulate huntingtin aggregation, nuclear entry and toxicity.* Human molecular genetics, 2007. **16**(21): p. 2600-2615.
19. Saudou, F. and S. Humbert, *The biology of huntingtin.* Neuron, 2016. **89**(5): p. 910-926.
20. Kim, M.W., et al., *Secondary structure of Huntingtin amino-terminal region.* Structure, 2009. **17**(9): p. 1205-1212.
21. Sivanandam, V., et al., *The aggregation-enhancing huntingtin N-terminus is helical in amyloid fibrils.* Journal of the American Chemical Society, 2011. **133**(12): p. 4558-4566.
22. Maiuri, T., et al., *The huntingtin N17 domain is a multifunctional CRM1 and Ran-dependent nuclear and cilial export signal.* Human molecular genetics, 2013. **22**(7): p. 1383-1394.
23. Harjes, P. and E.E. Wanker, *The hunt for huntingtin function: interaction partners tell many different stories.* Trends in biochemical sciences, 2003. **28**(8): p. 425-433.
24. Palidwor, G.A., et al., *Detection of alpha-rod protein repeats using a neural network and application to huntingtin.* PLoS Comput Biol, 2009. **5**(3): p. e1000304.

25. Takano, H. and J.F. Gusella, *The predominantly HEAT-like motif structure of huntingtin and its association and coincident nuclear entry with dorsal, an NF-kB/Rel/dorsal family transcription factor.* BMC neuroscience, 2002. **3**(1): p. 15.
26. Seong, I.S., et al., *Huntingtin facilitates polycomb repressive complex 2.* Human molecular genetics, 2010. **19**(4): p. 573-583.
27. Lontay, B., et al., *How Do Post-Translational Modifications Influence the Pathomechanistic Landscape of Huntington's Disease? A Comprehensive Review.* International journal of molecular sciences, 2020. **21**(12): p. 4282.
28. Warby, S.C., et al., *Activated caspase-6 and caspase-6-cleaved fragments of huntingtin specifically colocalize in the nucleus.* Human molecular genetics, 2008. **17**(15): p. 2390-2404.
29. Gafni, J. and L.M. Ellerby, *Calpain activation in Huntington's disease.* Journal of Neuroscience, 2002. **22**(12): p. 4842-4849.
30. Hermel, E., et al., *Specific caspase interactions and amplification are involved in selective neuronal vulnerability in Huntington's disease.* Cell Death & Differentiation, 2004. **11**(4): p. 424-438.
31. Kim, Y.J., et al., *Lysosomal proteases are involved in generation of N-terminal huntingtin fragments.* Neurobiology of disease, 2006. **22**(2): p. 346-356.
32. Lunkes, A., et al., *Proteases acting on mutant huntingtin generate cleaved products that differentially build up cytoplasmic and nuclear inclusions.* Molecular cell, 2002. **10**(2): p. 259-269.
33. Ratovitski, T., et al., *Mutant huntingtin N-terminal fragments of specific size mediate aggregation and toxicity in neuronal cells.* Journal of Biological Chemistry, 2009. **284**(16): p. 10855-10867.
34. Tebbenkamp, A.T., et al., *Analysis of proteolytic processes and enzymatic activities in the generation of huntingtin n-terminal fragments in an HEK293 cell model.* PLoS One, 2012. **7**(12).
35. Graham, R.K., et al., *Cleavage at the 586 amino acid caspase-6 site in mutant huntingtin influences caspase-6 activation in vivo.* Journal of Neuroscience, 2010. **30**(45): p. 15019-15029.
36. Riechers, S.-P., et al., *Interactome network analysis identifies multiple caspase-6 interactors involved in the pathogenesis of HD.* Human molecular genetics, 2016. **25**(8): p. 1600-1618.
37. Kim, Y.J., et al., *Caspase 3-cleaved N-terminal fragments of wild-type and mutant huntingtin are present in normal and Huntington's disease brains, associate with membranes, and undergo calpain-dependent proteolysis.* Proceedings of the National Academy of Sciences of the United States of America, 2001. **98**(22): p. 12784-12789.
38. El-Daher, M.T., et al., *Huntingtin proteolysis releases non-polyQ fragments that cause toxicity through dynamin 1 dysregulation.* The EMBO journal, 2015. **34**(17): p. 2255-2271.
39. Nasir, J., et al., *Targeted disruption of the Huntington's disease gene results in embryonic lethality and behavioral and morphological changes in heterozygotes.* Cell, 1995. **81**(5): p. 811-823.
40. Duyao, M.P., et al., *Inactivation of the mouse Huntington's disease gene homolog Hdh.* Science, 1995. **269**(5222): p. 407-410.
41. Zeitlin, S., et al., *Increased apoptosis and early embryonic lethality in mice nullizygous for the Huntington's disease gene homologue.* Nature genetics, 1995. **11**(2): p. 155-163.
42. Rigamonti, D., et al., *Wild-type huntingtin protects from apoptosis upstream of caspase-3.* Journal of Neuroscience, 2000. **20**(10): p. 3705-3713.
43. Zhang, Y., et al., *Depletion of wild-type huntingtin in mouse models of neurologic diseases.* Journal of neurochemistry, 2003. **87**(1): p. 101-106.
44. Leavitt, B.R., et al., *Wild-type huntingtin protects neurons from excitotoxicity.* Journal of neurochemistry, 2006. **96**(4): p. 1121-1129.
45. Rigamonti, D., et al., *Huntingtin's neuroprotective activity occurs via inhibition of procaspase-9 processing.* Journal of Biological Chemistry, 2001. **276**(18): p. 14545-14548.
46. Schulte, J. and J.T. Littleton, *The biological function of the Huntingtin protein and its relevance to Huntington's Disease pathology.* Current trends in neurology, 2011. **5**: p. 65.
47. Zuccato, C., et al., *Huntingtin interacts with REST/NRSF to modulate the transcription of NRSE-controlled neuronal genes.* Nature genetics, 2003. **35**(1): p. 76-83.

48. Gauthier, L.R., et al., *Huntingtin controls neurotrophic support and survival of neurons by enhancing BDNF vesicular transport along microtubules.* Cell, 2004. **118**(1): p. 127-138.
49. Her, L.-S. and L.S. Goldstein, *Enhanced sensitivity of striatal neurons to axonal transport defects induced by mutant huntingtin.* Journal of Neuroscience, 2008. **28**(50): p. 13662-13672.
50. Smith, R., P. Brundin, and J.-Y. Li, *Synaptic dysfunction in Huntington's disease: a new perspective.* Cellular and Molecular Life Sciences CMLS, 2005. **62**(17): p. 1901-1912.
51. Trushina, E., et al., *Mutant huntingtin impairs axonal trafficking in mammalian neurons in vivo and in vitro.* Mol Cell Biol, 2004. **24**(18): p. 8195-209.
52. Martin, D.D., et al., *Identification of a post-translationally myristoylated autophagy-inducing domain released by caspase cleavage of huntingtin.* Human molecular genetics, 2014. **23**(12): p. 3166-3179.
53. Steffan, J.S., *Does Huntingtin play a role in selective macroautophagy?* Cell cycle, 2010. **9**(17): p. 3401-3413.
54. Wong, Y.C. and E.L. Holzbaur, *The regulation of autophagosome dynamics by huntingtin and HAP1 is disrupted by expression of mutant huntingtin, leading to defective cargo degradation.* Journal of Neuroscience, 2014. **34**(4): p. 1293-1305.
55. Mangiarini, L., et al., *Exon 1 of the HD gene with an expanded CAG repeat is sufficient to cause a progressive neurological phenotype in transgenic mice.* Cell, 1996. **87**(3): p. 493-506.
56. Scherzinger, E., et al., *Huntingtin-encoded polyglutamine expansions form amyloid-like protein aggregates in vitro and in vivo.* Cell, 1997. **90**(3): p. 549-558.
57. Wellington, C.L., et al., *Toward understanding the molecular pathology of Huntington's disease.* Brain Pathology, 1997. **7**(3): p. 979-1002.
58. Huang, C.C., et al., *Amyloid formation by mutant huntingtin: threshold, progressivity and recruitment of normal polyglutamine proteins.* Somatic cell and molecular genetics, 1998. **24**(4): p. 217-233.
59. Shen, K., et al., *Control of the structural landscape and neuronal proteotoxicity of mutant Huntingtin by domains flanking the polyQ tract.* Elife, 2016. **5**: p. e18065.
60. Sugars, K.L. and D.C. Rubinsztein, *Transcriptional abnormalities in Huntington disease.* Trends in genetics, 2003. **19**(5): p. 233-238.
61. Sassone, J., et al., *Huntington's disease: the current state of research with peripheral tissues.* Experimental neurology, 2009. **219**(2): p. 385-397.
62. Halliday, G., et al., *Regional specificity of brain atrophy in Huntington's disease.* Experimental neurology, 1998. **154**(2): p. 663-672.
63. Vonsattel, J.P.G. and M. DiFiglia, *Huntington disease.* Journal of neuropathology and experimental neurology, 1998. **57**(5): p. 369.
64. Politis, M., et al., *Hypothalamic involvement in Huntington's disease: an in vivo PET study.* Brain, 2008. **131**(11): p. 2860-2869.
65. Martin, B., et al., *Therapeutic perspectives for the treatment of Huntington's disease: treating the whole body.* Histology and histopathology, 2008. **23**(2): p. 237.
66. Gardiner, S.L., et al., *Bioenergetics in fibroblasts of patients with Huntington disease are associated with age at onset.* Neurology Genetics, 2018. **4**(5): p. e275.
67. Jędrak, P., et al., *Mitochondrial alterations accompanied by oxidative stress conditions in skin fibroblasts of Huntington's disease patients.* Metabolic brain disease, 2018. **33**(6): p. 2005-2017.
68. Aziz, N.A., et al., *Weight loss in Huntington disease increases with higher CAG repeat number.* Neurology, 2008. **71**(19): p. 1506-1513.
69. Lakra, P., K. Aditi, and N. Agrawal, *Peripheral expression of mutant huntingtin is a critical determinant of weight loss and metabolic disturbances in Huntington's disease.* Scientific reports, 2019. **9**(1): p. 1-15.
70. Petersén, Å., et al., *Orexin loss in Huntington's disease.* Human molecular genetics, 2005. **14**(1): p. 39-47.
71. Aziz, A., et al., *Hypocretin and melanin-concentrating hormone in patients with Huntington disease.* Brain pathology, 2008. **18**(4): p. 474-483.
72. Saleh, N., et al., *Neuroendocrine disturbances in Huntington's disease.* PloS one, 2009. **4**(3).

73. Markianos, M., et al., *Plasma testosterone in male patients with Huntington's disease: relations to severity of illness and dementia.* Annals of neurology, 2005. **57**(4): p. 520-525.
74. Mihm, M.J., et al., *Cardiac dysfunction in the R6/2 mouse model of Huntington's disease.* Neurobiology of disease, 2007. **25**(2): p. 297-308.
75. Lanska, D.J., et al., *Conditions associated with huntington's disease at death: a case-control study.* Archives of neurology, 1988. **45**(8): p. 878-880.
76. Goodman, A.O., et al., *The metabolic profile of early Huntington's disease-a combined human and transgenic mouse study.* Experimental neurology, 2008. **210**(2): p. 691-698.
77. Hofer, S., et al., *Studying Huntington's disease in yeast: from mechanisms to pharmacological approaches.* Frontiers in molecular neuroscience, 2018. **11**: p. 318.
78. Wang, H.-Q., et al., *Overexpression of F0F1-ATP synthase α suppresses mutant huntingtin aggregation and toxicity in vitro.* Biochemical and biophysical research communications, 2009. **390**(4): p. 1294-1298.
79. Jędrak, P., et al., *Mitochondrial alterations accompanied by oxidative stress conditions in skin fibroblasts of Huntington's disease patients.* Metabolic brain disease, 2018. **33**(6): p. 2005-2017.
80. Liu, Y., et al., *Direct reprogramming of Huntington's disease patient fibroblasts into neuron-like cells leads to abnormal neurite outgrowth, increased cell death, and aggregate formation.* PloS one, 2014. **9**(10).
81. Xue, Y., et al., *Direct conversion of fibroblasts to neurons by reprogramming PTB-regulated microRNA circuits.* Cell, 2013. **152**(1-2): p. 82-96.
82. Davies, S.W., et al., *Formation of neuronal intranuclear inclusions underlies the neurological dysfunction in mice transgenic for the HD mutation.* Cell, 1997. **90**(3): p. 537-548.
83. Gu, X., et al., *Serines 13 and 16 are critical determinants of full-length human mutant huntingtin induced disease pathogenesis in HD mice.* Neuron, 2009. **64**(6): p. 828-840.
84. Bates, G.P., et al., *Huntington disease.* Nature reviews Disease primers, 2015. **1**(1): p. 1-21.
85. Seredenina, T. and R. Luthi-Carter, *What have we learned from gene expression profiles in Huntington's disease?* Neurobiology of disease, 2012. **45**(1): p. 83-98.
86. Reddy, P.H. and U.P. Shirendeb, *Mutant huntingtin, abnormal mitochondrial dynamics, defective axonal transport of mitochondria, and selective synaptic degeneration in Huntington's disease.* Biochimica et Biophysica Acta (BBA)-Molecular Basis of Disease, 2012. **1822**(2): p. 101-110.
87. Kim, M., et al., *Mutant huntingtin expression in clonal striatal cells: dissociation of inclusion formation and neuronal survival by caspase inhibition.* Journal of Neuroscience, 1999. **19**(3): p. 964-973.
88. Nithianantharajah, J. and A. Hannan, *Dysregulation of synaptic proteins, dendritic spine abnormalities and pathological plasticity of synapses as experience-dependent mediators of cognitive and psychiatric symptoms in Huntington's disease.* Neuroscience, 2013. **251**: p. 66-74.
89. Luthi-Carter, R., et al., *Dysregulation of gene expression in the R6/2 model of polyglutamine disease: parallel changes in muscle and brain.* Human molecular genetics, 2002. **11**(17): p. 1911-1926.
90. Strand, A.D., et al., *Gene expression in Huntington's disease skeletal muscle: a potential biomarker.* Human molecular genetics, 2005. **14**(13): p. 1863-1876.
91. Chaturvedi, R.K., et al., *Impaired PGC-1α function in muscle in Huntington's disease.* Human molecular genetics, 2009. **18**(16): p. 3048-3065.
92. Seo, H., K.C. Sonntag, and O. Isacson, *Generalized brain and skin proteasome inhibition in Huntington's disease.* Annals of neurology, 2004. **56**(3): p. 319-328.
93. Seo, H., et al., *Proteasome activator enhances survival of Huntington's disease neuronal model cells.* PloS one, 2007. **2**(2).
94. Saft, C., et al., *Mitochondrial impairment in patients and asymptomatic mutation carriers of Huntington's disease.* Movement disorders: official journal of the Movement Disorder Society, 2005. **20**(6): p. 674-679.
95. Oliveira, J.M. and R.N. Lightowlers, *Could successful (mitochondrial) networking help prevent Huntington's disease?* EMBO molecular medicine, 2010. **2**(12): p. 487-489.

96. Marchina, E., et al., *Gene expression profile in fibroblasts of Huntington's disease patients and controls.* Journal of the Neurological Sciences, 2014. **337**(1-2): p. 42-46.
97. Reddy, P.H., *Increased mitochondrial fission and neuronal dysfunction in Huntington's disease: implications for molecular inhibitors of excessive mitochondrial fission.* Drug discovery today, 2014. **19**(7): p. 951-955.
98. STAHL, W.L. and P.D. SWANSON, *Biochemical abnormalities in Huntington's chorea brains.* Neurology, 1974. **24**(9): p. 813-813.
99. GOEBEL, H.H., et al., *Juvenile Huntington chorea: clinical, ultrastructural, and biochemical studies.* Neurology, 1978. **28**(1): p. 23-23.
100. Tellez-Nagel, I., A.B. Johnson, and R.D. Terry, *Studies on brain biopsies of patients with Huntington's chorea.* Journal of Neuropathology & Experimental Neurology, 1974. **33**(2): p. 308-332.
101. Browne, S.E., et al., *Oxidative damage and metabolic dysfunction in Huntington's disease: selective vulnerability of the basal ganglia.* Annals of Neurology: Official Journal of the American Neurological Association and the Child Neurology Society, 1997. **41**(5): p. 646-653.
102. Gu, M., et al., *Mitochondrial defect in Huntington's disease caudate nucleus.* Annals of Neurology: Official Journal of the American Neurological Association and the Child Neurology Society, 1996. **39**(3): p. 385-389.
103. Mann, V., et al., *Mitochondrial function and parental sex effect in Huntington's disease.* The Lancet, 1990. **336**(8717): p. 749.
104. Seong, I.S., et al., *HD CAG repeat implicates a dominant property of huntingtin in mitochondrial energy metabolism.* Human molecular genetics, 2005. **14**(19): p. 2871-2880.
105. Lodi, R., et al., *Abnormal in vivo skeletal muscle energy metabolism in Huntington's disease and dentatorubropallidoluysian atrophy.* Annals of neurology, 2000. **48**(1): p. 72-76.
106. Zorova, L.D., et al., *Mitochondrial membrane potential.* Analytical biochemistry, 2018. **552**: p. 50-59.
107. Sawa, A., et al., *Increased apoptosis of Huntington disease lymphoblasts associated with repeat length-dependent mitochondrial depolarization.* Nature medicine, 1999. **5**(10): p. 1194-1198.
108. Singh, A., et al., *Oxidative stress: a key modulator in neurodegenerative diseases.* Molecules, 2019. **24**(8): p. 1583.
109. Vinogradov, A.D. and V.G. Grivennikova, *Oxidation of NADH and ROS production by respiratory complex I.* Biochimica et Biophysica Acta (BBA)-Bioenergetics, 2016. **1857**(7): p. 863-871.
110. Bleier, L. and S. Dröse, *Superoxide generation by complex III: from mechanistic rationales to functional consequences.* Biochimica et Biophysica Acta (BBA)-Bioenergetics, 2013. **1827**(11-12): p. 1320-1331.
111. Browne, S.E., R.J. Ferrante, and M.F. Beal, *Oxidative stress in Huntington's disease.* Brain pathology, 1999. **9**(1): p. 147-163.
112. Kim, G.H., et al., *The role of oxidative stress in neurodegenerative diseases.* Experimental neurobiology, 2015. **24**(4): p. 325-340.
113. Pisoschi, A.M. and A. Pop, *The role of antioxidants in the chemistry of oxidative stress: A review.* European journal of medicinal chemistry, 2015. **97**: p. 55-74.
114. Votyakova, T.V. and I.J. Reynolds, *ΔΨm-Dependent and-independent production of reactive oxygen species by rat brain mitochondria.* Journal of neurochemistry, 2001. **79**(2): p. 266-277.
115. Angelova, P.R. and A.Y. Abramov, *Role of mitochondrial ROS in the brain: from physiology to neurodegeneration.* FEBS letters, 2018. **592**(5): p. 692-702.
116. Jahani-Asl, A., et al., *Mitofusin 2 protects cerebellar granule neurons against injury-induced cell death.* Journal of Biological Chemistry, 2007. **282**(33): p. 23788-23798.
117. Chen, X.J. and R.A. Butow, *The organization and inheritance of the mitochondrial genome.* Nature Reviews Genetics, 2005. **6**(11): p. 815-825.
118. Pfanner, N. and A. Geissler, *Versatility of the mitochondrial protein import machinery.* Nature reviews Molecular cell biology, 2001. **2**(5): p. 339-349.
119. Neupert, W. and J.M. Herrmann, *Translocation of proteins into mitochondria.* Annu. Rev. Biochem., 2007. **76**: p. 723-749.

120. Westermann, B., *Mitochondrial fusion and fission in cell life and death.* Nature reviews Molecular cell biology, 2010. **11**(12): p. 872-884.
121. Youle, R.J. and A.M. Van Der Bliek, *Mitochondrial fission, fusion, and stress.* Science, 2012. **337**(6098): p. 1062-1065.
122. Novak, I. and I. Dikic, *Autophagy receptors in developmental clearance of mitochondria.* Autophagy, 2011. **7**(3): p. 301-303.
123. Knott, A.B. and E. Bossy-Wetzel, *Impairing the mitochondrial fission and fusion balance: a new mechanism of neurodegeneration.* Annals of the New York Academy of Sciences, 2008. **1147**: p. 283-292.
124. Knott, A.B., et al., *Mitochondrial fragmentation in neurodegeneration.* Nature Reviews Neuroscience, 2008. **9**(7): p. 505-518.
125. Losón, O.C., et al., *Fis1, Mff, MiD49, and MiD51 mediate Drp1 recruitment in mitochondrial fission.* Molecular biology of the cell, 2013. **24**(5): p. 659-667.
126. Hatch, A.L., P.S. Gurel, and H.N. Higgs, *Novel roles for actin in mitochondrial fission.* Journal of cell science, 2014. **127**(21): p. 4549-4560.
127. Ingerman, E., et al., *Dnm1 forms spirals that are structurally tailored to fit mitochondria.* The Journal of cell biology, 2005. **170**(7): p. 1021-1027.
128. Knott, A.B. and E. Bossy-Wetzel, *Impairing the mitochondrial fission and fusion balance: a new mechanism of neurodegeneration.* Annals of the New York Academy of Sciences, 2008. **1147**: p. 283.
129. Griffin, E.E., S.A. Detmer, and D.C. Chan, *Molecular mechanism of mitochondrial membrane fusion.* Biochimica et Biophysica Acta (BBA)-Molecular Cell Research, 2006. **1763**(5-6): p. 482-489.
130. Chen, H., et al., *Mitofusins Mfn1 and Mfn2 coordinately regulate mitochondrial fusion and are essential for embryonic development.* The Journal of cell biology, 2003. **160**(2): p. 189-200.
131. Ishihara, N., Y. Eura, and K. Mihara, *Mitofusin 1 and 2 play distinct roles in mitochondrial fusion reactions via GTPase activity.* Journal of cell science, 2004. **117**(26): p. 6535-6546.
132. Koshiba, T., et al., *Structural basis of mitochondrial tethering by mitofusin complexes.* Science, 2004. **305**(5685): p. 858-862.
133. Duvezin-Caubet, S., et al., *OPA1 processing reconstituted in yeast depends on the subunit composition of the m-AAA protease in mitochondria.* Molecular biology of the cell, 2007. **18**(9): p. 3582-3590.
134. Griparic, L., T. Kanazawa, and A.M. van der Bliek, *Regulation of the mitochondrial dynamin-like protein Opa1 by proteolytic cleavage.* Journal of Cell Biology, 2007. **178**(5): p. 757-764.
135. Song, Z., et al., *OPA1 processing controls mitochondrial fusion and is regulated by mRNA splicing, membrane potential, and Yme1L.* The Journal of cell biology, 2007. **178**(5): p. 749-755.
136. Twig, G., et al., *Fission and selective fusion govern mitochondrial segregation and elimination by autophagy.* The EMBO journal, 2008. **27**(2): p. 433-446.
137. Kim, J., et al., *Mitochondrial loss, dysfunction and altered dynamics in Huntington's disease.* Human molecular genetics, 2010. **19**(20): p. 3919-3935.
138. Shirendeb, U., et al., *Abnormal mitochondrial dynamics, mitochondrial loss and mutant huntingtin oligomers in Huntington's disease: implications for selective neuronal damage.* Human molecular genetics, 2011. **20**(7): p. 1438-1455.
139. Costa, V. and L. Scorrano, *Shaping the role of mitochondria in the pathogenesis of Huntington's disease.* The EMBO journal, 2012. **31**(8): p. 1853-1864.
140. Cereghetti, G., et al., *Dephosphorylation by calcineurin regulates translocation of Drp1 to mitochondria.* Proceedings of the National Academy of Sciences, 2008. **105**(41): p. 15803-15808.
141. Cherubini, M., L. Lopez-Molina, and S. Gines, *Mitochondrial fission in Huntington's disease mouse striatum disrupts ER-mitochondria contacts leading to disturbances in Ca2+ efflux and Reactive Oxygen Species (ROS) homeostasis.* Neurobiology of Disease, 2020. **136**: p. 104741.
142. Song, W., et al., *Mutant huntingtin binds the mitochondrial fission GTPase dynamin-related protein-1 and increases its enzymatic activity.* Nature medicine, 2011. **17**(3): p. 377-382.

143. Barsoum, M.J., et al., *Nitric oxide-induced mitochondrial fission is regulated by dynamin-related GTPases in neurons.* The EMBO journal, 2006. **25**(16): p. 3900-3911.
144. McGahan, L., A. Hakim, and G. Robertson, *Hippocampal Myc and p53 expression following transient global ischemia.* Molecular brain research, 1998. **56**(1-2): p. 133-145.
145. Beal, M.F. and R.J. Ferrante, *Experimental therapeutics in transgenic mouse models of Huntington's disease.* Nature Reviews Neuroscience, 2004. **5**(5): p. 373-384.
146. Rebec, G.V., et al., *Ascorbate treatment attenuates the Huntington behavioral phenotype in mice.* Neuroreport, 2003. **14**(9): p. 1263-1265.
147. Klivenyi, P., et al., *Increased survival and neuroprotective effects of BN82451 in a transgenic mouse model of Huntington's disease.* Journal of neurochemistry, 2003. **86**(1): p. 267-272.
148. Young, A.J., et al., *Coenzyme Q10: a review of its promise as a neuroprotectant.* CNS spectrums, 2007. **12**(1): p. 62-68.
149. Ferrante, R.J., et al., *Therapeutic effects of coenzyme Q10 and remacemide in transgenic mouse models of Huntington's disease.* Journal of Neuroscience, 2002. **22**(5): p. 1592-1599.
150. Smith, K.M., et al., *Dose ranging and efficacy study of high-dose coenzyme Q10 formulations in Huntington's disease mice.* Biochimica et Biophysica Acta (BBA)-Molecular Basis of Disease, 2006. **1762**(6): p. 616-626.
151. Damiano, M., et al., *Mitochondria in Huntington's disease.* Biochimica et Biophysica Acta (BBA)-Molecular Basis of Disease, 2010. **1802**(1): p. 52-61.
152. Naia, L., et al., *Histone deacetylase inhibitors protect against pyruvate dehydrogenase dysfunction in Huntington's disease.* Journal of Neuroscience, 2017. **37**(10): p. 2776-2794.
153. Naia, L., et al., *Comparative mitochondrial-based protective effects of resveratrol and nicotinamide in Huntington's disease models.* Molecular neurobiology, 2017. **54**(7): p. 5385-5399.
154. Yin, X., M. Manczak, and P.H. Reddy, *Mitochondria-targeted molecules MitoQ and SS31 reduce mutant huntingtin-induced mitochondrial toxicity and synaptic damage in Huntington's disease.* Human molecular genetics, 2016. **25**(9): p. 1739-1753.
155. Manczak, M. and P.H. Reddy, *Mitochondrial division inhibitor 1 protects against mutant huntingtin-induced abnormal mitochondrial dynamics and neuronal damage in Huntington's disease.* Human molecular genetics, 2015. **24**(25): p. 7308-7325.
156. Ruan, L., et al., *Cytosolic proteostasis through importing of misfolded proteins into mitochondria.* Nature, 2017. **543**(7645): p. 443-446.
157. Labbadia, J., et al., *Mitochondrial stress restores the heat shock response and prevents proteostasis collapse during aging.* Cell reports, 2017. **21**(6): p. 1481-1494.
158. Kim, H.-E., et al., *Lipid biosynthesis coordinates a mitochondrial-to-cytosolic stress response.* Cell, 2016. **166**(6): p. 1539-1552. e16.
159. Yerbury, J.J., et al., *Walking the tightrope: proteostasis and neurodegenerative disease.* Journal of neurochemistry, 2016. **137**(4): p. 489-505.
160. Li, W. and Y. Ye, *Polyubiquitin chains: functions, structures, and mechanisms.* Cellular and Molecular Life Sciences, 2008. **65**(15): p. 2397-2406.
161. Rubio, I., et al., *Effects of partial suppression of parkin on huntingtin mutant R6/1 mice.* Brain research, 2009. **1281**: p. 91-100.
162. Komander, D. and M. Rape, *The ubiquitin code.* Annual review of biochemistry, 2012. **81**: p. 203-229.
163. Chen, Z.J. and L.J. Sun, *Nonproteolytic functions of ubiquitin in cell signaling.* Molecular cell, 2009. **33**(3): p. 275-286.
164. Menzies, F.M., K. Moreau, and D.C. Rubinsztein, *Protein misfolding disorders and macroautophagy.* Current opinion in cell biology, 2011. **23**(2): p. 190-197.
165. Rubinsztein, D.C., et al., *Potential therapeutic applications of autophagy.* Nature reviews Drug discovery, 2007. **6**(4): p. 304-312.
166. Yang, Z. and D.J. Klionsky, *Eaten alive: a history of macroautophagy.* Nature cell biology, 2010. **12**(9): p. 814-822.
167. Martin, D.D., et al., *Autophagy in Huntington disease and huntingtin in autophagy.* Trends in neurosciences, 2015. **38**(1): p. 26-35.

168. Ashkenazi, A., et al., *Polyglutamine tracts regulate beclin 1-dependent autophagy.* Nature, 2017. **545**(7652): p. 108-111.
169. Rui, Y.-N., et al., *Huntingtin functions as a scaffold for selective macroautophagy.* Nature cell biology, 2015. **17**(3): p. 262-275.
170. Rui, Y.-N., et al., *HTT/Huntingtin in selective autophagy and Huntington disease: a foe or a friend within?* Autophagy, 2015. **11**(5): p. 858-860.
171. Livneh, I., et al., *Monoubiquitination joins polyubiquitination as an esteemed proteasomal targeting signal.* BioEssays, 2017. **39**(6): p. 1700027.
172. Glickman, M.H., et al., *The regulatory particle of the Saccharomyces cerevisiae proteasome.* Molecular and cellular biology, 1998. **18**(6): p. 3149-3162.
173. Voges, D., P. Zwickl, and W. Baumeister, *The 26S proteasome: a molecular machine designed for controlled proteolysis.* Annual review of biochemistry, 1999. **68**(1): p. 1015-1068.
174. Pickart, C.M. and R.E. Cohen, *Proteasomes and their kin: proteases in the machine age.* Nature reviews Molecular cell biology, 2004. **5**(3): p. 177-187.
175. Heo, J.-M. and J. Rutter, *Ubiquitin-dependent mitochondrial protein degradation.* The international journal of biochemistry & cell biology, 2011. **43**(10): p. 1422-1426.
176. Bragoszewski, P., M. Turek, and A. Chacinska, *Control of mitochondrial biogenesis and function by the ubiquitin-proteasome system.* Open biology, 2017. **7**(4): p. 170007.
177. Waelter, S., et al., *Accumulation of mutant huntingtin fragments in aggresome-like inclusion bodies as a result of insufficient protein degradation.* Molecular biology of the cell, 2001. **12**(5): p. 1393-1407.
178. Díaz-Hernández, M., et al., *Inhibition of 26S proteasome activity by huntingtin filaments but not inclusion bodies isolated from mouse and human brain.* Journal of neurochemistry, 2006. **98**(5): p. 1585-1596.
179. Schipper-Krom, S., et al., *Dynamic recruitment of active proteasomes into polyglutamine initiated inclusion bodies.* FEBS letters, 2014. **588**(1): p. 151-159.
180. Bennett, E.J., et al., *Global impairment of the ubiquitin-proteasome system by nuclear or cytoplasmic protein aggregates precedes inclusion body formation.* Molecular cell, 2005. **17**(3): p. 351-365.
181. Harding, R.J. and Y.-f. Tong, *Proteostasis in Huntington's disease: disease mechanisms and therapeutic opportunities.* Acta Pharmacologica Sinica, 2018. **39**(5): p. 754-769.
182. Holmberg, C.I., et al., *Inefficient degradation of truncated polyglutamine proteins by the proteasome.* The EMBO journal, 2004. **23**(21): p. 4307-4318.
183. Venkatraman, P., et al., *Eukaryotic proteasomes cannot digest polyglutamine sequences and release them during degradation of polyglutamine-containing proteins.* Molecular cell, 2004. **14**(1): p. 95-104.
184. Michalik, A. and C. Van Broeckhoven, *Proteasome degrades soluble expanded polyglutamine completely and efficiently.* Neurobiology of disease, 2004. **16**(1): p. 202-211.
185. Juenemann, K., et al., *Expanded polyglutamine-containing N-terminal huntingtin fragments are entirely degraded by mammalian proteasomes.* Journal of Biological Chemistry, 2013. **288**(38): p. 27068-27084.
186. Kish-Trier, E. and C.P. Hill, *Structural biology of the proteasome.* Annual review of biophysics, 2013. **42**: p. 29-49.
187. Jung, T., B. Catalgol, and T. Grune, *The proteasomal system.* Molecular aspects of medicine, 2009. **30**(4): p. 191-296.
188. Basler, M. and M. Groettrup, *Immunoproteasome-specific inhibitors and their application*, in *Ubiquitin Family Modifiers and the Proteasome*. 2012, Springer. p. 391-401.
189. Nandi, D., et al., *The ubiquitin-proteasome system.* Journal of biosciences, 2006. **31**(1): p. 137-155.
190. Tanaka, K., *The proteasome: overview of structure and functions.* Proceedings of the Japan Academy, Series B, 2009. **85**(1): p. 12-36.
191. Jung, T. and T. Grune, *The proteasome and its role in the degradation of oxidized proteins.* IUBMB life, 2008. **60**(11): p. 743-752.

192. Baugh, J.M., E.G. Viktorova, and E.V. Pilipenko, *Proteasomes can degrade a significant proportion of cellular proteins independent of ubiquitination.* Journal of molecular biology, 2009. **386**(3): p. 814-827.
193. Asher, G., et al., *A mechanism of ubiquitin-independent proteasomal degradation of the tumor suppressors p53 and p73.* Genes & development, 2005. **19**(3): p. 316-321.
194. Davies, K.J., *Degradation of oxidized proteins by the 20S proteasome.* Biochimie, 2001. **83**(3-4): p. 301-310.
195. Shringarpure, R., et al., *Ubiquitin conjugation is not required for the degradation of oxidized proteins by proteasome.* Journal of Biological Chemistry, 2003. **278**(1): p. 311-318.
196. Asher, G., N. Reuven, and Y. Shaul, *20S proteasomes and protein degradation "by default".* Bioessays, 2006. **28**(8): p. 844-849.
197. Hochstrasser, M., *Ubiquitin-dependent protein degradation.* Annual review of genetics, 1996. **30**(1): p. 405-439.
198. Ju, D. and Y. Xie, *Proteasomal degradation of RPN4 via two distinct mechanisms, ubiquitin-dependent and-independent.* Journal of Biological Chemistry, 2004. **279**(23): p. 23851-23854.
199. Grune, T., et al., *Tau protein degradation is catalyzed by the ATP/ubiquitin-independent 20S proteasome under normal cell conditions.* Archives of biochemistry and biophysics, 2010. **500**(2): p. 181-188.
200. Stadtmueller, B.M. and C.P. Hill, *Proteasome activators.* Molecular cell, 2011. **41**(1): p. 8-19.
201. Brehm, A. and E. Krüger. *Dysfunction in protein clearance by the proteasome: impact on autoinflammatory diseases*. in *Seminars in immunopathology*. 2015. Springer.
202. Rêgo, A.T. and P.C. da Fonseca, *Characterization of fully recombinant human 20S and 20S-PA200 proteasome complexes.* Molecular cell, 2019. **76**(1): p. 138-147. e5.
203. Sugiyama, M., et al., *Spatial arrangement and functional role of α subunits of proteasome activator PA28 in hetero-oligomeric form.* Biochemical and biophysical research communications, 2013. **432**(1): p. 141-145.
204. Whitby, F.G., et al., *Structural basis for the activation of 20S proteasomes by 11S regulators.* Nature, 2000. **408**(6808): p. 115-120.
205. Song, X., et al., *A model for the quaternary structure of the proteasome activator PA28.* Journal of Biological Chemistry, 1996. **271**(42): p. 26410-26417.
206. Ahn, J.Y., et al., *Primary structures of two homologous subunits of PA28, a γ-interferon-inducible protein activator of the 20S proteasome.* FEBS letters, 1995. **366**(1): p. 37-42.
207. Huber, E.M. and M. Groll, *The Mammalian Proteasome Activator PA28 Forms an Asymmetric α4β3 Complex.* Structure, 2017. **25**(10): p. 1473-1480.e3.
208. Soza, A., et al., *Expression and subcellular localization of mouse 20S proteasome activator complex PA28.* FEBS letters, 1997. **413**(1): p. 27-34.
209. Wójcik, C., et al., *Proteasome activator (PA28) subunits, α, β and γ (Ki antigen) in NT2 neuronal precursor cells and HeLa S3 cells.* European journal of cell biology, 1998. **77**(2): p. 151-160.
210. Jeon, J., et al., *Gene therapy by proteasome activator, PA28γ, improves motor coordination and proteasome function in Huntington's disease YAC128 mice.* Neuroscience, 2016. **324**: p. 20-28.
211. Ustrell, V., et al., *PA200, a nuclear proteasome activator involved in DNA repair.* The EMBO Journal, 2002. **21**(13): p. 3516-3525.
212. Moore, C., *Further characterizations of bleomycin-sensitive (blm) mutants of Saccharomyces cerevisiae with implications for a radiomimetic model.* Journal of bacteriology, 1991. **173**(11): p. 3605-3608.
213. Rechsteiner, M. and C.P. Hill, *Mobilizing the proteolytic machine: cell biological roles of proteasome activators and inhibitors.* Trends in cell biology, 2005. **15**(1): p. 27-33.
214. Febres, D.E., et al., *The novel BLM3 gene encodes a protein that protects against lethal effects of oxidative damage.* Cellular and molecular biology (Noisy-le-Grand, France), 2001. **47**(7): p. 1149-1162.
215. McCullock, S., et al., *blm3-1 is an allele of UBP3, a ubiquitin protease that appears to act during transcription of damaged DNA.* Journal of molecular biology, 2006. **363**(3): p. 660-672.

216. Iwanczyk, J., et al., *Structure of the Blm10–20 S proteasome complex by cryo-electron microscopy. Insights into the mechanism of activation of mature yeast proteasomes.* Journal of molecular biology, 2006. **363**(3): p. 648-659.
217. Toste Rêgo, A. and P.C.A. da Fonseca, *Characterization of Fully Recombinant Human 20S and 20S-PA200 Proteasome Complexes.* Molecular Cell, 2019. **76**(1): p. 138-147.e5.
218. Guan, H., et al., *Cryo-EM structures of the human PA200 and PA200-20S complex reveal regulation of proteasome gate opening and two PA200 apertures.* PLoS biology, 2020. **18**(3): p. e3000654.
219. Schmidt, M., et al., *The HEAT repeat protein Blm10 regulates the yeast proteasome by capping the core particle.* Nature structural & molecular biology, 2005. **12**(4): p. 294-303.
220. Blickwedehl, J., et al., *Role for proteasome activator PA200 and postglutamyl proteasome activity in genomic stability.* Proceedings of the National Academy of Sciences, 2008. **105**(42): p. 16165-16170.
221. Ortega, J., et al., *The axial channel of the 20 S proteasome opens upon binding of the PA200 activator.* Journal of molecular biology, 2005. **346**(5): p. 1221-1227.
222. Qian, M.-X., et al., *Acetylation-mediated proteasomal degradation of core histones during DNA repair and spermatogenesis.* Cell, 2013. **153**(5): p. 1012-1024.
223. Dange, T., et al., *Blm10 protein promotes proteasomal substrate turnover by an active gating mechanism.* Journal of Biological Chemistry, 2011. **286**(50): p. 42830-42839.
224. Rapić-Otrin, V., et al., *Sequential binding of UV DNA damage binding factor and degradation of the p48 subunit as early events after UV irradiation.* Nucleic acids research, 2002. **30**(11): p. 2588-2598.
225. Ciechanover, A. and Y.T. Kwon, *Degradation of misfolded proteins in neurodegenerative diseases: therapeutic targets and strategies.* Experimental & molecular medicine, 2015. **47**(3): p. e147-e147.
226. Sorrentino, V., K.J. Menzies, and J. Auwerx, *Repairing mitochondrial dysfunction in disease.* Annual review of pharmacology and toxicology, 2018. **58**: p. 353-389.
227. Wyant, K.J., A.J. Ridder, and P. Dayalu, *Huntington's disease—update on treatments.* Current neurology and neuroscience reports, 2017. **17**(4): p. 33.
228. Wild, E.J. and S.J. Tabrizi, *Therapies targeting DNA and RNA in Huntington's disease.* The Lancet Neurology, 2017. **16**(10): p. 837-847.
229. Tabrizi, S.J., et al., *Huntington disease: new insights into molecular pathogenesis and therapeutic opportunities.* Nature Reviews Neurology, 2020. **16**(10): p. 529-546.
230. Kwon, D., *Failure of genetic therapies for Huntington's devastates community.* Nature, 2021.
231. McKinnon, C. and S.J. Tabrizi, *The ubiquitin-proteasome system in neurodegeneration.* Antioxidants & redox signaling, 2014. **21**(17): p. 2302-2321.
232. Bhat, K.P., et al., *Differential ubiquitination and degradation of huntingtin fragments modulated by ubiquitin-protein ligase E3A.* Proceedings of the National Academy of Sciences, 2014. **111**(15): p. 5706-5711.
233. Jana, N.R., et al., *Co-chaperone CHIP associates with expanded polyglutamine protein and promotes their degradation by proteasomes.* Journal of Biological Chemistry, 2005. **280**(12): p. 11635-11640.
234. Luo, H., et al., *Herp promotes degradation of mutant huntingtin: involvement of the proteasome and molecular chaperones.* Molecular neurobiology, 2018. **55**(10): p. 7652-7668.
235. Koyuncu, S., et al., *The ubiquitin ligase UBR5 suppresses proteostasis collapse in pluripotent stem cells from Huntington's disease patients.* Nature communications, 2018. **9**(1): p. 2886.
236. Kumarapeli, A.R., et al., *A novel transgenic mouse model reveals deregulation of the ubiquitin-proteasome system in the heart by doxorubicin.* The FASEB journal, 2005. **19**(14): p. 2051-2053.
237. Liu, Y., et al., *Sulforaphane enhances proteasomal and autophagic activities in mice and is a potential therapeutic reagent for Huntington's disease.* Journal of neurochemistry, 2014. **129**(3): p. 539-547.
238. Jang, M. and I.-H. Cho, *Sulforaphane ameliorates 3-nitropropionic acid-induced striatal toxicity by activating the Keap1-Nrf2-ARE pathway and inhibiting the MAPKs and NF-κB pathways.* Molecular neurobiology, 2016. **53**(4): p. 2619-2635.

239. Luis-García, E.R., et al., *Sulforaphane prevents quinolinic acid-induced mitochondrial dysfunction in rat striatum.* Journal of biochemical and molecular toxicology, 2017. **31**(2): p. e21837.
240. DeMarch, Z., et al., *Beneficial effects of rolipram in the R6/2 mouse model of Huntington's disease.* Neurobiology of disease, 2008. **30**(3): p. 375-387.
241. Wong, H.K., et al., *Blocking acid-sensing ion channel 1 alleviates Huntington's disease pathology via an ubiquitin-proteasome system-dependent mechanism.* Human molecular genetics, 2008. **17**(20): p. 3223-3235.
242. Tomoshige, S., et al., *Discovery of small molecules that induce the degradation of huntingtin.* Angewandte Chemie International Edition, 2017. **56**(38): p. 11530-11533.
243. Butler, D.C. and A. Messer, *Bifunctional anti-huntingtin proteasome-directed intrabodies mediate efficient degradation of mutant huntingtin exon 1 protein fragments.* PloS one, 2011. **6**(12).
244. Evers, M.M., et al., *Making (anti-) sense out of huntingtin levels in Huntington disease.* Molecular neurodegeneration, 2015. **10**(1): p. 21.
245. Douida, A., et al., *The proteasome activator PA200 regulates expression of genes involved in cell survival upon selective mitochondrial inhibition in neuroblastoma cells.* Journal of Cellular and Molecular Medicine, 2020.
246. Baker Brachmann, C., et al., *Designer deletion strains derived from Saccharomyces cerevisiae S288C: a useful set of strains and plasmids for PCR-mediated gene disruption and other applications.* Yeast, 1998. **14**(2): p. 115-132.
247. Gietz, R.D., et al., *Studies on the transformation of intact yeast cells by the LiAc/SS-DNA/PEG procedure.* Yeast, 1995. **11**(4): p. 355-360.
248. Mortimer, R.K. and J.R. Johnston, *Genealogy of principal strains of the yeast genetic stock center.* Genetics, 1986. **113**(1): p. 35-43.
249. Anton, F., et al., *Two deubiquitylases act on mitofusin and regulate mitochondrial fusion along independent pathways.* Molecular cell, 2013. **49**(3): p. 487-498.
250. Tar, K., et al., *Proteasomes associated with the Blm10 activator protein antagonize mitochondrial fission through degradation of the fission protein Dnm1.* Journal of Biological Chemistry, 2014. **289**(17): p. 12145-12156.
251. Kruegel, U., et al., *Elevated proteasome capacity extends replicative lifespan in Saccharomyces cerevisiae.* PLoS Genet, 2011. **7**(9): p. e1002253.
252. Narain, Y., et al., *A molecular investigation of true dominance in Huntington's disease.* Journal of medical genetics, 1999. **36**(10): p. 739-746.
253. Hipp, M.S., et al., *Indirect inhibition of 26S proteasome activity in a cellular model of Huntington's disease.* Journal of Cell Biology, 2012. **196**(5): p. 573-587.
254. Meriin, A.B., et al., *Huntingtin toxicity in yeast model depends on polyglutamine aggregation mediated by a prion-like protein Rnq1.* The Journal of cell biology, 2002. **157**(6): p. 997-1004.
255. Ocampo, A. and A. Barrientos, *Quick and reliable assessment of chronological life span in yeast cell populations by flow cytometry.* Mechanisms of ageing and development, 2011. **132**(6-7): p. 315-323.
256. Alberti, S., R. Halfmann, and S. Lindquist, *Biochemical, cell biological, and genetic assays to analyze amyloid and prion aggregation in yeast*, in *Methods in enzymology*. 2010, Elsevier. p. 709-734.
257. Dange, T., et al., *Blm10 protein promotes proteasomal substrate turnover by an active gating mechanism.* The Journal of biological chemistry, 2011. **286**(50): p. 42830-42839.
258. Elsasser, S., M. Schmidt, and D. Finley, *Characterization of the proteasome using native gel electrophoresis.* Methods in enzymology, 2005. **398**: p. 353-363.
259. Ishihama, Y., J. Rappsilber, and M. Mann, *Modular stop and go extraction tips with stacked disks for parallel and multidimensional Peptide fractionation in proteomics.* Journal of proteome research, 2006. **5**(4): p. 988-994.
260. Wickham, H., et al., *Welcome to the Tidyverse.* Journal of Open Source Software, 2019. **4**(43): p. 1686.
261. Polidori, M.C., et al., *Oxidative damage to mitochondrial DNA in Huntington's disease parietal cortex.* Neuroscience letters, 1999. **272**(1): p. 53-56.

262. Sorolla, M.A., et al., *Proteomic and oxidative stress analysis in human brain samples of Huntington disease.* Free Radical Biology and Medicine, 2008. **45**(5): p. 667-678.
263. Lin, M.T. and M.F. Beal, *Mitochondrial dysfunction and oxidative stress in neurodegenerative diseases.* Nature, 2006. **443**(7113): p. 787-795.
264. Kumar, A. and R.R. Ratan, *Oxidative stress and Huntington's disease: The good, the bad, and the ugly.* Journal of Huntington's disease, 2016. **5**(3): p. 217-237.
265. Mookerjee, S.A., et al., *Quantifying intracellular rates of glycolytic and oxidative ATP production and consumption using extracellular flux measurements.* Journal of Biological Chemistry, 2017. **292**(17): p. 7189-7207.
266. Ott, M., et al., *Mitochondria, oxidative stress and cell death.* Apoptosis, 2007. **12**(5): p. 913-922.
267. Westermann, B., *Bioenergetic role of mitochondrial fusion and fission.* Biochimica et Biophysica Acta (BBA)-Bioenergetics, 2012. **1817**(10): p. 1833-1838.
268. Pagliuso, A., P. Cossart, and F. Stavru, *The ever-growing complexity of the mitochondrial fission machinery.* Cellular and molecular life sciences, 2018. **75**(3): p. 355-374.
269. Mishra, P. and D.C. Chan, *Metabolic regulation of mitochondrial dynamics.* Journal of Cell Biology, 2016. **212**(4): p. 379-387.
270. Chen, H. and D.C. Chan, *Mitochondrial dynamics in regulating the unique phenotypes of cancer and stem cells.* Cell metabolism, 2017. **26**(1): p. 39-48.
271. Han, Y.H., et al., *The effect of MG132, a proteasome inhibitor on HeLa cells in relation to cell growth, reactive oxygen species and GSH.* Oncology reports, 2009. **22**(1): p. 215-221.
272. Roelofs, J., et al., *Native gel approaches in studying proteasome assembly and chaperones*, in *The Ubiquitin Proteasome System*. 2018, Springer. p. 237-260.
273. Yamamoto, A., et al., *Bafilomycin A1 prevents maturation of autophagic vacuoles by inhibiting fusion between autophagosomes and lysosomes in rat hepatoma cell line, H-4-II-E cells.* Cell structure and function, 1998. **23**(1): p. 33-42.
274. Tanida, I., T. Ueno, and E. Kominami, *LC3 and Autophagy*, in *Autophagosome and Phagosome*. 2008, Springer. p. 77-88.
275. Ichimura, Y. and M. Komatsu. *Selective degradation of p62 by autophagy*. in *Seminars in immunopathology*. 2010. Springer.
276. Narendra, D., et al., *Parkin is recruited selectively to impaired mitochondria and promotes their autophagy.* The Journal of cell biology, 2008. **183**(5): p. 795-803.
277. Um, J.W., et al., *Parkin directly modulates 26S proteasome activity.* Journal of Neuroscience, 2010. **30**(35): p. 11805-11814.
278. Wahabi, K., A. Perwez, and M.A. Rizvi, *Parkin in Parkinson's disease and Cancer: a double-edged sword.* Molecular neurobiology, 2018. **55**(8): p. 6788-6800.
279. Glauser, L., et al., *Parkin promotes the ubiquitination and degradation of the mitochondrial fusion factor mitofusin 1.* Journal of neurochemistry, 2011. **118**(4): p. 636-645.
280. Schneider-Poetsch, T., et al., *Inhibition of eukaryotic translation elongation by cycloheximide and lactimidomycin.* Nature chemical biology, 2010. **6**(3): p. 209-217.
281. de Loubresse, N.G., et al., *Structural basis for the inhibition of the eukaryotic ribosome.* Nature, 2014. **513**(7519): p. 517-522.
282. McColgan, P. and S.J. Tabrizi, *Huntington's disease: a clinical review.* European journal of neurology, 2018. **25**(1): p. 24-34.
283. Ross, C.A. and S.J. Tabrizi, *Huntington's disease: from molecular pathogenesis to clinical treatment.* The Lancet Neurology, 2011. **10**(1): p. 83-98.
284. Ocampo, A., A. Zambrano, and A. Barrientos, *Suppression of polyglutamine-induced cytotoxicity in Saccharomyces cerevisiae by enhancement of mitochondrial biogenesis.* The FASEB Journal, 2010. **24**(5): p. 1431-1441.
285. Mason, R.P. and F. Giorgini, *Modeling Huntington disease in yeast: perspectives and future directions.* Prion, 2011. **5**(4): p. 269-276.
286. Jiang, T.-X., et al., *Proteasome activator PA200 maintains stability of histone marks during transcription and aging.* Theranostics, 2021. **11**(3): p. 1458.

287. Chen, L.-B., et al., *Transcriptional upregulation of proteasome activator Blm10 antagonizes cellular aging.* Biochemical and Biophysical Research Communications, 2020. **532**(2): p. 211-218.
288. Lopez, A.D., et al., *Proteasomal degradation of Sfp1 contributes to the repression of ribosome biogenesis during starvation and is mediated by the proteasome activator Blm10.* Molecular biology of the cell, 2011. **22**(5): p. 528-540.
289. Bolte, S. and F.P. Cordelières, *A guided tour into subcellular colocalization analysis in light microscopy.* Journal of microscopy, 2006. **224**(3): p. 213-232.
290. Zou, K.H., K. Tuncali, and S.G. Silverman, *Correlation and simple linear regression.* Radiology, 2003. **227**(3): p. 617-628.
291. Mukaka, M.M., *A guide to appropriate use of correlation coefficient in medical research.* Malawi medical journal, 2012. **24**(3): p. 69-71.
292. Berger, A. and I. Schechter, *Mapping the active site of papain with the aid of peptide substrates and inhibitors.* Philosophical Transactions of the Royal Society of London. B, Biological Sciences, 1970. **257**(813): p. 249-264.
293. Turk, B.E., et al., *Determination of protease cleavage site motifs using mixture-based oriented peptide libraries.* Nature biotechnology, 2001. **19**(7): p. 661-667.
294. Coradin, M., K.R. Karch, and B.A. Garcia, *Monitoring proteolytic processing events by quantitative mass spectrometry.* Expert review of proteomics, 2017. **14**(5): p. 409-418.
295. Gumeni, S. and I.P. Trougakos, *Cross talk of proteostasis and mitostasis in cellular homeodynamics, ageing, and disease.* Oxidative Medicine and Cellular Longevity, 2016. **2016**.
296. Olivero, P., et al., *Proteostasis and mitochondrial role on psychiatric and neurodegenerative disorders: current perspectives.* Neural plasticity, 2018. **2018**.
297. del Hoyo, P., et al., *Oxidative stress in skin fibroblasts cultures of patients with Huntington's disease.* Neurochemical research, 2006. **31**(9): p. 1103-1109.
298. Suski, J.M., et al., *Relation between mitochondrial membrane potential and ROS formation*, in *Mitochondrial bioenergetics*. 2012, Springer. p. 183-205.
299. Nicholls, D.G., *Mitochondrial membrane potential and aging.* Aging cell, 2004. **3**(1): p. 35-40.
300. Korshunov, S.S., V.P. Skulachev, and A.A. Starkov, *High protonic potential actuates a mechanism of production of reactive oxygen species in mitochondria.* FEBS letters, 1997. **416**(1): p. 15-18.
301. Wojtczak, L., et al., *Effect of glucose and deoxyglucose on the redistribution of calcium in Ehrlich ascites tumour and Zajdela hepatoma cells and its consequences for mitochondrial energetics: Further arguments for the role of Ca2+ in the mechanism of the Crabtree effect.* European journal of biochemistry, 1999. **263**(2): p. 495-501.
302. Lebiedzinska, M., et al., *Oxidative stress-dependent p66Shc phosphorylation in skin fibroblasts of children with mitochondrial disorders.* Biochim Biophys Acta, 2010. **1797**(6-7): p. 952-60.
303. Wang, H., et al., *Effects of overexpression of huntingtin proteins on mitochondrial integrity.* Human molecular genetics, 2009. **18**(4): p. 737-752.
304. Parone, P.A., et al., *Preventing mitochondrial fission impairs mitochondrial function and leads to loss of mitochondrial DNA.* PloS one, 2008. **3**(9).
305. Benard, G., et al., *Mitochondrial bioenergetics and structural network organization.* Journal of cell science, 2007. **120**(5): p. 838-848.
306. Schmitt, K., et al., *Circadian control of DRP1 activity regulates mitochondrial dynamics and bioenergetics.* Cell metabolism, 2018. **27**(3): p. 657-666. e5.
307. Gegg, M.E., et al., *Mitofusin 1 and mitofusin 2 are ubiquitinated in a PINK1/parkin-dependent manner upon induction of mitophagy.* Human molecular genetics, 2010. **19**(24): p. 4861-4870.
308. Tanaka, A., et al., *Proteasome and p97 mediate mitophagy and degradation of mitofusins induced by Parkin.* Journal of Cell Biology, 2010. **191**(7): p. 1367-1380.
309. Shiratori, R., et al., *Glycolytic suppression dramatically changes the intracellular metabolic profile of multiple cancer cell lines in a mitochondrial metabolism-dependent manner.* Scientific reports, 2019. **9**(1): p. 1-15.
310. Sadre-Bazzaz, K., et al., *Structure of a Blm10 complex reveals common mechanisms for proteasome binding and gate opening.* Molecular cell, 2010. **37**(5): p. 728-735.

9. List of publications

UNIVERSITY AND NATIONAL LIBRARY
UNIVERSITY OF DEBRECEN
H-4002 Egyetem tér 1, Debrecen
Phone: +3652/410-443, email: publikaciok@lib.unideb.hu

Registry number: DEENK/212/2021.PL
Subject: PhD Publication List

Candidate: Azzam Aladdin
Doctoral School: Doctoral School of Molecular Medicine

List of publications related to the dissertation

1. **Aladdin, A.**, Yao, Y., Yang, C., Kahlert, G., Ghani, M., Király, N., Boratkó, A., Uray, K., Dittmar, G., Tar, K.: The Proteasome Activators Blm10/PA200 Enhance the Proteasomal Degradation of N-Terminal Huntingtin.
Biomolecules. 10 (11), 1-33, 2020.
DOI: http://dx.doi.org/10.3390/biom10111581
IF: 4.082 (2019)

2. **Aladdin, A.**, Király, R., Botó, P., Regdon, Z., Tar, K.: Juvenile Huntington's disease skin fibroblasts respond with elevated parkin level and increased proteasome activity as a potential mechanism to counterbalance the pathological consequences of mutant huntingtin protein.
Int. J. Mol. Sci. 20 (5338), 1-39, 2019.
IF: 4.556

List of other publications

3. Alatshan, A., Kovács, G. E., **Aladdin, A.**, Czimmerer, Z., Tar, K., Benkő, S.: All-Trans Retinoic Acid Enhances both the Signaling for Priming and the Glycolysis for Activation of NLRP3 Inflammasome in Human Macrophage.
Cells. 9, 1-21, 2020.
DOI: http://dx.doi.org/10.3390/cells9071591
IF: 4.366 (2019)

4. Douida, A., Batista, F., Robaszkiewicz, A., Botó, P., **Aladdin, A.**, Szenykiv, M., Czinege, R., Virág, L., Tar, K.: The proteasome activator PA200 regulates expression of genes involved in cell survival upon selective mitochondrial inhibition in neuroblastoma cells.
J. Cell. Mol. Med. 24 (12), 6716-6730, 2020.
DOI: http://dx.doi.org/10.1111/jcmm.15323
IF: 4.486 (2019)

5. **Aladdin, A.**, Dib, J. R., Malek, R. A., Enshasy, H. A. E.: Killer Yeast, a novel biological control of soilborne diseases for good agriculture practice.
In: Sustainable Technologies for the Management of Agricultural Wastes. Ed.: Zainul, Akmar Zakaria, Springer Nature Singapore Pte Ltd., Singapore, 71-86, 2018.

6. Perez, M. F., Isas, A. S., **Aladdin, A.**, Enshasy, H. A. E., Dib, J. R.: Killer yeasts as biocontrol agents of postharvest fungal diseases in lemons.
In: Sustainable Technologies for the Management of Agricultural Wastes. Ed.: Zainul, Akmar Zakaria, Springer Nature Singapore Pte Ltd., Singapore, 87-98, 2018.

7. **Aladdin, A.**, Yarar, E., Batool, T., Al-Astal, H. I. M., AlMatar, M., Makky, E. A.: Antiulcerogenic activity of Ageratum conyzoides: a review.
J. Biotech. Sci. Res. 4 (3), 204-213, 2017.

8. **Aladdin, A.**, Alsaheb, R. A. A., Pareek, A., Othman, N. Z., Malek, R. A., Enshasy, H. A. E.: Biotechnological Aspects and Pharmaceutical Applications of Bacterial Proteases.
Pharm Lett. 9 (2), 9-20, 2017.

9. Malek, K., Norazan, M., Ramaness, P., Othman, N. Z., Malek, R. A., Aziz, R., **Aladdin, A.**, Enshasy, H. A. E.: Cysteine Proteases from Carica papaya: An important enzyme group of many industrial applications.
IOSR J. Pharm. Biol. Sci. 11 (2), 11-16, 2016.
DOI: http://dx.doi.org/10.9790/3008-11211116

10. Malek, K., Norazan, M., Parasuraman, R., Othman, N. Z., Malek, R. A., Aziz, R., **Aladdin, A.**, Enshasy, H. A. E.: Production of Cysteine Proteases by Recombinant Microorganisms: a Critical Review.
IOSR J. Pharm. Biol. Sci. 11 (2), 35-40, 2016.

11. Alsaheb, R. A. A., **Aladdin, A.**, Othman, N. Z., Malek, R. A., Leng, O. M., Aziz, R., Enshasy, H. A. E.: Lactic acid applications in pharmaceutical and cosmeceutical industries.
J. Chem. Pharm. Res. 7 (10), 729-735, 2015.

12. Alsaheb, R. A. A., **Aladdin, A.**, Othman, N. Z., Malek, R. A., Leng, O. M., Aziz, R., Enshasy, H. A. E.: Recent applications of polylactic acid in pharmaceutical and medical industries.
J. Chem. Pharm. Res. 7 (12), 51-63, 2015.

13. **Aladdin, A.**, Bouna, A., Ibrahim, A., Noor, R. M., Ramli, F., Shamsir, M. S.: Homology Modeling and Molecular Dynamics Simulation of a Novel [beta]-galactosidase from Antarctic Psychrophilic Bacterium Planococcus Antarcticus DSM 14505.
J. Biotech. Sci. Res. 2 (1), 63-70, 2014.

UNIVERSITY AND NATIONAL LIBRARY
UNIVERSITY OF DEBRECEN
H-4002 Egyetem tér 1, Debrecen
Phone: +3652/410-443, email: publikaciok@lib.unideb.hu

14. Ali, A. A. M., AlMatar, M., Al-Astal, H. I. M., Hawege, E. F., **Aladdin, A.**: Production of Xylanase Enzyme from Aspergillus Terreus SUK-1.
Int. J. Chemtech Res. 6 (11), 4884-4889, 2014.

Total IF of journals (all publications): 17,49
Total IF of journals (publications related to the dissertation): 8,638

The Candidate's publication data submitted to the iDEa Tudóstér have been validated by DEENK on the basis of the Journal Citation Report (Impact Factor) database.

21 April, 2021

DEBRECENI EGYETEM
Egyetemi és Nemzeti Könyvtár

10. Keywords

Huntington’s disease (HD)

Juvenile HD fibroblast

26S

Blm10/PA200-proteasomes

Mitochondria

Parkin

Ubiquitin-proteasome system (UPS)

PolyQ

20S-CP

Blm10/PA200

Degradation

Huntingtin (Htt)

N-Htt fragments

Aggregates

Cell protection

11. Acknowledgments

I am immensely thankful to my supervisor Dr. Krisztina Tar for the professional guidance, encouragement, and continuous support throughout my Ph.D. study. I deeply appreciate her confidence bestowed upon me.

I would like to extend my gratitude to Prof. Dr. László Virág the head of the Department of Medical Chemistry, for giving me the chance to work within the department. Special thanks to Prof. Dr. Péter Bay for enabling us to use several devices in his Lab. I would like to thank Prof. Dr. László Csernoch the head of the Doctoral School of Molecular Medicine for his support to us.

I am grateful to Dr. Róbert Király for guiding me during the initial stage of my Ph.D., teaching me several techniques. I am also thankful to Prof. Dr. László Fésüs for allowing me to perform many experiments in his Lab. Very special thanks to all my colleagues/friends in Fesus's Lab for their help and cooperation.

I would like to thank Abdennour Douida, Andrea Tankáné Farkas, and Marvi Ghani for the valuable discussions and good time together. My sincere gratitude goes to all my colleagues/friends and staff of the Department of Medical Chemistry for helping me in any condition I needed.

Very special thanks to Prof. Dr. Hesham A. El Enshasy for his great support and help to take the first step in my research life. Special thanks to our international collaborators Prof. Dr. Gunnar Dittmar from Luxembourg Institute of Health, Dr. Ciyu Yang from Albert Einstein University, Dr. Günther Kahlert from Institute for Systems Biology, Dr. Yanhua Yao from Shanghai Jiao Tong University for their valuable contribution and feedback in my project.

Warm thanks to my mom Subhia Aladdin, I would like to thank her for all her prayers and tears, I am really missing you, mom. I also would like to thank my siblings and all my friends for the ongoing emotional support.

This work is a special dedication to Hiba, and my kids Maria and Mahmoud. Thanks for all the love, and patience. They give me continuous spiritual support, and I always drew strength from them throughout the difficult times.

12. Appendix

The thesis is based on the following publications: